Inaugural dissertation

for obtaining the doctoral degree

of the

Combined Faculty of Mathematics, Engineering and Natural Sciences

of the Ruprecht Karls University Heidelberg

Presented by

M.Sc. Bahardokht Tolou Dabbaghian

Born in Tehran, Iran

Oral examination: 07.05.2024

Use of pharmaceutical and transgenic interventions in dissection of neuropathic pain mechanisms in spinal cord injury

Referees:

Prof. Dr. Hilmar Bading

Dr. Radhika Puttagunta

Prof. Dr. med. Thomas Kuner

Prof. Dr. Marc Freichel

To Erfan and my mother…

Abstract

After experimental spinal cord injury (SCI), the emergence of neuropathic pain below the injury site is linked to heightened structural plasticity of nociceptive fibers into deeper laminae of the dorsal horn. I have examined the role of prophylactic pregabalin (PGB), a commonly prescribed drug for SCI patients following neuropathic pain development, on this aberrant plasticity and the development of neuropathic pain. Prophylactic PGB administration (46 mg/kg, i.p., 2x/day, for 7 days) effectively averted mechanical allodynia and the plasticity of peptidergic nociceptors into laminae III-IV in the lumbar spinal cord of male and female C57BL/6J mice subjected to a T11 moderate contusion. These beneficial effects against mechanical allodynia and the plasticity of nociceptive fibers persisted for up to two weeks post-PGB discontinuation. To learn more about the specific role of nociceptors and their voltage-gated calcium channel (VGCC) α2-δ2 subunit (Cacna2d2) −a selective PGB target− in the development of the neuropathic pain and aberrant plasticity I employed $SNS^{Cacna2d2}$ mice with a partial knockout of the α2-δ2 subunit specifically in nociceptors. Remarkably, these mice did not manifest thermal hyperalgesia nor mechanical allodynia post-SCI, as confirmed by Hargreaves, von Frey hair filaments, and the place escape/avoidance paradigm. Importantly, non-noxious mechanical hindpaw stimulation induced dorsal horn activation (c-fos) with significantly lower activation in both the PGB-treated and partial knockout mice. Laminae III-V of the dorsal horn exhibited the highest neuronal activation, aligning with the observed plasticity. Utilizing 3D imaging of nociceptor-labeled transgenic mice ($SNS^{tdTomato}$), this study reveals a post-SCI increase in volume of nociceptors in lower laminae of the dorsal horn, specifically starting from lamina III. This expansion suggests ventral sprouting rather than lateral. This thesis work underscores the pivotal role of nociceptors in neuropathic pain development following SCI, indicating their plasticity into deeper laminae establishes new connections transmitting mechanical allodynia potentially through wide dynamic neurons.

Zusammenfassung

Nach experimenteller Rückenmarksverletzung (SCI) ist das Auftreten von mechanischer Allodynie unterhalb der Verletzungsstelle mit einer gesteigerten Plastizität der nozizeptiven Afferenzen in tiefere Laminae des dorsalen Horns verbunden. Ich habe die Rolle der prophylaktischen Anwendung von Pregabalin (PGB), einem häufig verschriebenen Medikament für SCI-Patienten nach der Entwicklung neuropathischer Schmerzen, bei dieser abnormen Plastizität und der Entwicklung neuropathischer Schmerzen untersucht. Die prophylaktische Verabreichung von PGB (46 mg/kg, i.p., 2x/Tag, für 7 Tage) verhinderte effektiv mechanische Allodynie und die Plastizität peptiderger Nozizeptoren in den Laminae III-IV im lumbalen Rückenmark von männlichen und weiblichen C57BL/6J-Mäusen, die einer mäßigen Quetschung von T11 unterzogen wurden. Diese vorteilhaften Effekte gegen mechanische Allodynie und Plastizität nozizeptiver Afferenzen hielten bis zu zwei Wochen nach Absetzen von PGB an. Um mehr über die spezifische Rolle von Nozizeptoren und ihres spannungsgesteuerten Calciumkanal-α2-δ2-subunit (Cacna2d2) - einem PGB-Ziel - bei der Entwicklung von neuropathischen Schmerzen und abnormer Plastizität zu erfahren, setzte ich $SNS^{Cacna2d2}$ Mäuse mit einem partiellen Knockout der α2-δ2-subunit spezifisch in Nozizeptoren ein. Diese Mäuse zeigten post-SCI bemerkenswerterweise keine thermische Hyperalgesie oder mechanische Allodynie, wie durch Hargreaves, von Frey-Haarfilamente und das Place-Escapen/Avoidance-Paradigme bestätigt wurde. Wichtig ist, dass nicht-nociceptive mechanische Stimulierung der Hinterpfote eine Aktivierung des dorsalen Horns (c-fos) mit signifikant geringerer Aktivierung sowohl bei den PGB-behandelten als auch bei den teilweisen Knockout-Mäusen induzierte. Laminae III-V des dorsalen Horns zeigte die höchste neuronale Aktivierung, was mit der beobachteten Plastizität übereinstimmt. Durch die Verwendung von 3D-Bildgebung von nozizeptor-markierten transgenen Mäusen ($SNS^{tdTomato}$) zeigt diese Studie eine post-SCI-Zunahme des Volumens von Nozizeptoren in der unteren Laminae des dorsalen Horns, die speziell ab Lamina III beginnt. Diese Expansion deutet auf eine ventrale Auswucherung hin, anstatt seitlich. Diese

Doktorarbeit unterstreicht die entscheidende Rolle von Nozizeptoren bei der Entwicklung neuropathischer Schmerzen nach SCI und deutet darauf hin, dass ihre Plastizität in tiefere Laminae neue Verbindungen etabliert, die möglicherweise mechanische Allodynie-Signale durch weitreichende dynamische Neuronen übertragen.

Acknowledgement

I want to extend my thanks to everyone who played a meaningful role in my academic and personal life during this doctoral journey.

I am deeply thankful to my direct supervisor, Dr. Radhika Puttagunta, for giving me the opportunity to do my PhD in their lab and the unwavering guidance, insightful feedback, and continuous support throughout this research journey. I am also grateful to Prof. Dr. Norbert Weidner for his valuable input and expertise.

I am deeply grateful to Prof. Dr. Hilmar Bading and Prof. Dr. Thomas Kuner, members of my Thesis Advisory Committee. Their invaluable expertise significantly contributed to the effective management of my projects. I am especially thankful for their constructive feedback, which played a pivotal role in the successful completion of my studies. I am also very grateful to Prof. Dr. Hilmar Bading for being my first supervisor. I extend my gratitude to Prof. Dr. Marc Freichel for agreeing to serve as the fourth member of my committee.

My sincere thanks go to Dr. Jarred Griffin for his collaboration and wonderful work with the lightsheet microscopy as well as his assistance and insights, enriching the scope and depth of my research. I am also grateful to Prof. Dr. Frank Bradke, for sharing his resources for this project.

This research would not have been possible without the financial support from the Heidelberg Pain SFB 1158, enabling me to focus on my studies and contribute to the academic community.

I extend my sincere appreciation to my fellow PhD candidates, colleagues, and friends for fostering a stimulating academic environment and generously sharing valuable insights and experiences. Special gratitude is owed to Dr. Xing Chen who introduced me to the lab. I am grateful to Dr. Vasileios Kampanis for not only introducing me to the lab but also for making our collaboration on multiple projects enjoyable and fulfilling. I would like to thank Dr. Naëmi Kühn for her friendship and emotional support throughout my PhD journey. I would like to express my heartfelt thanks to Jing Chen for her valuable assistance with my project, coupled

with her kindness, enduring friendship, and emotional support. Additionally, I am grateful to Dr. Yifeng Zheng for the enriching conversations, friendship, kindness, and support. I am also thankful to Melanie Motsch for her help with mice breeding and genotyping. Also, a special thanks goes to my student Patrick Wisser for trusting me as a mentor and for helping me further my project.

To my family, especially my mother who stood by me with unwavering support and encouragement, I express my deepest gratitude. Your understanding and patience have been the pillar of my strength.

With heartfelt gratitude, I want to express my thanks to Erfan, my amazing best friend and husband. I might not have been standing here today, if not for your unwavering support, encouragement, and understanding, which have been my greatest pillars. Your sacrifices, patience, and belief in me have been instrumental in my success. I am truly fortunate to have a partner who understands everything I go through so well and can provide emotional support and encouragement when it is needed the most. Thank you for being my rock and sharing this academic adventure with me. Your love and support have made this accomplishment all the more meaningful.

Table of contents

Abstract I

Zusammenfassung II

Acknowledgement IV

Table of contents VI

Abbreviations X

List of Figures XII

List of Tables XV

1 Introduction 2

1.1. Background 2

1.1.1 Spinal cord injury and neuropathic pain 2

1.1.2 Somatosensory neurons 2

1.1.3 Spinothalamic tract and wide dynamic range neurons 4

1.1.4 Voltage-gated calcium channels 6

1.1.5 Localization of α2δ subunit in the CNS and DRG 9

1.1.6 Involvement of α2δ subunit in nerve injury and neuropathic pain 9

1.1.7 Gabapentinoids 11

1.1.8 Microglia, neuropathic pain and gabapentinoids 12

1.2. Hypothesis and Aims 14

1.2.1. Hypothesis 14

1.2.2. Aims 14

2. Material and Methods 17

2.1. Materials 17

2.1.1. Animals 17

2.1.2. Equipment and instruments 18
2.1.3. Chemicals 22
2.1.4. Antibodies 27
2.1.5. Buffer and solutions 30
2.1.6. Primers 35
2.1. Methods 35
2.2.1 Animal guidelines and housing conditions 35
2.2.2 Spinal Cord Injury 36
2.2.3 Behavioral Testing 37
2.2.3.1 Motor recovery: Basso Mouse Scale (BMS) 37
2.2.3.2 Mechanical Sensitivity Testing: von Frey hair filaments 38
2.2.3.3 Supraspinal pain processing: Place Escape/Avoidance Paradigm (PEAP) 39
2.2.3.4 Thermal sensitivity testing: Hargreaves' method 39
2.2.3.5 Hindpaw stimulation 40
2.2.4 Transgenic animal breeding 40
2.2.4.1 $SNS^{tdTomato}$ mice 41
2.2.4.2 $SNS^{Cacna2d2}$ mice 42
2.2.5 Genotyping 43
2.2.5.1 DNA isolation 43
2.2.5.2 Genotyping PCR 43
2.2.5.3 Primer and Cycling Protocols 44
2.2.6 Tissue processing 45
2.2.7 Eriochrome Cyanine staining 46
2.2.8 Immunohistochemistry on slides 47
2.2.9 Immunohistochemistry of free-floating sections 48

2.2.10 Clearing and staining of intact lumbar spinal cord 49
2.2.11 Analysis of microscopic images 51
2.2.11.1 Quantification of CGRP labeling density in the spinal cord 51
2.2.11.2 Quantification of c-fos labeling in the spinal cord 51
2.2.11.3 Quantification of KCC2, PKCγ and Iba1 intensity in the spinal cord 52
2.2.11.4 Quantification of 5HT in the spinal cord 52
2.2.11.5 Quantification of Cacna2d2 intensity in the DRG 53
2.2.11.6 Quantification of pCAMKII, pCREB and CREB intensity in the DRG 53
2.2.12 Statistical analysis 53
2.2.13 Illustration 54
3 Results 56
3.1 Aberrant nociceptor plasticity to deeper laminae occurs rapidly after spinal cord injury 56
3.2 Prophylactic pregabalin treatment prevents mechanical allodynia development, associated peptidergic nociceptor plasticity and reduces microglia activation 58
3.3 The prevention of mechanical hypersensitivity by pregabalin is partially conserved beyond two weeks post-discontinuation 66
3.4 Nociceptors contribute to SCI-induce neuropathic pain through voltage-gated calcium channels 70
4. Discussion 79
4.1 Nociceptors plasticity contributes to neuropathic pain 79
4.2 Effect of Gabapentinoids on nociceptor plasticity and neuropathic pain 81
4.3 Effect of α2δ-2 subunit of VGCCs on nociceptor plasticity and neuropathic pain 82
4.4 Role of microglia in neuropathic pain 83
4.5 Further mechanisms of neuropathic pain 84
4.6 Sex differences in neuropathic pain development 85

5. Conclusions and Future Perspective 88

6. Bibliography 91

Abbreviations

5-HT	5-hydroxytryptamine
BDNF	Brain-derived neurotrophic factor
BMS	Basso Mouse Scale
CACNA2D2	Calcium Channel, Voltage-Dependent, α2δ-2 subunit
CGRP	Calcitonin gene-related peptide
CSF1	Colony stimulating factor 1
dpi	Days post injury
DMSO	Dimethylsulfoxid
DRG	Dorsal root ganglion
du/du	Ducky mouse mutants
EC	Eriochrome Cyanine
ECM	Extracellular matrix
EDTA	Ethylenediaminetetraacetic acid
GABA	Gamma-Aminobutyric acid
GBP	Gabapentin
Iba1	Ionized calcium-binding adapter molecule 1
IL-6, -10, -1β	Interleukin 6, -10, -1 beta
i.p.	Intraperitoneal
IB4	Isolectin B4
KCC2	K^+/Cl^- cotransporter 2
KO	Knockout
LRP1	Lipoprotein receptor-related protein 1
LTMRs	Low-threshold mechanoreceptors
MAPKs	Mitogen Activated Protein Kinases
Mrgprd/A3	MAS-related G-protein coupled receptor member D/A3
NEFH	Neurofilament heavy chain protein

NeuN	Neuronal nuclei
NMDA	N-methyl-D-aspartate
NMDARs	N-methyl-D-aspartate receptors
PBS	Phosphate-Buffered Saline
PEAP	Place Escape/Avoidance Paradigm
PFA	Paraformaldehyde
PGB	Pregabalin
PKCγ	Protein kinase Cγ
s.c.	Subcutaneous
SCI	Spinal cord injury
SD	Standard deviation
SP	Substance P
STT	Spinothalamic tracts
TBS	Tris buffered saline
TH	Tyrosine hydroxylase
TNF-α	Tumor necrosis factor α
TRIS	Tris(hydroxymethyl)aminomethan
TrkA	Tropomyosin receptor kinase A
TrkB	Tropomyosin receptor kinase B or Tyrosine receptor kinase B
TrkC	Tropomyosin receptor kinase C
VGCCs	Voltage-gated calcium channels
VWA	von Willebrand factor A
WDR	Wide-dynamic range

List of Figures

Figure 1: Wide dynamic range neurons

Figure 2: Voltage-gated calcium channels

Figure 3: Pregabalin and Gabapentin structure

Figure 4: $SNS^{tdTomato}$ mice

Figure 5: $SNS^{CACNA2D2}$ mice

Figure 6: 3D reconstructed SCI-induced nociceptive plasticity

Figure 7: Prophylactic PGB treatment inhibits the development of mechanical allodynia in both sexes

Figure 8: Prophylactic PGB treatment reduces SCI-induced $CGRP^{+}$ fiber plasticity and neuronal activation below injury level in the lumbar spinal cord

Figure 9: Prophylactic PGB treatment has no effect on white matter sparing or lesion length after SCI

Figure 10: Prophylactic PGB treatment reduces microglia reactivity below injury level in the lumbar spinal cord, one-week post-SCI

Figure 11: Prophylactic PGB treatment has no effect on PKCγ in the dorsal horn of the lumbar spinal cord after SCI

Figure 12: Prophylactic PGB treatment has no effect on KCC2 intensity in the dorsal horn of the lumbar spinal cord after SCI

Figure 13: Prophylactic PGB treatment has no effect on 5HT fiber neuroprotection in lumbar spinal cord after SCI

Figure 14: Seven-day PGB treatment has lasting effects on mechanical sensitivity for nearly 2 weeks post-PGB removal

Figure 15: Seven-day PGB treatment has lasting effects on the reduction of $CGRP^{+}$ fiber plasticity but not Iba1 intensity two weeks following removal

Figure 16: Discontinuation of prophylactic PGB treatment following SCI has no effect on white matter sparing or lesion extent

Figure 17: Discontinuation of prophylactic PGB treatment following SCI has no effect on PKCγ in the lumbar spinal cord

Figure 18: Partial knockout of CACNA2D2 in nociceptors of male mice stops the development of mechanical allodynia and thermal hyperalgesia following SCI

Figure 19: Partial CACNA2D2 nociceptor-specific knockout in female mice has a similar beneficial effect as males after SCI

Figure 20: Significant reduction in CACNA2D2 intensity in the nociceptors after partial α2δ-2 subunit of VGCCs nociceptor-specific knockout

Figure 21: Significant reduction in pCAMKII intensity in the nociceptors after partial α2δ-2 subunit of VGCCs nociceptor-specific knockout

Figure 22: Significant reduction in nuclear pCREB/CREB intensity in the nociceptors after partial α2δ-2 subunit of VGCCs nociceptor-specific knockout

Figure 23: Partial knockout of CACNA2D2 in nociceptors reduces SCI-induced CGRP-expressing fiber plasticity and neuronal activation in laminae III-V but has no effect on Iba1 levels below injury level in the dorsal horn of lumbar spinal cord

Figure 24: Partial CACNA2D2 nociceptor-specific knockout does not alter PKCγ levels in the lumbar spinal cord after SCI

Figure 25: White matter sparing and lesion length remains similar in partial knockout and control mice after SCI

List of Tables

Table 1: Classification of DRG sensory neurons

Table 2: VGCC subclasses

Table 3: List of animals

Table 4: Equipment for DNA preparation and genotyping

Table 5: Equipment and instruments for surgery and tissue processing

Table 6: Equipment and instruments for behavioral testing

Table 7: Equipment and instruments for microscopic imaging

Table 8: Software

Table 9: List of chemicals and kits

Table 10: List of Antibodies

Table 11: Buffer and solutions

Table 12: List of primers for genotyping

Table 13: PCR Master mix for genotyping

Table 14: PCR protocol for genotyping Rosa26$^{LSL\text{-}tdTomato}$ mice

Table 15: PCR protocol for genotyping SNS^{Cre} mice

Table 16: PCR protocol for genotyping of Cacna2d2$^{fl/fl}$ mice

Table 17: SNS^{CACNA2D2} breeding and offspring details

Introduction

1 Introduction

1.1. Background

1.1.1 Spinal cord injury and neuropathic pain

Spinal cord injury (SCI) happens following trauma or damage to the spinal cord resulting in various levels of motor, sensory and autonomic dysfunction. Depending on severity and location of the injury, SCI can result in lifelong impairment of these functions, significantly diminishing the patient's quality of life. Moreover, nearly 50% of these patients also suffer from neuropathic pain. This pain can be localized at or below lesion level and often persists for many years after the initial injury[1–3]. The primary symptoms of neuropathic pain include allodynia (lowered threshold for pain), hyperalgesia (intensified sensitivity to pain) and hypoalgesia (heightened threshold for pain). Allodynia and hyperalgesia are believed to indicate an exaggerated reaction to an otherwise normal mechanical or thermal stimulus below the threshold[4]. SCI-induced neuropathic pain has a complex and multifactorial pathophysiology and due to the lack of knowledge about the direct mechanisms, it remains difficult to treat. To better treat the patients, it is necessary to learn more about the driving mechanisms, contributing factors and neuronal populations involved.

1.1.2 Somatosensory neurons

The nerve endings of the primary sensory neurons which are in the trigeminal ganglia and dorsal root ganglia (DRG), in head and trunk region respectively, are responsible for receiving sensations such as pain perception, joint orientation, muscle extension, temperature detection, pressure sensitivity, and tactile sensations. Primary sensory neurons, pseudounipolar in structure, divide into two branches: one projecting to peripheral tissues and the other terminating in the spinal cord[5].

DRG neurons display a variety of populations: unmyelinated small-diameter C-fibers, Aδ-fibers with thin myelination, and large-diameter Aα/β-fibers with thick myelination. The small population can be peptidergic (release neuropeptides like calcitonin gene-related peptide (CGRP) and substance P(SP)) or non-peptidergic (lack neuropeptide expression but bind to isolectin B4; IB4). The large population express neurofilament 200 (NF200). There is also another subpopulation of small diameter neuron comprised of tyrosine hydroxylase (TH)-positive neurons. Additionally, DRG neurons can be classified according to their expression of receptors for neurotrophic factors. Peptidergic fibers express tropomyosin receptor-kinase A (TrkA), which serves as a receptor for nerve growth factor (NGF). Nonpeptidergic fibers have the Ret receptor and Gfra2 (Glial cell line-derived neurotrophic factor/GDNF family receptor α2), and large neurons express of TrkB or TrkC[6].

scRNA-seq investigations conducted in mice have categorized neurons in DRG into 11 cell types[6–11]. The different types are summarized in Table 1. The cluster containing neurofilament (NF) expresses lactate dehydrogenase B (LDHB) and neurofilament heavy chain (NEFH). The peptidergic nociceptors (PEP) cluster expresses substance P, TRKA, and CGRP. The non-peptidergic nociceptors (NP) cluster expresses Mrgprd (MAS-related G-protein coupled receptor D) and P2rx3 (purinergic receptor P2X ligand-gated ion channel 3). The TH (tyrosine hydroxylase) cluster are unmyelinated neurons with distinct expression of TH[10]. The NF1-3 subtypes are identified as low-threshold mechanoreceptors (LTMRs) with myelination, which are responsible for conveying sensory touch signals, while NF4-5 neurons act as proprioceptors, sensing both body motion and posture. TH expressing cells (unmyelinated C-fiber LTMRs) responded to a various harmful stimulus, such as intense pressure, temperature extremes, or tissue damage. PEP1 (unmyelinated peptidergic fibers) coexpress genes for neuropeptides such as SP and CGRP. PEP2 (peptidergic fibers with myelination) consist of Aδ nociceptors and express CGRP and NEFH, but no SP. NP1 (express Mrgprd) are nociceptors with no myelination, which responds to polymodal painful stimuli (thermal, mechanical and pruritic). NP2 neurons (Mrgpra3^{+}; MAS-related G-protein coupled receptor member A3) and

NP3 fibers (Nppb^{+}; natriuretic polypeptide b) are vital in sensing itch, although they may also transmit pain-related information[5,7,8,11].

Classic classification	New classification	Identification markers	Common products	Myelination
C-LTMRS	TH	VGLUT3, PIEZO2	$Na_v1.8$/9	NO
Peptidergic nociceptors	PEP1	TRKA, CGRP	$Na_v1.8$/9	NO
	PEP2	TRKA, CGRP	$Na_v1.8$/9, NEFH	YES
Non-peptidergic nociceptors	NP1	PLXNC1, P2X3	$Na_v1.8$/9	NO
	NP2	PLXNC1, P2X3	$Na_v1.8$/9	
	NP3	PLXNC1, P2X3	$Na_v1.8$/9	
LTMRs	NF1	LDBH, TRKB (high)	NEFH	YES
	NF2	LDBH, TRKB (low)	NEFH	
	NF3	LDBH, TRKC (high)	NEFH	
Proprioceptors	NF4	LDBH, PV, TRKC (low)	NEFH	YES
	NF5	LDBH, PV, TRKC (low)	NEFH	

Table 1. Classification of DRG sensory neurons. Different DRG classes include tyrosine hydroxylase containing (TH), peptidergic nociceptors (PEP), non-peptidergic nociceptors (NP), neurofilament containing (NF). Further designation is through the following markers; CGRP (calcitonin gene-related peptide), LDHB (lactate dehydrogenase B), NEFH (neurofilament heavy chain protein), P2X3 (purinergic receptor P2X ligand-gated ion channel 3), PIEZO2 (mechanically activated ion channels conferring proprioception, touch and noxious mechanical stimuli) PLXNC1 (plexin C1), PV (parvalbumin), TRKA (Tropomyosin receptor kinase A), TRKB, TRKC, TH (tyrosine hydroxylase), VGLUT3 (Vesicular Glutamate Transporter 3). Modified from Usoskin et al.[10].

1.1.3 Spinothalamic tract and wide dynamic range neurons

The somatosensory information received from the periphery is conveyed to thalamus and cerebral cortex through ascending spinal pathways. Pain and thermal sensations are transmitted through spinothalamic tract (STT). The ventral

STT is responsible for conveying sensations of crude touch and pressure. The lateral STT transmits signals related to pain and temperature. The dorsolateral STT (described in the rat, cat, macaque monkey) also serves as a nociceptive ascending spinal pathway[12].

Most of STT neurons in rats are situated contralaterally within the spinal cord, primarily in laminae I, III-VII, and X. In the lumbar region, neurons are particularly noticeable in the medial portion of lamina V[13]. In the deep dorsal horn (laminae III-V), most second-order neurons are wide dynamic range (WDR; Figure 1) neurons which are an important part of pain processing[14]. Aδ and C-nociceptors provide synaptic input to these neurons. WDR neurons additionally receive synaptic signals from Aβ mechanoreceptors[15–18]. WDR neurons exhibit distinctive characteristics and display differential responses across a broad spectrum of stimulus intensities, ranging from gentle to painful stimulation. In comparison to non-painful stimuli, painful stimuli elevate the impulse frequencies and a activate greater number of WDR neurons[15–19]. Sharper or hotter objects elicit an increase in their impulse frequency, and this allows discrimination of small temperature differences[15]. Research indicates that the destruction of nociceptors in superficial dorsal horn results in alterations in WDR neurons, and these neurons no longer show amplification in their reaction to repeated C-fiber stimulation and demonstrate a significant decline in their ability to undergo sensitization[20,21].

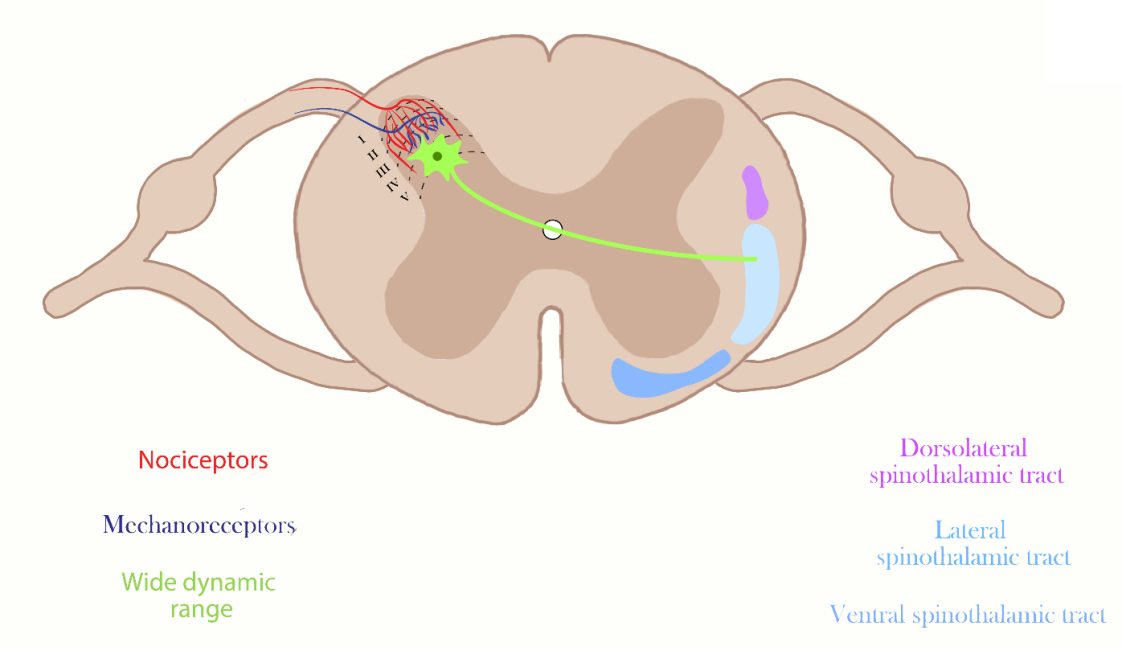

Figure 1. Wide dynamic range neurons. Wide dynamic range neurons are mostly located in laminae III-V. They are involved in transmitting the pain signal through the spinothalamic tract. Painted in Adobe Illustrator (Adapted by Watson and Harrison[88] and Willis et al.[130])

1.1.4 Voltage-gated calcium channels

Voltage-gated calcium channels (VGCCs) are an important part for the functioning of excitable cells. They can be categorized into three classes, namely Ca_V1–3. As seen in Figure 2, VGCCs have of a pore-forming α1 subunit, and except for Ca_V3 (T type) channels, all the other classes are accompanied by auxiliary subunits known as α2δ and β, along with an additional γ subunit in skeletal muscle[22]. These auxiliary subunits play a role in trafficking and activation kinetics [23,24].

The α2δ subunits are widely recognized for their established role in modulating the trafficking and function of Ca_V1 and Ca_V2 channels (different types explained in Table 2). They have been shown to increase the density of these channels on the plasma membrane. Moreover, the α2δ subunits play a role in directing the channels to specific subcellular locations, such as neuronal processes. Furthermore, they contribute to enhancement of functional Ca_V channels by influencing the biophysical features of calcium currents, extending

their impact beyond just trafficking. These subunits also exert an influence on various voltage-related features and kinetics of the channels, such as activation and inactivation [22,25]. Research on Purkinje cells involving the genetic removal of the α2δ-2 subunit has revealed notable impacts on neuronal and synaptic morphology, including a reduction in the size of the dendritic tree along with other abnormalities such as weeping willow dendrites (bending downwards) and dendritic thickening, indicating potential roles for α2δ that extend beyond calcium channel kinetics [26,27].

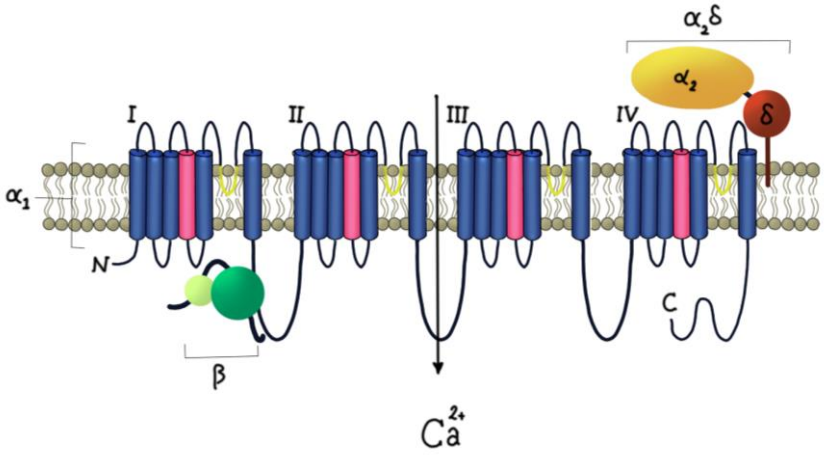

Figure 2. Voltage-gated calcium channels. VGCCs α1 subunits have 24 transmembrane α-helices, which are divided into four homologous repeats (I–IV). Each repeat's fourth transmembrane segment (shown in pink) contains five amino acids with positive charges. It creates the channel's voltage-sensing component, together with the adjacent segments. The α2δ subunit consists of an extracellular component (α2), which is bond by disulphide to the membrane-associated component (δ).

Ca^{2+} current type	α1 Subunits	Principal physiological functions
L	$Ca_V1.1$	Skeletal muscle
	$Ca_V1.2$	Cardiac muscle, smooth muscle, secretion of endocrine hormones, Ca^{2+} transients in neuronal cell bodies and dendrites
	$Ca_V1.3$	Secretion of endocrine hormones, cardiac pacemaking, Ca^{2+} transients in neuronal cell bodies and dendrites, inner hair cells in cochlea
	$Ca_V1.4$	Retinal synapses
P/Q	$Ca_V2.1$	Central synapses, Neurotransmitter release, Dendritic Ca^{2+} transients, neuromuscular junction, cochlea
N	$Ca_V2.2$	Central and peripheral synapses, Neurotransmitter release, Dendritic Ca^{2+} transients
R	$Ca_V2.3$	Central and peripheral synapses (asynchronous release), Neurotransmitter release, Dendritic Ca^{2+} transients, cochlea, cardiac
T	$Ca_V3.1$	Many excitable cells including those with pacemaker function and subthreshold oscillations
	$Ca_V3.2$	
	$Ca_V3.3$	

Table 2. VGCC subclasses. α1 subunits can be categorized into three subclasses based on their amino acid sequence. The Ca_V1 and Ca_V2 classes are also called the high-voltage-activated (HVA) channels, although relatively mid to low voltages activate $Ca_V1.3$ and $Ca_V1.4$. The Ca_V3 are called low-voltage-activated (LVA) channels. (Modified from Dolphin and Lee [131]; Dolphin[113])

α2δ-2 subunits are extracellular membrane-associated and consist of various domains, notably the von Willebrand factor A (VWA) domain, which is frequently involved in facilitating protein-protein interactions. Specifically, the VWA domain plays a crucial role in mediating interactions between cell-adhesion

proteins and the extracellular matrix (ECM). Experiments involving mutagenesis indicate that the VWA domain plays a critical role in regulating the interaction between α2δ-2 and ECM components, such as thrombospondins and tenascin. These interactions are vital for the formation of synapses[28,29].

1.1.5 Localization of α2δ subunit in the CNS and DRG

The α2δ subunits play a critical role in trafficking calcium channels to synapse active zones, regulating calcium influx, and subsequent neurotransmitter release[30]. It has been shown that α2δ expression is widespread in both peripheral and central neurons[31,32]. Brain regions tied to pain perception, including the dorsal raphe, periaqueductal gray, locus coeruleus, and amygdala, have strong expression of α2δ subunits[31,32]. In the spinal cord, the α2δ-1 subunit is mainly found in the presynaptic terminals of primary afferents that terminate in the superficial laminae of the dorsal horn, accompanied by a moderate presence in postsynaptic sites of deeper neurons[33,34], however, the expression of α2δ-2 mRNA is significantly higher compared to α2δ-1 mRNA in the spinal cord. Importantly, it's worth noting that α2δ-1 exhibits expression in non-neuronal tissues, including cardiac tissue, smooth muscle, and endocrine organs[35]. In contrast, α2δ-2 is primarily found in the neurons[35]. Although both α2δ-1 and α2δ-2 mRNA are present in all DRG neurons, the abundance of α2δ-2 mRNA in large-diameter neurons is comparatively lower than that of α2δ-1 mRNA[31].

1.1.6 Involvement of α2δ subunit in nerve injury and neuropathic pain

In damaged DRG neurons, there is a consistent increase in both α2δ-1 mRNA and protein levels[34,36–38]. Additionally, mice with a knockout of α2δ-1 subunit have a significant reduction in their baseline responses to mechanical and cold stimuli, and a delay in development of hyperalgesia following sciatic nerve injury[39]. These findings underscore the crucial role of α2δ in modulating pain processing and sensitivity in other neuropathic conditions.

Studies revealed that in mice lacking the α2δ-1 gene (complete conventional knockout), there is a significant decrease in sensitivity to mechanical and cold stimuli, which is associated with decreased transportation of N-type calcium channels to presynaptic terminals of primary sensory neurons in the dorsal horn [30,39]. A decrease in presynaptic input was observed following electrical stimulation in α2δ-1 knockout (KO) mice which likely indicates a reduction in synaptic transmitter release from primary afferents that connect to neurons in the dorsal horn. Furthermore, the absence of changes in windup responses further supports the idea of presynaptic alterations[39]. Moreover, DRG neurons lacking α2δ-1 demonstrate notably reduced calcium channel currents[39]. α2δ subunit has also been found to aid in the formation of excitatory synapses through its interaction with thrombospondin[28]. In mice lacking α2δ-1, there is a reduction of $Ca_V2.2$ protein level in brain and spinal cord synaptosomes. Overexpression of α2δ-1, shortens action potential duration, indicating a key role of these subunits in shaping DRG neuronal action potentials[30]. The duration of action potentials is associated with the maximum firing frequency, with C-nociceptors exhibiting the longest durations and Aα/β fibers displaying the shortest durations[40]. Consequently, when α2δ-1 upregulates after peripheral nerve injury in DRG neurons[37,41,42] and the presynaptic terminals of the primary afferent neurons in spinal cord[34,43]. This is associated with mechanical allodynia[41] and enables DRG to sustain a higher frequency of spontaneous action potential and increase neurotransmitter release[39]. In transgenic mice with overexpression of α2δ-1 (mimicking this characteristic of sensory nerve damage), mechanical allodynia will occur even without nerve damage[33]. Although thus far most studies have concentrated on the involvement of the α2δ-1 subunit in neuropathic pain, the substantial impact it exerts suggests that the α2δ-2 subunit may also play a significant role. Given the prevalence of α2δ-2 in small diameter DRG (predominantly nociceptors), they should be explored for their contributions to neuropathic pain.

1.1.7 Gabapentinoids

Gabapentinoids (including gabapentin, pregabalin, and mirogabalin), were initially developed as derivatives of Gamma-Aminobutyric acid (GABA), however, receptor-binding and electrophysiological techniques show that neither gabapentin nor pregabalin interact with $GABA_A$ or $GABA_B$ receptors, nor do they have noticeable effects on GABA levels[44–48]. These antiepileptic drugs are first-line treatments for neuropathic pain after SCI[49,50]. Pregabalin (PGB) is similar in structure to gabapentin (GBP) (Figure 3), and both selectively bind to α2δ-1 and α2δ-2 subunit of VGCCs, while lacking affinity for α2δ-3 or α2δ-4[44–46,51]. In particular, α2δ-1 and α2δ-2 subunits of the N-type calcium channels have been proposed as the main targets of gabapentinoids[52]. GBP and PGB, both interact with VGCCs however, they exhibit varied affinities for different α2δ calcium channel subunits. Specifically, GBP demonstrates a stronger binding affinity for the α2δ-1 subunit, while PGB displays greater specificity for α2δ-2[53]. Receptor autoradiography showed that PGB binds to different regions in CNS. These regions include the cortex, amygdala, hippocampus, cerebellum and spinal cord dorsal horn. Spinal cord white matter shows very little specific binding to PGB, whereas in the dorsal horn superficial layers (laminae I and II) highest level of receptor binding is observed[44]. PGB decreases calcium influx at nerve terminals, resulting in a subsequent reduction in the release of excitatory neurotransmitters such as CGRP, glutamate, SP and noradrenaline[54–56].

Studies conducted *in vivo* where pregabalin was chronically administered to rats with spinal nerve ligation, revealed a decrease in the heightened levels of pre-synaptic α2δ-1 in the dorsal horn. This indicates a potential inhibition of trafficking[34]. Consequently, gabapentinoids can impact the activity of other proteins which α2δ subunit interacts with. Long-term incubation of cultured cells with gabapentinoids, reduced calcium currents. This reduction was evident in transfected cells co-expressing α2δ-1 or α2δ-2 subunit of VGCCs, as well as in DRG neurons[57–59]. Additionally, there was a decrease in the expression of α1 subunits of Ca_V2 family of VGCCs on the cell surface[57,60]. These findings highlight the ability of gabapentinoids to modulate calcium currents and influence the

presence of VGCCs on the cell surface when applied for extended periods of time.

Figure 3. Pregabalin and Gabapentin structure. The structure of gabapentin and pregabalin compared to GABA (Gamma-Aminobutyric acid).

1.1.8 Microglia, neuropathic pain and gabapentinoids

It has been shown that activated microglia play a role in neuropathic pain after SCI[61–67]. Furthermore, research on peripheral nerve injury has shown that microglia can have a role in peripheral neuropathic pain. Peripheral nerve injury rapidly triggers colony stimulating factor 1 (CSF1) expression in damaged DRG neurons. CSF1 is transported to the presynaptic terminals in the spinal dorsal horn, where it interacts with the microglia CSF1 receptor, leading to proliferation[68–70]. Activated microglia, release various pro-inflammatory cytokines, which can impact spinal dorsal horn neuronal function through both direct and indirect mechanisms. Activation of microglia results in release of brain-derived neurotrophic factor (BDNF) in the spinal dorsal horn after peripheral nerve injury[71,72]. BDNF activates tyrosine kinase receptor B (TrkB), which in turn downregulates K^+/Cl^- cotransporter 2 (KCC2) and leads to a rise in intracellular Cl^- levels. The elevation of intracellular Cl^- enhances glutamatergic excitation through NMDA receptors by switching GABAergic inhibition to excitation. In the end, this change in equilibrium favoring synaptic excitation results in the firing of

action potentials in projection neurons from the spino-parabrachial lamina I, primarily associated with nociceptive output[73,74].

It has been shown that after peripheral nerve injury, repeated gabapentinoid administration can reduce spinal levels of Iba1 (Ionized calcium-binding adapter molecule 1; a microglia/macrophage marker)[75,76]. Similarly, after diabetic neuropathic pain gabapentinoids diminished spinal microglial activation[77]. Studies on the mitogen-activated protein kinase (MAPK) family, showed that gabapentinoids can diminish phospho-p38/p38 levels which are enhanced in spinal microglia after nerve injury[75]. Studies have shown that gabapentinoids can increase the expression of the spinal anti-inflammatory cytokine interleukin 10 (IL-10) and and β-endorphin in microglia, and consequently inhibit proinflammatory cytokines such as tumor necrosis factor α (TNF-α), IL-6, and IL-1β[78].

1.2. Hypothesis and Aims

1.2.1. Hypothesis

Research indicates that structural changes of nociceptors occur in the dorsal horn below the level of injury after SCI, correlating with neuropathic pain. Recognizing that these changes manifest early post-injury, I aimed to explore the feasibility of halting the initiation of structural changes that occur post-SCI, thereby preventing the onset of associated neuropathic pain. Despite pregabalin's common prescription for neuropathic pain in clinical settings, its administration typically follows the onset of pain. Consequently, I hypothesized that the effectiveness of prophylactic pregabalin treatment in SCI mice could prevent the initiation of pain. Additionally, analyzing structural changes after prophylactic pregabalin treatment offers insights into the primary neuronal population contributing to neuropathic pain, potentially paving the way for more effective treatments for patients.

1.2.2. Aims

I explored the effect of prophylactic treatment on these structural changes and neuropathic pain. Additionally, I delved into the durability of the effects of prophylactic pregabalin treatment. Furthermore, I explored the distinct contribution of nociceptors to the initiation of neuropathic pain by specifically knocking out the pregabalin target, VGCC α2δ-2 subunit, in nociceptors. My collective aims are listed below:

#1 Investigating the structural changes of nociceptors in below-injury level dorsal horn post-SCI through 3D imaging.

#2 Investigating the effect of prophylactic pregabalin treatment on neuropathic pain development post-SCI and nociceptive structural changes in below-injury level dorsal horn.

#3 Investigating the durability of prophylactic pregabalin treatment effects post-SCI.

#4 Investigating the specific role of VGCCs α2δ-2 subunit in neuropathic pain post-SCI through its specific nociceptor knockout.

Materials and Methods

2. Material and Methods

2.1. Materials

2.1.1. Animals

Table 3. List of animals

Short name	Full name	Description
C57BL/6J		Wildtype mice
SNS^{Cre}	C57BL/6-Tg(SCN10ACre)1Rkun/Uhg	Cre recombinase under the control of the nociceptor specific promoter SCN10a (encodes $Na_v1.8$)
$Rosa26^{LSL\text{-}tdTomato}$	B6.CgGt(ROSA)26Sor$^{tm14(CAG\text{-}tdTomato)Hze}$/J	Mice containing a loxP-flanked STOP cassette, which hinders the transcription of tdTomato driven by the strong and widespread CAG promoter
$SNS^{tdTomato}$	C57BL/6-Tg(SCN10ACre)1Rkun/Uhg X B6.CgGt(ROSA)26Sor$^{tm14(CAG\text{-}tdTomato)Hze}$/J	All $Na_v1.8^+$ nociceptors and their projections are labeled by tdTomato
$Cacna2d2^{fl/fl}$	C57BL/6N-Cacna2d2$^{tm1c(KOMP)Wtsi}$	Cacna2d2 (expressing α2δ-2 of VGCCs) is protected by floxed loxP

$SNS^{Cacna2d2}$	C57BL/6-Tg(SCN10ACre)1Rkun/Uhg X C57BL/6N-$Cacna2d2^{tm1c(KOMP)Wtsi}$	Cacna2d2 is knocked out in all $Na_v1.8^+$ nociceptors and their projections

2.1.2. Equipment and instruments

Table 4. Equipment for DNA preparation and genotyping

Equipment/Instrument	Usage	Manufacturer
ThermoMixer	Digestion of biopsies for DNA isolation	Eppendorf AG, Hamburg, Germany
T100 TM Thermal Cycler	PCR	Bio-Rad Laboratories Inc., Hercules, California, USA
UV Detector	Agarose gel image acquisition	PeqLab, VWR, Leuven, Belgium

Table 5. Equipment and instruments for surgery and tissue processing

Equipment/Instrument	Usage	Manufacturer
Braunol®	Disinfection	Braun Melsungen AG, Melsungen, Germany
Cryostat Blades	Cryo-sectioning	Fine Science Tools, Foster City, California, USA
Cryostat Hyrax C60	Cryo-sectioning	Microm GmbH, Walldorf, Germany

Disposable scalpel #11, #15	Opening the skin and dissection	FEATHER Safety Razor Co. Ltd, Osaka, Japan
Dumont #2, #5, #55 forceps	Surgeries and dissections	Fine Science Tools, Foster City, California, USA
Extra Fine Micro Dissecting Scissors	Dissections	Roboz surgical instrument Co., Inc., Maryland, USA
Infinite Horizon Impactor (IH-0400 Impactor)	Contusion	Precision Systems and Instrumentation, Lexington, Kentucky, USA
ISMATEC® REGLO Digital MS-4/8	Transcardial perfusion	IDEX Health & Science Oak Harbor, Washington, USA
McPherson-Westcott conjunctival scissors	Laminectomy	World precision instruments, Freiberg, Germany
Michel suture clips	Surgeries	Fine Science Tools, Foster City, USA
Remington Razor	Surgery preparation	Remington, Wisconsin, USA
Standard mouse impact tip (1.3 mm)	Contusion	Precision Systems and Instrumentation, Lexington, Kentucky, USA
Steri250 surgical tool sterilizer	Tool Sterilization	Simon Keller AG, Switzerland
Stereomicroscope Stemi 2000-C	Surgeries and dissections	Carl Zeiss Microscopy GmbH, Jena, Germany

Stryker Gaymar TP700 TPump	Temperature regulation	VWR, Leuven, Belgium
Surgical Microscope	Contusion	Olympus Deutschland GmbH, Hamburg, Germany
Terylene (4/0, HR-12)	Surgeries	SERAG-WIESSNER GmbH & Co.K
96 well plates (U shape bottom)	Tissue storing and staining	Thermo Fisher Scientific, Invitrogen, Waltham, Massachusetts, USA

Table 6. Equipment and instruments for behavioral testing

Equipment/Instrument	**Usage**	**Manufacturer**
Hargreaves Apparatus	Thermal sensitivity test	Ugo Basile Srl, Gemonio, VA, Italy
Modular Animal Enclosure	Mechanical/thermal sensitivity tests	Ugo Basile Srl, Gemonio, Varese, Italy
Open Field (round)	Motor recovery tets	Custom-made
Perforated metal platform	Mechanical/thermal sensitivity tests	Ugo Basile Srl, Gemonio, Varese, Italy
Place Escape/Avoidance paradigm chamber	Place Escape/Avoidance paradigm test	Custom-made
Stimulation base (large platform and supporting columns)	Mechanical/thermal sensitivity tests	Ugo Basile Srl, Gemonio, Varese, Italy
Touch Test® Sensory Evaluators	Mechanical sensitivity test	North Coast Medical Inc, Gilroy, California, USA

Table 7. Equipment and instruments for microscopic imaging

Equipment/Instrument	Usage	Manufacturer
ORCA spark Digital CMOS camera (C11440-36U)	Image Acquisition	Hamamamatsu, Shizuoka, Japan
Fluoview FV1000 confocal laser scanning microscope	Image Acquisition	Olympus Deutschland GmbH, Hamburg, Germany
System Microscope BX53	Image Acquisition	Olympus Deutschland GmbH, Hamburg, Germany
Wacom Cintiq 16	Illustrations	Wacom, Kazo, Japan

Table 8. Software

Software	Usage	Company
Adobe Illustrator 2023 (27.1)	Illustrations	Adobe Systems Inc., San Jose, California, USA
Adobe Photoshop 2020 (21.2.1)	Illustrations	Adobe Systems Inc., San Jose, California, USA
cellSens (Olympus cellSens Standard 3.2)	Imaging software for bright-field microscope	Olympus Deutschland GmbH, Hamburg, Germany
FV10-ASW (Olympus Fluoview Ver.4.2c)	Imaging software for fluorescence microscope	Olympus Deutschland GmbH, Hamburg, Germany
ImageJ	Image processing and Evaluation	NIH
Prism 9	Data analysis and representation	GraphPad Software Inc., La Jolla, California, USA

2.1.3. Chemicals

Table 9. List of chemicals and kits

Chemicals/solutions/Kits	Usage	Company
5 Prime Master Mix	Genotyping/PCR	5 PRIME GmbH, Hamburg, Germany
Agarose Ultrapure	Gel preparation	Thermo Fisher Scientific, Invitrogen, Waltham, Massachusetts, USA
Ammonium iron (III) sulfate dodecahydrate ($NH_4Fe(SO_4)_2$)	EC Staining	Carl Roth GmbH & Co. KG, Karlsruhe, Germany
Ampicillin (Ampicillin-ratiopharm® 5.0 g)	Post-surgery treatment	Ratiopharm GmbH, Ulm, Germany
Atipamezol 5 mg/ml	Antagonize for anesthesia	Prodivet pharmaceuticals, Belgium
Buprenorphin HCl (Temgesic®)	Post-surgery treatment	Reckitt Benckiser, Slough, UK
Citric acid (anhydrous)	Antigen retrieval	Carl Roth GmbH & Co. KG, Karlsruhe, Germany
CUBIC-L	Tissue clearing	TCI Chemicals, Tokyo, Japan
CUBIC-R^+	Tissue clearing	TCI Chemicals, Tokyo, Japan

D(+)-Saccharose (sucrose)	Tissue preparation	Carl Roth GmbH & Co. KG, Karlsruhe, Germany
Destilled water (ultra-pure type 1 water)	Solution preparation	ELGA LabWater, UK
Dimethylsulfoxid (DMSO)	Solution preparation	Merck KGaA, Darmstadt, Germany
Disodium hydrogen phosphate (Na_2HPO_4)	Solution preparation	Carl Roth GmbH & Co. KG, Karlsruhe, Germany
Disodium tetraborate decahydrate ($Na_2[B_4O_5(OH)_4]x8H_2O$; Borax)	EC staining	Carl Roth GmbH & Co. KG, Karlsruhe, Germany
DNA Ladder (100 bp)	DNA electrophoresis	New England Biolabs Inc., Ipswich, Massachusetts, USA
DNeasy Blood & Tissue Kit	DNA preparation	Qiagen GmbH, Hilden, Germany
Eriochrome cyanine R (EC)	EC staining	Merck KGaA, Darmstadt, Germany
Ethanol denatured	EC staining	Carl Roth GmbH & Co. KG, Karlsruhe, Germany
Ethylenediaminetetraacetic acid (EDTA)	Genotyping	Carl Roth GmbH & Co. KG, Karlsruhe, Germany

Ethylene glycol	Cryopreservation	NeoLab Migge GmbH, Heidelberg, Germany
Fentanyl 0.05 mg/ml	Anesthesia	Janssen-Cilag, Neuss, Germany
Flumazenil 0.1 mg/ml	Antagonize for anesthesia	Fresenius, Bad Homburg, Germany
Fluoromount-G®	Imaging	Southern Biotechnology Associates, Birmingham, Alabama, USA
Gel Loading Dye, Blue (6x)	DNA electrophoresis	New England Biolabs Inc., Ipswich, Massachusetts, USA
Heparin	Tissue clearing and staining	Merck KGaA, Darmstadt, Germany
Ketamine 10%	Killing mix	Bremer Pharma GmbH, Warburg, Germany
Liquid blocker-PAP PEN Immunostaining pen-5 mm	Immunohistochemistry	Kisker Biotech GmbH & Co., Steinfurt, Germany
Medetomidine 1 mg/ml	Anesthesia	Alvetra, Neumünster, German

Methylphenyl silicone oil (HIVAC F-4)	Imaging	Shin-Etsu Co. Ltd., Ohio, USA
Midazolam 5 mg/ml	Anesthesia	Hameln pharma plus, Hameln, Germany
Mineral oil (M8410)	Imaging	Merck KGaA, Darmstadt, Germany,
Neo-clear®	Imaging	Merck KGaA, Darmstadt, Germany
Neo-Mount®	Imaging	Merck KGaA, Darmstadt, Germany
Paraformaldehyde (PFA)	Tissue fixation	Carl Roth GmbH & Co. KG, Karlsruhe, Germany
PeqGreen DNA/RNA dye	DNA electrophoresis	VWR, Leuven, Belgium
Phosphate-Buffered Saline (10X) (PBS) pH 7.4	Solution preparations	Merck KGaA, Darmstadt, Germany
Pregabalin (M3599)	Analgesia	Abmole Bioscience Inc., Houston, Texas, USA
Potassium hexacyanoferrate(III) ($C_6N_6FeK_3$)	EC staining	neoLab Migge Laborbedarf-Vertriebs GmbH, Heidelberg, Germany

Ringer's solution	Post-surgery treatment	Braun Melsungen AG, Melsungen, Germany
Sterile Saline Solution (0.9%)	Dilution of drugs	Braun Melsungen AG, Melsungen, Germany
Steriled filtered donkey serum	Immunostaining	Equitech-Bio Inc., Kerrville, Texas, USA
Sodium Chloride (NaCl)	Solution preparations	VWR, Leuven, Belgium
Sodium dihydrogen phosphate (NaH_2PO_4)	Solution preparations	Carl Roth GmbH & Co. KG, Karlsruhe, Germany
Sodium hydroxide solution 40 % (10 M, NaOH)	Solution preparations	Carl Roth GmbH & Co. KG, Karlsruhe, Germany
Sulfuric acid (H_2SO_4)	EC staining	neoLab Migge Laborbedarf-vertriebs GmbH, Heidelberg, Germany
Tissue Tek® OCT™ compound	Cryosectioning	Sakura Finetek Germany GmbH, Staufen, Germany
Triton X-100	Solution preparations	neoLab Migge Laborbedarf-Vertriebs GmbH, Heidelberg, Germany

Tween-20	Solution preparations	neoLab Migge GmbH, Heidelberg, Germany
Xylazine 20 mg (XYLARIEM ®)	Killing mix	Ecuphar N.V., Oostkamp, Belgium

2.1.4. Antibodies

Table 10. List of Antibodies

Antibody	Host	Type	Dilution	Company	Catalog number
5HT	Rabbit	Polyclonal	1:1000 (IHC)	Immunostar, Hudson, Wisconsin, USA	20080
Cacna2d2 ($Ca_v\alpha2\delta2$) extracellular	Rabbit	IgG Polyclonal	1:200 (IHC)	Alomone labs, Jerusalem, Israel	ACC-102
c-fos	Rat	Monoclonal	1:600 (IHC)	Synaptic systems, Göttingen, Germany	26017
CGRP	Rabbit	IgG polyclonal	1:600 (IHC)	Immunostar, Hudson, Wisconsin, USA	24112

CREB	Mouse	Unconjugated IgG Monoclonal	1:200 (IHC)	Abcam plc, Cambridge, UK	ab178322
Iba1	Rabbit	Polyclonal	1:600 (IHC)	Wako, Osaka, Japan	019-19741
KCC2	Rabbit	Polyclonal	1:750 (IHC)	ThermoFischer, Massachusetts, USA	PA5-78544
NeuN	Guinea pig	Unpurified serum IgG polyclonal	1:2000 (IHC), 1:200 (clearing)	Millipore, Merck KGaA, Darmstadt, Germany	ABN90
Phospho-CaMK2 (Thr287)	Rabbit	Unconjugated IgG polyclonal	1:200 (IHC)	ThermoFischer, Massachusetts, USA	bs-1647R
Phospho-CREB(Ser133)	Rabbit	Affinity Purified polyclonal	1:200 (IHC)	Millipore, Merck KGaA, Darmstadt, Germany	06-519
PKCγ	Guinea pig	Polyclonal	1:600 (IHC)	Frontier Institute co., ltd., Hokkaido, Japan	AB_2571826
TrkA	Goat	IgG Polyclonal	1:200 (IHC)	R&D systems, Minneapolis, Minnesota, USA	AF1056
Alexa Fluor® 488 anti-rabbit	Donkey	IgG (H+L)	1:600 (IHC)	ThermoFischer, Massachusetts, USA	A21206

Alexa Fluor® 594 anti-rabbit	Donkey	IgG (H+L)	1:600 (IHC)	ThermoFischer, Massachusetts, USA	A21207
Alexa Fluor® 594 anti-rat	Donkey	IgG (H+L)	1:600 (IHC)	ThermoFischer, Massachusetts, USA	A21209
Alexa Fluor® 594 anti-guinea pig	Donkey	IgG (H+L)	1:600 (IHC)	Jackson Immunoresearch Laboratories, Pennsylvania, USA	706-585-148
Alexa Fluor® 594 anti-goat	Donkey	IgG (H+L)	1:600 (IHC)	ThermoFischer, Massachusetts, USA	A11055
Cy5 anti-guinea pig	Donkey	IgG (H+L)	1:600 (IHC)	Jackson Immunoresearch Laboratories, Pennsylvania, USA	706-175-148
Cy5 anti-mouse	Donkey	IgG (H+L)	1:600 (IHC)	Jackson Immunoresearch Laboratories, Pennsylvania, USA	715-175-151
Red fluorescent Protein (RFP)	Rabbit		1:400 (clearing)	Clontech Laboratories GmbH, Heidelberg, Germany	8370-2

Alexa Fluor® 594 anti-rabbit	Donkey	IgG (H+L)	1:400 (clearing)	ThermoFischer, Massachusetts, USA	A21207
Alexa Fluor® 488 anti-guinea pig	Donkey	IgG (H+L)	1:400 (clearing)	Jackson Immunoresearch Laboratories, Pennsylvania, USA	706-545-148

2.1.5. Buffer and solutions

Table 11. Buffer and solutions

Buffer/Solution	Reagent	Add
Animal Perfusion		
0.2 M Sodium Phosphate Monobasic solution	NaH_2PO_4 ddH_2O	27.6 g fill up to 1 L
0.2 M Sodium Phosphate dibasic solution	Na_2HPO_4 ddH_2O	28.6 g fill up to 1 L
Phosphate Buffer (0.2 M)	Sodium Phosphate Monobasic solution Sodium Phosphate dibasic solution	230 ml 770 ml
Perfusion Saline (0.9 %)	NaCl 0.2 M Phosphate Buffer ddH_2O	9.0 g 0.5 L 0.5 L

PFA solution (4% w/v)	paraformaldehyde 10 M NaOH 0.2 M Phosphate Buffer ddH_2O	40.0 g 4 drops 0.5 L 0.5 L • Heat ddH2O to 65°C • Add 40.0 g PFA • Dissolve by continuous stirring • Add 10 M NaOH • Wait until fully dissolved • Filter solution • Add phosphate buffer
30% (w/v) Sucrose	D(+)-sucrose 0.2 M Phosphate Buffer ddH_2O	300 g 350 mL 350 mL
Immunofluorescence and Histology		
Borax Ferricyanide Solution	Sodium tetraborate dechydrate ($Na_2B_4O_7$**.**$10H_2O$, Borax) Potassium Ferricyanide $K_3Fe(CN)_6$ ddH_2O	2 g 2.5 g 200 ml • Stir until dissolved • Protect solution from light (Reusable, filter if needed)
Ferric Ammonium Sulfate Solution [10%]	Ammonium iron(III) sulfate dodecahydrate	10 g

	($NH_4Fe(SO_4)_2.12H_2O$) ddH_2O	 100 ml • Stir until dissolved (protect from light)
Ferric Ammonium Sulfate Solution [5%]	Ammonium iron (III) sulfate dodecahydrate ($NH_4Fe(SO_4)_2.12H_2O$) ddH_2O	5 g 200 ml • Stir until dissolved (protect from light, do not reuse)
Eriochrome Cyanine solution	Eriochrome Cyanine R Concentrated H_2SO_4 10% Ferric Ammonium Sulfate Solution ddH_2O	0.4 g 1.0 ml 8 ml 192 ml • Stir until dye fully dissolves • Add 10 % Ferric Ammonium Sulfate Solution and mix • Filter solution (protect from light, reusable, filter if needed)
Tris buffered saline (TBS)	Tris-HCl Tris NaCl ddH_2O	13.22 g 1.94 g 9.0 g fill up to 1 L; adjust pH to 7.4
Blocking buffer for IHC (mounted slides)	TBS Triton X-100	9.475 ml

	Donkey serum	0.025 ml [0.25 % v/v] 0.5 ml [5% v/v]
Staining buffer for IHC (mounted slides, primary antibody)	TBS Triton X-100 Donkey serum	9.875 ml 0.025 ml [0.25 % v/v] 0.1 ml [1% v/v]
Staining buffer for IHC (mounted slides, secondary antibody)	TBS Donkey serum	9.9 ml 0.1 ml [1% v/v]
Citrate buffer (10 mM) for antigen retrieval	Citric acid ddH_2O Tween-20	1.92 g 800 ml Adjust pH to 6.0 and fill up to 1 L with ddH_2O Add 0.5 ml of Tween-20 and mix
Blocking buffer for IHC (free floating)	Donkey serum Triton X-100 PBS	0.5 ml [5% v/v] 0.02 ml [0.2% v/v] 9.48 ml
Staining buffer for IHC (free floating, primary antibody)	Donkey serum Triton X-100 PBS	0.5 ml [5% v/v] 0.02 ml [0.2% v/v] 9.48 ml
Staining buffer for IHC (free floating, secondary antibody)	Donkey serum PBS	0.5 ml [5% v/v] 9.5 ml
Clearing and staining		
PTwH	10X PBS 2ml Tween-20 1ml Heparin stock 10mg/ml	100 ml 2 ml 1 ml Fill up to 1 L

	ddH_2O	
PTx.2	10X PBS	100 ml
	TritonX-100	2 ml
	ddH_2O	Fill up to 1 L
Blocking solution	PTx.2	42 ml
	Donkey serum	3 ml
	DMSO	5 ml
Staining buffer for primary antibody	DMSO	0.5 ml
	Donkey Serum	0.3 ml
	PTwH	9.2 ml
Staining buffer for secondary antibody	Donkey Serum	0.3 ml
	PTwH	9.7 ml
Cryopreservation solution		
Cryopreservation solution for storing free floating sections	$NaH_2PO_4.2H_2O$ (Sodium dihydrogen phosphate dihydrate)	1.2 g
	Na_2HPO_4 (Sodium phosphate dibasic)	4.53 g
	Sucrose	150 g
	Ethylene glycol	150 ml
	ddH_2O	Fill up to 500 ml
Genptyping		
Tris acetate EDTA (TAE, 10X)	tris base	48.5 g
	glacial acetic acid	11.4 mL
	0.5 M EDTA solution (pH 8.0)	20 mL
	ddH_2O	Fill up to 1 L

2.1.6. Primers

Table 12. List of primers for genotyping

Primer	Neucleotide sequence (5`– 3`)
Cacna2d2-CSD-5'-F	CACTCAGAACTGAAAGCAGACCA
Cacna2d2-CSD-ttR	GTGATCCACGGGGACAGAAG
CSD-en2-R	CCAACTGACCTTGGGCAAGAACAT
SNS5 arm outer	ACA GAC ATA CTC ATA ATA TTT CTG TGA TT
SNS3 arm outer	GCT GAG TGC AGA CAT TCT TAC CC
Cre E	GCG CGC CTG AAG ATA TAG AAG A
mtmG #1	CTC TGC TGC CTC CTG GCT TCT
mtmG #2	CGA GGC GGA TCA CAA GCA ATA
mtmG #3	TCA ATG GGC GGG GGT CGT T

2.1. Methods

2.2.1 Animal guidelines and housing conditions

All experiments were carried out following the regulations stipulated in the European Communities Council Directive (EU and institutional guidelines) and received approval from the local governing body (Regierungspräsidium Karlsruhe). Adult female and male C57BL/6J mice (8-12 weeks old; wildtype JANVIER LABS) with various genotypes were used for the experiments. Apart from the mice, the facility was also monitored daily to ensure optimal conditions regarding temperature (22°C ± 1°C) and humidity (45-65%). In each cage 3-4 littermates were housed together on a 12/12-hour light/dark cycle and provided with ad libitum access to food and water. The mice weighed between 20-30 g at the time of surgery. To maintain consistency in behavioral testing, I personally handled the animals in each experiment. To prevent potential conflicts,

particularly among the male mice, all male mice were housed together with their littermates for the entire duration of the experiments. This approach ensured that no new mice were introduced, minimizing the likelihood of dominance-related fights. Additionally, in experiments involving both sham and SCI male mice, the sham males were grouped together and housed in a separate cage, while the SCI males were housed together in another cage. Similarly, for the pregabalin studies, special precautions were taken due to the potential drowsiness in PGB-treated mice and higher alertness and activity in vehicle-treated mice. To mitigate the risk of dominance-related conflicts, the PGB-treated and vehicle-treated male mice were housed separately in distinct cages. The treatment labels were removed from the cages prior to behavioral testing, and the mice were then randomly placed in the testing area by another experimenter without any predetermined order. Therefore, the experimenter conducting the behavioral test was blinded to each mouse identity.

2.2.2 Spinal Cord Injury

Contusion injuries are considered fitting traumatic SCI models from a clinical perspective. The Infinite Horizon Impact Device (IH-0400 Impactor; Precision Systems & Instrumentation, Lexington, KY, USA) was adjusted for the mouse spinal cord (mouse steel-tipped impactor with a 1.3 mm diameter) and used for all contusion surgeries[79–81]. Using an impactor device offers the advantage of causing well defined contusions with specific force which is also reproducible. Before the surgery, the mice were deeply anesthetized through intraperitoneal (i.p.) injection of a sleeping mix Fentanyl (0.01 mg/kg), Medetomidine (0.3 mg/kg) and Midazolam (4 mg/kg). Under a surgical microscope, the vertebral column was exposed, and the target region was identified. For all mice, a T9 laminectomy was performed, which exposes the T11 spinal level. To prevent dehydration during the surgical procedure, the animals were given 100 µl of lactated Ringer's solution (s.c.) in the middle of surgery. In SCI mice, extra fine forceps were used to stabilize the spinal column by gripping the spinal processes of the adjacent vertebrae (T8 and T10). The tip was

positioned 4-5 mm above the exposed spinal cord, and a moderate contusion with the force of 50 kDyn was induced[79–81]. Afterwards the muscles were sutured using 4/0 terylene, and the skin incision was closed with suture clips. General anesthesia was antagonized with i.p. doses of Buprenorphine (0.04 mg/kg) and s.c. Flumazenil (0.5 mg/kg) and Atipamezole (2.5 mg/kg) without additional analgesic treatment.

Following surgery, the mice were closely monitored, and their bladders were emptied manually at least twice per day. Antibiotics (100 µl ampicillin s.c., 33 mg/kg, twice per day) were administered for approximately 10-14 days following the surgery. This antibiotic treatment aimed to prevent bladder infections until the mice regained their reflexive bladder function. To manage post-operative pain, analgesics (0.04 mg/kg buprenorphine-HCL, 100 µl s.c., Temgesic) were administered to both injured and sham-operated mice twice daily during the first two days after surgery. In the PGB-treated animals, buprenorphine injections were substituted with PGB injections. The surgical clips were removed around one week after the injury from conscious mice.

2.2.3 Behavioral Testing

Before the behavioral testing, the mice were familiarized with each test set-up for at least 1 hour/day for 2 days. On the testing days, the mice were additionally habituated to each set-up for 30 minutes. All behavioral assessments were conducted in conscious and unrestrained mice, while I was blinded to the group's identity.

2.2.3.1 Motor recovery: Basso Mouse Scale (BMS)

Motor functional recovery was evaluated using the Basso Mouse Scale (BMS) for locomotion[82]. Each mouse was placed in an open field and observed by two investigators, who were blinded to group identity. The BMS is a 9-point scoring system tailored and approved for assessing spinal cord injuries in mice.

The assessment includes various parameters related to motor function, including extent of ankle movement, weight support, plantar or dorsal placement of the paws, stepping, paw rotations, coordination, stability of the trunk, and the positioning of the tail. A score of 9 indicates normal movement in an uninjured mouse and a score of 0 indicates complete hindlimb paralysis with no ankle movement. Scores between 0 and 3 represent changes in ankle movement and plantar placement of the hindpaw, scores between 4 and 6 indicate stepping and coordination and scores between 7 and 9 reflect stability of the trunk and tail positioning. Weekly assessments were initiated 7 days post-injury. Each hindpaw was individually scored, and the scores were averaged to obtain a single score per testing day for each animal.

2.2.3.2 Mechanical Sensitivity Testing: von Frey hair filaments

To assess changes in mechanical sensitivity, von Frey hair filaments (Nylon monofilaments) were utilized. These filaments were selected in ascending diameter and force (0.16 g, 0.4 g, 0.6 g, 1.4 g)[79–81], and applied to the hindpaws of the mice. The mice were situated within plexiglass enclosures (10 cm length x 10 cm width x 14 cm height), which were placed on an elevated grid floor (90 cm x 39 cm) that served as the testing surface. von Frey hair filaments were applied to the plantar surface of the hindpaws in an ascending order, starting with the smallest filament (0.16 g). Each hindpaw was stimulated five times (total of 10 stimuli per filament for each mouse). To avoid stimulus-induced sensitization of the paw, there was an interval of 3-5 minutes before the stimulus was re-applied to the same animal. Paw withdrawal frequency (number of positive responses for both hindpaws divided by the total number of stimulations by each filament) defined mechanical sensitivity. Mechanical sensitivity was conducted on two consecutive days before the surgical procedure, to establish the baseline sensitivity. The mean value per animal and filament was considered the pre-injury baseline value. Following surgery, the mechanical sensitivity was assessed weekly.

Following SCI, prior to sensory testing, the BMS[82] was employed to confirm adequate recovery. A BMS score of ≥ 3, indicating weight support, was considered necessary for proceeding with sensory assessments.

2.2.3.3 Supraspinal pain processing: Place Escape/Avoidance Paradigm (PEAP)

To assess the aversiveness and emotional aspect of innocuous mechanical stimulation in animals, the place escape/avoidance paradigm (PEAP) was utilized[83,84]. This test was conducted as the last behavioral test in the last week of survival. The testing setup involved placing the animals in a two-compartment arena (each 10 cm length x 10 cm width x 14 cm height). The arena was divided into a closed compartment and an open compartment connected by a 3.5 cm opening in the dividing wall. The arena was placed on an elevated grid floor. The enclosed compartment's roof and walls were covered in black adhesive foil, while the walls of the open compartment were lined with white adhesive foil.

Throughout the 25-minute examination, the initial 10-minute period functioned as an unstimulated reference baseline. Subsequently, after the 10 minutes, the hindpaws (altering between left and right) were stimulated every 15 seconds for the remaining 15 minutes if located in the dark compartment. An innocuous (0.16 g) von Frey filament was chosen for hindpaw stimulation since it only causes a more consistent response in SCI mice with mechanical allodynia.

2.2.3.4 Thermal sensitivity testing: Hargreaves' method

The Hargreaves' method (Hargreaves Apparatus, Ugo Basile) was used to evaluate thermal sensitivity of the hindpaws. Mice were placed in plexiglass chambers positioned on a glass floor (Ugo Basile) of a metal platform (90 cm x 39 cm). A movable infrared laser beam was directed to the plantar surface of the hindpaws, and the time passed until the paw was withdrawn was logged as the response latency to heat stimulus. The laser and timer both deactivated automatically the moment the mouse withdrew its paw (accuracy = 0.1

seconds)[85]. The laser intensity was modified to attain a latency of roughly 8-9 seconds in uninjured mice (190 ± 1 mW/cm^2). A 15-second cut-off time was implemented to prevent tissue damage, and a minimum interval of 3-5 minutes was maintained between consecutive trials for the same paw and mouse. Thermal sensitivity was expressed as the mean response latency of eight trials (4 left + 4 right hindpaw trial/mouse) in each animal. Thermal sensitivity assessment always followed the mechanical sensitivity test. The baseline thermal sensitivity was determined by calculating the average latency across two consecutive days of testing prior to the surgery[81]. Following surgery, the thermal sensitivity was assessed weekly.

2.2.3.5 Hindpaw stimulation

In some of the experiments, 1 hour before perfusion, the hindpaws were subjected to repeated stimulation using a non-noxious von Frey hair filament (0.16 g) every 30 s over a period of 20 minutes. This stimulation resulted in the activation of neurons in the spinal cord in response to mechanical allodynia.

2.2.4 Transgenic animal breeding

For transgenic mouse breeding, around three females were paired with a single male at the same time, by introducing him into their cage. After 2 weeks, the males and females were separated and put into individual cages. Males used for the breeding were within an age range of 10-50 weeks, while females were between 11-40 weeks. To mitigate the risk of excessive inbreeding, each line was crossbred with non-sibling wildtype animals, ensuring the maintenance of the line while minimizing the detrimental impacts of inbreeding. Pups were separated from their mother and weaned after 28 days.

2.2.4.1 SNS^{tdTomato} mice

SNS^{tdTomato} (SNS^{Cre}::Rosa26$^{LSL\text{-}tdTomato}$) mice were created by crossing C57BL/6-Tg(SCN10A-Cre)1Rkun/Uhg (SNS^{Cre}) mice with B6.Cg-Gt(ROSA)26Sor$^{tm14(CAG\text{-}tdTomato)Hze}$/J (Rosa26$^{LSL\text{-}tdTomato}$) reporter mice (Figure 4). Rosa26$^{LSL\text{-}tdTomato}$ mice carry a targeted mutation of the Gt(ROSA)26Sor locus with a loxP-flanked STOP cassette, hindering transcription of tdTomato under the widespread CAG promoter[86]. Rosa26 promoter is expressed in various tissues, and tdTomato can be expressed when the STOP cassette is removed in tissues expressing Cre recombinase.

In SNS^{Cre} mice, Cre recombinase is expressed under the control of the SCN10a promoter (expresses voltage-gated sodium channel $Na_v1.8$). Recombination is observable in all nociceptors of the DRG and trigeminal ganglia, and SNS^{Cre} mice facilitate reporter expression in all primary nociceptors[87]. Therefore, in SNS^{tdTomato} mice nociceptors (C-and Aδ-fiber, and potentially C-LTMRs) can be observed with tdTomato red fluorescence. Rosa26LSL-tdTomato and SNS^{Cre} mice were used in collaboration with Prof. Dr. Rohini Kuner, Institute for Pharmacology, University of Heidelberg. All SNS^{tdTomato} mice used have been heterozygous.

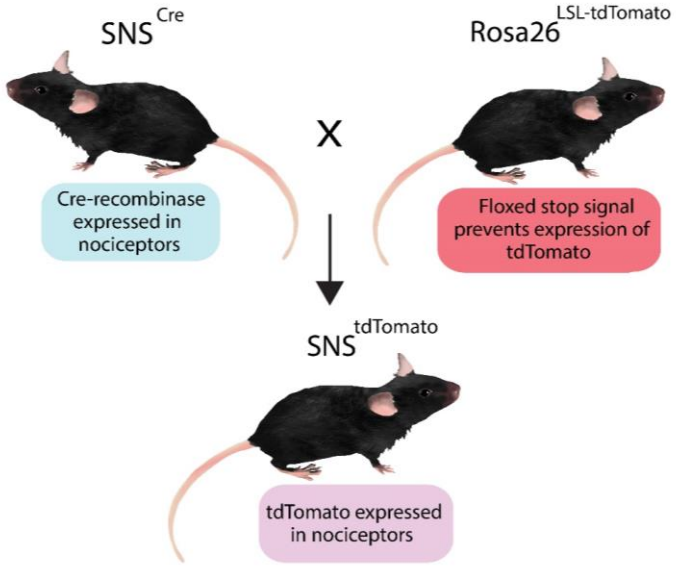

Figure 4: SNS^{tdTomato} mice. Crossing Rosa26$^{LSL\text{-}tdTomato}$ with SNS^{Cre} mice causes the floxed STOP signal (loxP-STOP-loxP) to be exclusively eliminated in Cre-expressing cells (nociceptive fibers) leading to expression of tdTomato.

2.2.4.2 SNS^{Cacna2d2} mice

SNS^{Cacna2d2} mice (Figure 5) were created by crossing SNS^{Cre} (C57BL/6-Tg(SCN10A-Cre)1Rkun/Uhg) mice with Cacna2d2$^{tm1c(KOMP)Wtsi}$ (Cacna2d2$^{fl/fl}$) which is a genetic mouse model developed by the Knockout Mouse Project (KOMP) at the Wellcome Trust Sanger Institute (WTSI). In the Cacna2d2$^{fl/fl}$ mice the Cacna2d2 gene (responsible for expression of α2δ-2 subunit of VGCCs) is protected by a floxed loxP and can be knocked out when Cre is expressed. There in SNS^{Cacna2d2} mice, α2δ-2 subunit of VGCCs is specifically knocked out in nociceptors ($Na_v1.8^+$ neurons, C-and Aδ-fiber, and potentially C-LTMRs). Cacna2d2$^{fl/fl}$ mice were used in collaboration with Prof. Dr. Frank Bradke, German Center for Neurodegenerative Diseases (DZNE), Bonn.

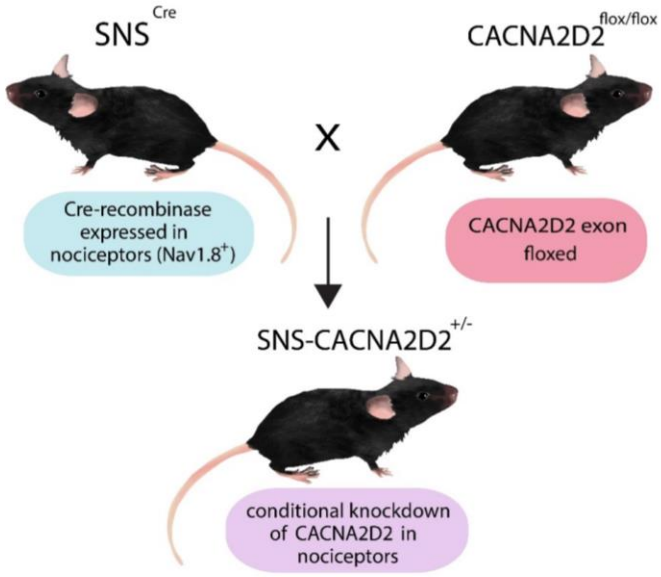

Figure 5: SNS^{CACNA2D2} mice. By crossing Cacna2d2$^{flox/flox}$ with SNS^{Cre} mice the floxed CACNA2D2 exon is only removed in Cre-expressing cells (nociceptive fibers) resulting in partial knock out of CACNA2D2 in nociceptors.

2.2.5 Genotyping

2.2.5.1 DNA isolation

Ear biopsies were taken from the transgenic mice at approximately 4-5 weeks of age. The biopsies were processed using DNeasy Blood & Tissue Kit (Qiagen). The tissue was digested by adding 20 µl of Proteinase K (600 mAU/ml solution) and overnight incubation at 56 °C in a water bath. Next, following the manufacturer's guidelines DNA precipitation steps were completed.

2.2.5.2 Genotyping PCR

5 Prime Master Mix (5 PRIME GmbH) was used for the PCR reactions. 2 µL DNA (~20-100 ng) from each mouse was used for the PCR. Eurofins Genomics synthesized all primers (lyophilized), which were then reconstituted in DNase/RNase-free ddH_2O to achieve a stock concentration of 100 µM, and subsequently stored at -20 °C. All primers necessary for a single reaction were pooled into a solution at a concentration of 25 µM per primer. 8 µl of prepared PCR master mix (details in Table 13) was added to each DNA sample (final volume = 10 µl).

Table 13. PCR Master mix for genotyping

Component	1x Reaction (10 µL total volume)
5 Prime Master Mix [2.5 x]	4 µl
Primer Mix [25 µM]	0.3 µl
DNase and RNase-free ddH_2O	3.7 µl
DNA	2 µl

A 2.0% w/v agarose gel was prepared (3 g of agarose powder (Thermo Fisher Scientific) + 150 ml of 1x TAE buffer). The agarose solution was boiled in

a microwave until fully dissolved (150 ml for one gel). After cooling down, 4.5 µL of PeqGreen (VWR) was added to the agarose, and the mixture was poured into a gel chamber with combs already inserted. Once solidified, each sample was mixed with 2 µl loading dye (New England Biolabs) and loaded into the gel pockets (12 µl per well). 3 µl of a 100 bp DNA ladder (New England Biolabs) was loaded into the first gel pocket. The gel was run for approximately 60 minutes at a constant voltage of 110 V to separate the PCR products. Images of the gels were captured using a PeqLab UV detector (VWR).

2.2.5.3 Primer and Cycling Protocols

Table 14. PCR protocol for genotyping Rosa26$^{LSL\text{-}tdTomato}$ mice

Primer	Cycle	Repeat	Step	Time	Temp [°C]
mtmG #1	1	1	1	2 min	95
mtmG #2	2	35	1	30 sec	95
mtmG #3			2	45 sec	61
			3	40 sec	72
	3	1	1	7 min	72
	4	1	1	∞	12
Expected results	wildtype: 330 bp transgenic homozygous: 250 bp heterozygous: 250 + 330 bp				

Table 15. PCR protocol for genotyping SNS^{Cre} mice

Primer	Cycle	Repeat	Step	Time	Temp [°C]
SNS5 arm outer	1	1	1	5 min	95
SNS3 arm outer	2	32	1	45 sec	95
Cre E			2	45 sec	55
			3	1 min	72

	3	1	1	5 min	72
	4	1	1	∞	12
Expected results	wildtype: 650 bp transgenic: 600 bp				

Table 16. PCR protocol for genotyping Cacna2d2$^{fl/fl}$ mice

Primer	Cycle	Repeat	Step	Time	Temp [°C]
Cacna2d2-CSD-5'-F	1	1	1	2 min	95
Cacna2d2-CSD-ttR	2	30	1	20 sec	95
CSD-en2-R			2	20 sec	58
			3	30 sec	72
	3	1	1	5 min	72
	4	1	1	∞	12
Expected results	wildtype: 233 bp transgenic homozygous: 424 bp heterozygous: 233 + 424 bp				

2.2.6 Tissue processing

At the end of the experiments, animals were put to sleep with an anesthesia cocktail overdose consisting of ketamine (31.25 mg/kg), xylazine (1.58 mg/kg), and acepromazine (0.31 mg/kg), and underwent transcardial perfusion with cold perfusion saline (0.9%) for 5 minutes followed by cold 4% paraformaldehyde (PFA) for 5 minutes (details in Table 11). The fur and organs were removed, and the rest was post-fixed at room temperature in 4% PFA for 1 hour. After briefly washing with ddH_2O to remove the residual PFA, the tissue was washed for 5 minutes in 0.1 M phosphate buffer. The lesion site (T11 spinal cord), L4-L6 spinal cord and L4-L6 DRGs, were identified[88] and dissected. The tissue was stored in PBS at 4°C and transferred to a solution of 30% sucrose

(details in Table 11) few days before sectioning. For sectioning, the tissue was immersed in Tissue-Tek® O.C.T compound (Sakura Finetek, Germany). The spinal cord sections were cut at either 16 or 25 µm thickness (coronal), while the DRG sections were cut at 10 µm thickness. The sections were either mounted on slides (Microscope Slides Superfrost® Plus; Thermo Fisher) in 7 or 14 series, or kept in 96-well plates filled with cryopreservation solution (see table 11 for details) as free-floating sections and stored in -20°C.

2.2.7 Eriochrome Cyanine staining

To analyze the lesion length and white matter sparing, multiple slides including the lesion epicenter, beginning and end of the lesion (25 µm sections, T11 spinal cord) were stained with eriochrome-cyanine (EC) to visualize myelin and the extent of degenerated myelinated axons. The slides were put in 37°C incubator for 3 hours and then placed for 5 minutes in fresh acetone. The slides were then dried for 20 minutes at room temperature by placing in open air. The sections were then stained at room temperature for 30 minutes with the EC solution (details in Table 11), followed by 5 minutes of rinsing with distilled water (ddH_2O). The sections were differentiated for 10-20 minutes in a 5% aqueous ferric ammonium solution (details in Table 11) until the gray matter became visible. After a 10-minute rinse in ddH_2O, the differentiation was completed after 10 minutes incubation in borax-ferricyanide solution (details in Table 11). Following an additional 5-minute rinse in ddH_2O, tissue dehydration was carried out using graded ethanol solutions (70%, 95%, and 100% ethanol). The sections were then cleared using three changes of Neo-clear (Merck, Darmstadt, Germany) each for 2 minutes, and cover-slipped with Neo-Mount (Merck). For white matter sparing, sections from the lesion epicenter, with the least spared white matter, were imaged using an Olympus BX53 microscope equipped with ORCA-spark C11440-36U (Hamamatsu Photonics, Shizuoka, Japan). Tissue sparing was assessed by delineating regions displaying light and dark blue staining and represented as a percentage of the cross-sectional area. This calculation involved dividing the white matter area by the total cross-sectional

area[81]. In sham mice, those without any injury, the cross-sectional area typically ranges between 60-70%. Following contusion, these values decrease to 20-30%. For lesion length the distance between the beginning and end of the lesion appearance was calculated.

2.2.8 Immunohistochemistry on slides

Immunohistochemical labeling was carried out on slides of the lumbar spinal cord (L4-L6 of 1-week female PGB study; 16 µm) and the L4-L6 DRGs (10 µm). After drying the slides at room temperature for 30 minutes, the slides were encircled with a liquid blocker. The slides were first washed three times (each 5 minutes) with 0.1 M Tris-buffered saline (TBS), and then incubated at room temperature in blocking solution (TBS + 0.25% Triton X-100 + 5% donkey serum) for 1 hour. The sections were incubated with the primary antibodies (diluted in TBS + 0.25% Triton X-100 + 1% donkey serum) overnight in a humid box at 4°C. Afterwards the slides were washed at room temperature three times (10 minutes each) with TBS + 1% donkey. The sections were incubated at room temperature with the secondary antibodies conjugated with fluorescent dyes (diluted in TBS + 1% donkey serum) for 2.5 hours in the dark. Subsequently, the slides were washed three times (each 10 minutes) with TBS, dried for 10 minutes, and cover-slipped using Fluoromount G (Southern Biotechnology Associates, Birmingham, AL)[81].

The primary antibodies used for L4-L6 spinal cord include rabbit anti-Calcitonin gene-related peptide (CGRP; 1:600; Immunostar, Hudson, Wisconsin, USA) to identify peptidergic nociceptors. To identify lamina IIi, guinea pig anti-PKCγ (1:600; Frontier Institute co., ltd., Hokkaido, Japan) was used. Furthermore, rabbit anti-Iba1 (1:600; Wako, Osaka, Japan), rabbit 5HT (1:1000; Immunostar, Wisconsin, USA), rabbit anti-KCC2 (1:750; ThermoFischer, Massachusetts, USA) and guinea pig anti-NeuN (1:2000; Millipore, Merck KGaA, Darmstadt, Germany) were used on lumbar sections. The following secondary antibodies were used: Alexa Fluor® 488 donkey anti-rabbit (1:600; ThermoFischer, Massachusetts, USA), Alexa Fluor® 594 donkey anti-rabbit (1:600;

ThermoFischer, Massachusetts, USA), Alexa Fluor® 594 donkey anti-guinea pig (1:600, Jackson Immunoresearch Laboratories, Pennsylvania, USA), anti-guinea pig Cy5 (1:600; Jackson Immunoresearch Laboratories, Pennsylvania, USA). For each animal, images of the left and right dorsal horn of three labeled sections with an intersection distance ranging from 700-1400 µm were taken at 20x magnification with Fluoview FV1000 confocal laser scanning microscope.

The primary antibodies used for L4-L6 DRGs include rabbit Cacna2d2 (1:200; Alomone labs, Jerusalem, Israel) and goat TrkA (1:200; R&D systems, Minnesota, USA), rabbit anti-pCAMKII (Thr287) (1:200; ThermoFischer, Massachusetts, USA), rabbit anti-phospho-CREB (Ser133) (1:200; Merck KGaA, Darmstadt, Germany), mouse anti-CREB (1:200; Abcam plc, Cambridge, UK). The following secondary antibodies were used: Alexa Fluor® 488 donkey anti-rabbit (1:600; ThermoFischer, Massachusetts, USA), Alexa Fluor® 594 donkey anti-goat (1:600; ThermoFischer, Massachusetts, USA) and Cy5 donkey anti-mouse (1:600; Jackson Immunoresearch Laboratories, Pennsylvania, USA).

2.2.9 Immunohistochemistry of free-floating sections

For c-fos staining, antigen retrieval was conducted by immersing the sections (25 µm L4-L6 spinal cord) in an antigen retrieval buffer (Citrate buffer, pH=6, see table 11 for details) placed in a 24-well plate. The plate was then incubated in a water bath at 85°C for 20 minutes. Following antigen retrieval, the tissue was rinsed three times with TBS for 5 minutes each to remove any residual buffer. Subsequently, the tissue was blocked in a solution of TBS containing 5% donkey serum and 0.2% Triton X-100 at room temperature with gentle shaking for 2.5 hours. Primary antibodies were diluted in TBS with 5% donkey serum and 0.2% Triton X-100. The tissue was then incubated with the primary antibody for 1 hour at room temperature, followed by an additional incubation at 4°C in a cold room with gentle shaking for 48 hours. After primary antibody incubation, the tissue was washed three times for 10 minutes each in TBS with 5% donkey serum and 0.2% Triton X-100 at room temperature. For secondary antibody labeling, the secondary antibodies were diluted in TBS with 5% donkey serum and incubated

with the tissue sections at room temperature for 2.5 hours in the dark with gentle shaking. Subsequently, the sections were washed three times for 10 minutes each with TBS and 5% donkey serum at room temperature. Finally, the sections were carefully flattened on a drop of TBS on a slide. The excess TBS was gently removed, and the slides were allowed to dry before cover-slipping using Fluoromount G.

The primary antibodies used for L4-L6 spinal cords include rabbit anti-CGRP (1:600; Immunostar, Hudson, Wisconsin, USA), guinea pig anti-PKCγ (1:600; Frontier Institute co., ltd., Hokkaido, Japan), Rat anti-c-fos (1:600; Synaptic systems, Göttingen, Germany), rabbit anti-Iba1 (1:600; Wako, Osaka, Japan). The following secondary antibodies were used: Alexa Fluor® 488 donkey anti-rabbit (1:600; ThermoFischer, Massachusetts, USA), Alexa Fluor® 594 donkey anti-rat (1:600; Invitrogen, Eugene, Oregon, USA), Cy5 donkey anti-guinea pig (1:600, Jackson Immunoresearch Laboratories, Pennsylvania, USA). Images with 20x magnification of the left and right dorsal horn of three labeled sections were taken for each animal, with an intersection distance of 700-1400 µm with Fluoview FV1000 confocal laser scanning microscope.

2.2.10 Clearing and staining of intact lumbar spinal cord

After perfusion and post-fixation in 4% PFA, the region of interest (L4-L6 spinal cord) was dissected. To facilitate the clearing process, a 2 mm segment on each caudal and rostral side was included along with the 5 mm segment of the L4-L6 spinal cord. These additional 2 mm segments on each side were used as attachment points on the sample holder during 3D imaging. The samples were then washed three times with phosphate-buffered saline (PBS), with each wash lasting at least 2 hours. Next, the samples underwent delipidation treatment using a 50% CUBIC-L solution (1:1 in ddH_2O) at 37°C for 24 hours with gentle shaking. Delipidation was continued using 100% CUBIC-L solution at 37°C, for 6 days with gentle shaking. The CUBIC-L solution was replaced with fresh solution on the 2nd, 4th, and 6th day. Following delipidation, the samples were washed five times

with PTwH solution (details provided in table 11), with each wash lasting at least 2 hours with gentle shaking. The samples were left in PTwH solution overnight. Subsequently, the samples were blocked (details provided in table 11) at 37°C, for 24 hours, with gentle shaking. Primary antibodies were diluted in PTwH solution containing 5% dimethylsulfoxide (DMSO) and 3% donkey serum. The tissue was then incubated with the primary antibodies at 37°C, with gentle shaking, for 6 days. Following the primary antibody incubation, the samples were washed five times with PTwH solution, with each wash lasting at least 2 hours. The samples were left in PTwH solution overnight. For the secondary antibody labeling, the antibodies were diluted in PTwH solution containing 3% donkey serum. The tissue was incubated with the secondary antibodies at 37°C, with gentle shaking, for 4 days. The samples were washed five times with PTwH solution at room temperature, with each wash lasting at least 2 hours and were incubated in PTwH solution overnight. To enable clearing and refractive index (RI) matching, the samples were pre-treated with a 50% CUBIC-R+ solution (1:1 in ddH_2O) at room temperature, with gentle shaking, for 24 hours. Clearing and RI matching were completed by treating the samples with 100% CUBIC-R^+ solution at room temperature for at least 2 days. Three hours prior to imaging, the samples were submerged in an oil mixture consisting of 65% silicon oil (ShinEtsu, Ohio, USA) and 35% mineral oil (Merck KGaA, Darmstadt, Germany) with a refractive index matching that of CUBIC-R^+ (1.522). The imaging was conducted using Zeiss 7 light sheet microscope using a 5x objective (EC Plan-Neofluar 5x/0.16) and dual light sheet illumination. Light sheet microscopy followed by analysis of the 3D images using Imaris 3D reconstructions were carried out by our collaborator, Dr. Jarred Griffin, from the Deutsches Zentrum für neurodegenerative Erkrankungen (DZNE) in Bonn, Germany. All the other steps including surgeries, behavioral tests, perfusion, dissection, clearing and staining of the tissues have been carried out by me.

Clearing was carried out on $SNS^{tdTomato}$ mice, however to amplify the red fluorescence of tdTomato, a primary antibody rabbit red fluorescent protein (RFP; 1:400; Clontech Laboratories GmbH, Heidelberg, Germany) was used together with guinea pig NeuN (1:200; Millipore, Merck KGaA, Darmstadt, Germany). As

secondary antibodies Alexa Fluor® 594 donkey anti-rabbit (1:400; ThermoFischer, Massachusetts, USA) and Alexa Fluor® 488 donkey anti-guinea pig (1:400; Jackson Immunoresearch Laboratories, Pennsylvania, USA) were used.

2.2.11 Analysis of microscopic images

All analyses were conducted on the original microscopic images without any modifications. However, slight adjustments have been made to the brightness and contrast of the presented images for improved visibility in this dissertation.

2.2.11.1 Quantification of CGRP labeling density in the spinal cord

The analysis of CGRP fiber labeling density was carried out as previously described[79–81]. The region of interest was determined using the mouse spinal cord atlas and the PKCγ-labeling of lamina IIi. The dorsoventral extent of lamina IIi, indicated by PKCγ-labeling, was measured and defined as “x”. A box was placed at the center of the dorsal horn below lamina IIi, with dimensions of 2x in the dorsoventral direction and 4x in the mediolateral direction. The quantification of labeling density was performed blindly with ImageJ software. The labeling threshold was set to minimize background noise while accurately capturing CGRP fiber labeling. The labeling density shows the percentage of positive labeling within the analysis box, and the values for each mouse were averaged from at least three sections.

2.2.11.2 Quantification of c-fos labeling in the spinal cord

Z-stack images (20x magnification) with a step size of 3 µm were taken from 25 µm sections. Analysis of c-fos expression followed established

protocols[83,84,89]. The Z-stack images were compressed into one maximum projection image in ImageJ. The 'analyze particles' function, with a size limit ranging from 10 to 400 µm and circularity between 0.23 and 1.0, was employed along with the threshold tool to quantify the number of c-fos$^+$ neurons. Automatic counting results were carefully reviewed manually to exclude false positives, such as auto-fluorescent particles. The mouse spinal cord atlas[90] together with PKCγ lamina (lamina IIi), were used in each image to manually overlay the outlined laminae I-V.

2.2.11.3 Quantification of KCC2, PKCγ and Iba1 intensity in the spinal cord

To assess KCC2 intensity in laminae I-II, lamina IIi was visualized through PKCγ staining on the same slide. Manual outlining was employed to outline lamina IIi along with the remaining dorsal part of the dorsal horn (laminae I and IIo). Within this defined region, KCC2 intensity was measured. For Iba1 intensity the dorsal horn (laminae I-V) was outlined and the intensity was measured. PKCγ intensity was quantified through manual outlining of lamina IIi. Furthermore, the number of PKCγ-positive cells located beneath lamina IIi was manually counted during the image analysis process. The average of PKCγ and Iba1 intensity in control SCI mice were calculated in ImageJ and the values for each animal were normalized by the SCI average value and reported as relative intensity.

2.2.11.4 Quantification of 5HT in the spinal cord

Thresholding technique in ImageJ was performed to binarize the image, remove the background and visualize the fibers accurately. The 5-HT image was the skeletonized and fiber length was analyzed with the 'analyze skeleton' function of ImageJ.

2.2.11.5 Quantification of Cacna2d2 intensity in the DRG

The Cacna2d2 intensity was assessed in small-diameter $TrkA^+$ L4-L6 DRG and large-diameter (≥ 40 µm) $TrkA^-$ DRG (non-nociceptive). The small diameter $TrkA^+$ and large-diameter $TrkA^-$ neurons in each image were outlined in ImageJ. Size measurement was used to make sure that in $TrkA^-$ fibers, $Nav1.8^+$ nociceptors which have medium to small diameters are not selected. The average intensity of Cacna2d2 channel was then measured for each neuron and subsequently each image and mice.

2.2.11.6 Quantification of pCAMKII, pCREB and CREB intensity in the DRG

The intensities of each channel were measured in $TrkA^+$ L4-L6 DRG, using ImageJ. The average intensity of each marker was calculated in control SCI mice and the values for each animal was normalized by the SCI average value and reported as relative intensity.

2.2.12 Statistical analysis

Behavioral analysis (mechanical and thermal sensitivity as well as the PEAP) was determined using mixed-effects 2-way ANOVA analysis followed by Sidak pairwise comparisons. The mixed-effect model was used to account for the missing values. C-fos and volume of nociceptors across different laminae were analyzed by repeated measures 2-way ANOVA followed by Sidak pairwise comparisons to reveal overall group and laminae differences. The motor function results as well as the tissue analysis results were analyzed by unpaired t-test. All data have been tested for normality and have been found to be normal. All data are presented as mean ± standard deviation (SD). Statistical analysis was done using GraphPad Prism 9 software (GraphPad Software Inc., Boston, Massachusetts, USA) with an alpha level of 0.05 for significance.

2.2.13 Illustration

All the illustrations featured in this thesis are original artworks crafted for this purpose. The artistic process involved the use of Adobe Photoshop 2020 in conjunction with a Wacom Cintiq 16 tablet (Wacom, Kazo, Japan). Notably, Seyederfan Moussavi Torshizi skillfully painted the depictions of mice, von Frey hair filaments, Hargreaves, PEAP, syringes and VGCCs following my instructions. I created the remaining illustrations in Adobe Illustrator.

Results

3 Results

The work presented here are currently in preparation for submission as my sole first author publication.

3.1 Aberrant nociceptor plasticity to deeper laminae occurs rapidly after spinal cord injury

Following SCI, the plasticity of nociceptors in the spinal dorsal horn correlates strongly with SCI-induced neuropathic pain, specifically mechanical allodynia[80,81,91,92]. To learn more about the termination pattern of nociceptors I have used $SNS^{tdTomato}$ mice and carried out either T11 spinal cord moderate contusion or sham surgery on them. Seven days post-injury (dpi), I conducted behavioral tests including the Basso Mouse Scale (BMS) to ensure weight support, followed by von Frey and Hargreaves tests to confirm that mechanical allodynia and thermal hyperalgesia developed in SCI mice. At 7 dpi I performed a transcardial perfusion and dissected the L4-L6 segment of the spinal cord followed by a 4-week clearing and staining protocol (4 weeks of tissue treatment). Afterwards I sent the tissue to our collaborator Dr. Jarred Griffin (Deutsches Zentrum für neurodegenerative Erkrankungen (DZNE), Bonn, Germany) for light sheet microscopy and analysis using Imaris 3D reconstructions.

I show that 7 dpi, SCI mice developed mechanical allodynia (**** $P<0.0001$ and $P<0.05$ for 0.16g and 0.4g filaments, respectively), thermal hyperalgesia (**** $P<0.0001$) and impaired motor function (*** $P<0.001$) compared to sham mice (Figure 6 A-C). Furthermore, 3D lightsheet imaging of the L4-L6 spinal cord in $SNS^{tdTomato}$ mice at 7 dpi demonstrated an increase in the volume of nociceptors ($Na_V1.8^+$ neurons, C-and Aδ-fiber, and potentially C-LTMRs) in lamina III (** $P<0.01$), IV (* $P<0.05$) and V (* $P<0.05$) of dorsal horn compared to sham (Figure 6 D and E). The substantial increase occurring in lamina III likely indicates ventral sprouting rather than mere lateral growth of existing ventral fibers.

.

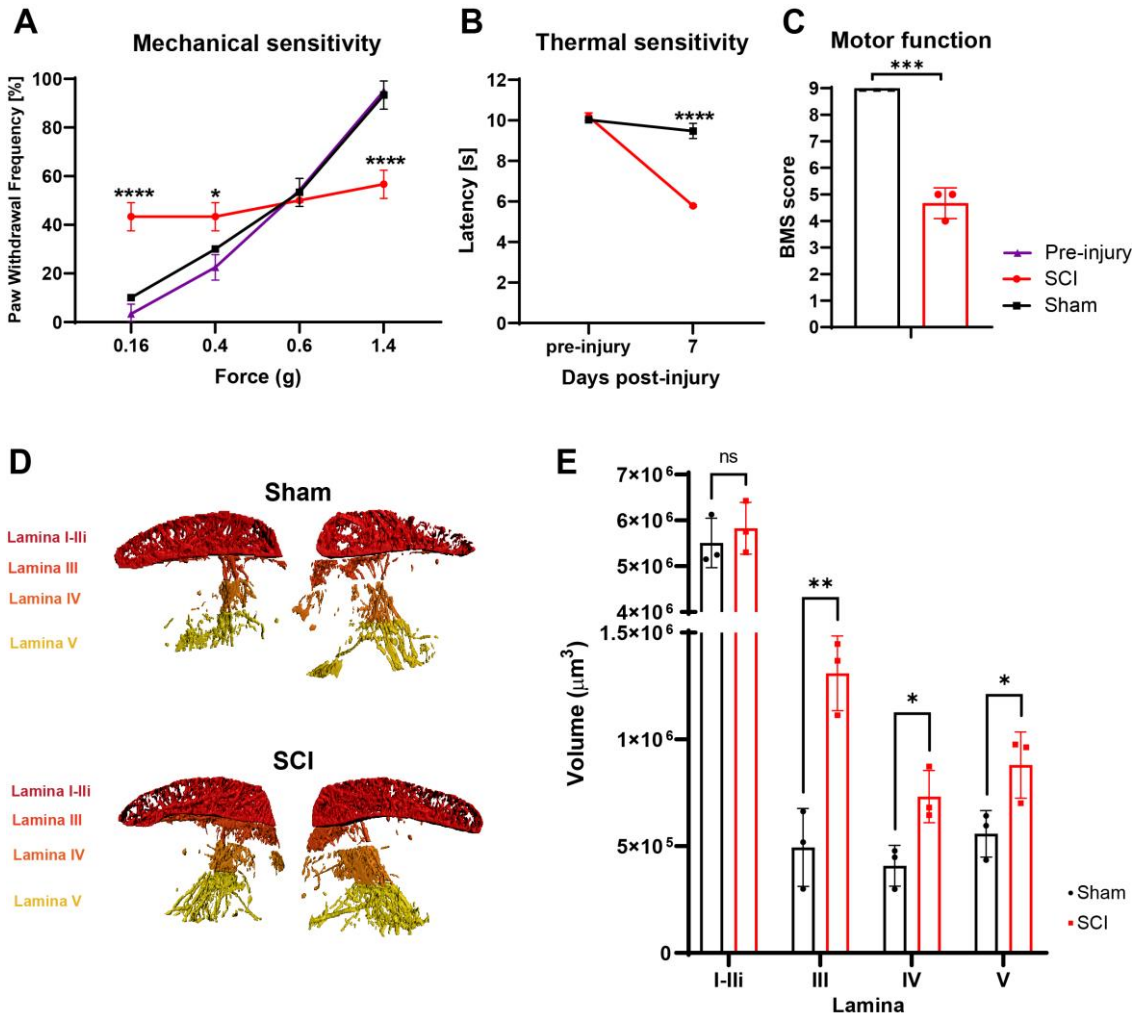

Figure 6 3D reconstructed SCI-induced nociceptive plasticity. A) 7 dpi mechanical allodynia (non-noxious von Frey hair filaments: 0.16 g and 0.4 g) developed in T11 SCI compared to sham mice (2-way ANOVA group comparison P<0.0001, Sidak's pairwise comparisons, 0.16g and 0.4g **** P<0.0001 and * P<0.05, respectively) **B)** Thermal hyperalgesia developed in SCI mice compared to sham (2-way ANOVA group differences with Sidak's pairwise comparisons, **** P<0.0001). **C)** Motor function is significantly impaired after SCI (*** P<0.001) **D)** 3D lightsheet imaging of lumbar spinal cord shows an increase in nociceptive fiber volume following SCI, as observed by Imaris surface rendering of nociceptive fibers in L4-L6 spinal cord of $SNS^{tdTomato+}$ sham and SCI mice. **E)** The volume of nociceptors increases after SCI (Repeated-measures 2-way ANOVA followed by Sidak's post hoc test showed a significant impact of injury, p=0.028) in laminae III, IV and V (significant impact across different laminae, p<0.0001). ** P<0.01, * P<0.05, ns = not significant. mean ± SD. n = 3/group.

3.2 Prophylactic pregabalin treatment prevents mechanical allodynia development, associated peptidergic nociceptor plasticity and reduces microglia activation

Given that neuropathic pain and associated structural changes arise acutely after experimental SCI in rodents, I examined pregabalin (PGB) treatment immediately after SCI in prevention of below-level SCI-induced neuropathic pain development. Further understanding the role sex may play in SCI-induced neuropathic pain treatment is key to understanding the role of hormones in this pathophysiology. Therefore, this study was carried out on C57BL/6J female (n=14) and male (n=14) mice that underwent T11 spinal cord moderate contusion (50kDyn) injury. Two groups (n = 7 female; n = 7 male) received PGB treatment (46 mg/kg, i.p., 2x/day, starting on the evening post-SCI), while the other two groups received saline injections for 7 dpi (Figure 7 A and B). PGB treatment prevented the development of mechanical allodynia in both female and male mice (0.16 g and 0.4 g von Frey hair filaments, $P<0.001$ for females and $P<0.0001$ and $P<0.01$ for males, Figure 7 C and D). Interestingly, the mechanical hypoalgesia, which is normally developed in response to the noxious 1.4g filament, was reduced in mice treated with PGB ($P<0.001$ for female and $P<0.05$ for male PGB-treated mice compared to vehicle-treated mice). PGB alleviated thermal hyperalgesia in male mice ($P<0.0001$, Figure 7 F), but did not in female mice (Figure 7 E). Furthermore, no difference in motor function (BMS) was observed between the treated and untreated groups (Figure 7 G and H). In male mice, place escape/avoidance paradigm (PEAP) was further performed to assess pain quality and supraspinal processing of mechanical sensitivity using the non-noxious 0.16g filament. The results indicate that PGB-treated male mice did not exhibit a change in place preference in response to the non-painful stimulus, confirming the absence of mechanical allodynia ($P<0.001$, Figure 7 I).

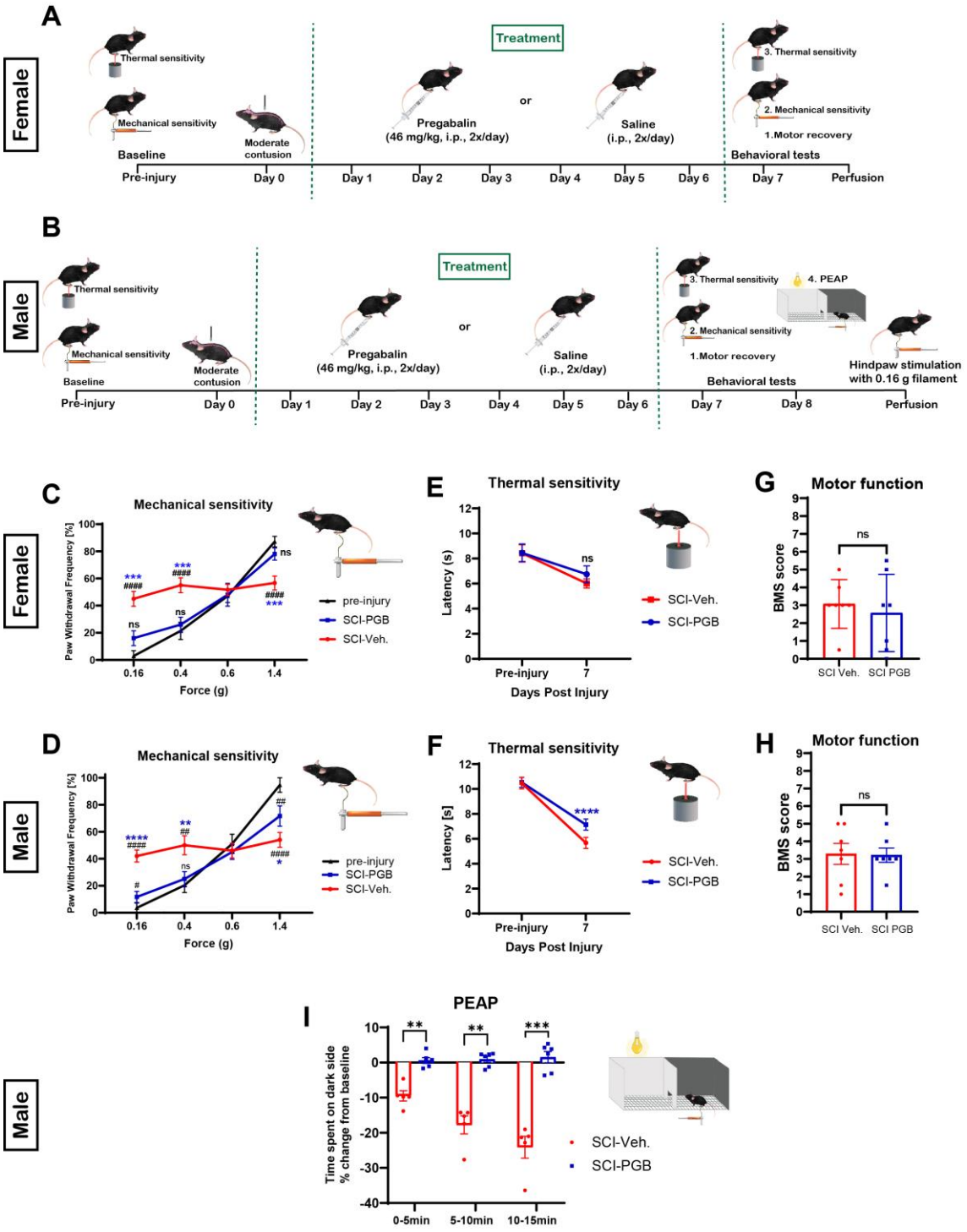
A
Female
Thermal sensitivity
Mechanical sensitivity
Baseline
Moderate contusion
Treatment
Pregabalin (46 mg/kg, i.p., 2x/day)
or
Saline (i.p., 2x/day)
3. Thermal sensitivity
2. Mechanical sensitivity
1.Motor recovery
Behavioral tests
Pre-injury
Day 0
Day 1
Day 2
Day 3
Day 4
Day 5
Day 6
Day 7
Perfusion
B
Male
Thermal sensitivity
Mechanical sensitivity
Baseline
Moderate contusion
Treatment
Pregabalin (46 mg/kg, i.p., 2x/day)
or
Saline (i.p., 2x/day)
3. Thermal sensitivity
4. PEAP
2. Mechanical sensitivity
1.Motor recovery
Behavioral tests
Hindpaw stimulation with 0.16 g filament
Pre-injury
Day 0
Day 1
Day 2
Day 3
Day 4
Day 5
Day 6
Day 7
Day 8
Perfusion
C
Female
Mechanical sensitivity
Paw Withdrawal Frequency [%]
Force (g)
pre-injury
SCI-PGB
SCI-Veh.
E
Thermal sensitivity
Latency (s)
Pre-injury
7
Days Post Injury
SCI-Veh.
SCI-PGB
G
Motor function
BMS score
SCI Veh.
SCI PGB
D
Male
Mechanical sensitivity
Paw Withdrawal Frequency [%]
Force (g)
pre-injury
SCI-PGB
SCI-Veh.
F
Thermal sensitivity
Latency [s]
Pre-injury
7
Days Post Injury
SCI-Veh.
SCI-PGB
H
Motor function
BMS score
SCI Veh.
SCI PGB
I
Male
PEAP
Time spent on dark side % change from baseline
0-5min
5-10min
10-15min
SCI-Veh.
SCI-PGB

Figure 7 Prophylactic PGB treatment inhibits the development of mechanical allodynia in both sexes. A-B) Experimental timeline in female and male mice. On the SCI evening, the mice were injected with PGB (i.p. 46 mg/kg, 2x/day, n=7) or saline (n=7) and then daily for 7 dpi. One week post-SCI, the mice were tested for motor function as well as mechanical and thermal sensitivity. Male mice were additionally tested for PEAP. **C-D)** SCI-induced mechanical allodynia (non-noxious von Frey hair filaments: 0.16 g and 0.4 g) did not develop in mice treated with prophylactic PGB (0.16g and 0.4g P<0.001 in females and P<0.0001 and P<0.01 males, 2-way ANOVA group comparison P=0.0034 in females and P=0.0021 in males, Sidak's pairwise comparisons; SCI-Veh. (saline) with pre-injury #### P<0.0001; SCI-PGB with pre-injury #### P<0.0001, ## P<0.01 or ns=not significant; SCI-PGB with SCI-Veh * P<0.05, ** P<0.01, *** P<0.001, **** P<0.0001). **E-F)** Thermal sensitivity shows only a trend in females, however in males a significant reduction in sensitivity is observed after treatment (2-way ANOVA group differences, P=0.0003, Sidak's pairwise comparisons, **** P<0.0001). **G-H)** Motor function is not altered with PGB treatment. **I)** Supraspinal processing of nociception using the PEAP (stimulation with non-noxious 0.16 g filament) shows that male SCI-PGB did not change their chamber preference in the presence of the stimulus compared to their baselines (absence of stimulus), confirming the lack of mechanical allodynia development (2-way ANOVA, group differences P= 0.0002, Sidak's pairwise comparisons to SCI-Veh., *** P<0.001, ** P<0.01). Mixed effects 2-way ANOVA followed by Sidak's post hoc test for mechanical and thermal sensitivity and PEAP, unpaired t-test for motor recovery, mean ± SD, n = 7/group. Each treatment group contained 7 animals during baseline testing and for assessing motor function Since some animals did not have weight support 7 dpi, the numbers after injury are lower: For females SCI-PGB (n=5) and SCI-Veh (n=6). For males SCI-PGB (n=6) and SCI-Veh (n=5).

Whilst there are studies regarding the mechanisms of pregabalin action as a blocker of α2–δ1 and α2–δ2 subunit of VGCCs[44,46], our understanding remains limited in the context of SCI-induced below-level neuropathic pain. I explored the potential mechanisms through which pregabalin prevents SCI-induced neuropathic pain development, including effects on nociceptor fiber plasticity in deeper laminae (III-IV), inflammatory response, neuroprotection (5HT, lesion length) and disinhibition imbalance (PKCγ, KCC2). Analysis revealed that $CGRP^+$ nociceptor fiber plasticity into the deeper laminae (III-IV) was significantly lower in SCI-PGB compared to the untreated group in both females and males (P<0.05 in females, Figure 8 A, B; P<0.01 in males, Figure 8 A, C). In males, additional c-fos staining revealed that hindpaw stimulation with a non-noxious 0.16 g filament

led to dorsal horn neuronal activation. This activation was significantly reduced in the SCI-PGB group (P<0.01) and laminae IIi-V showed the greatest reduction (Figure 8 A, D).

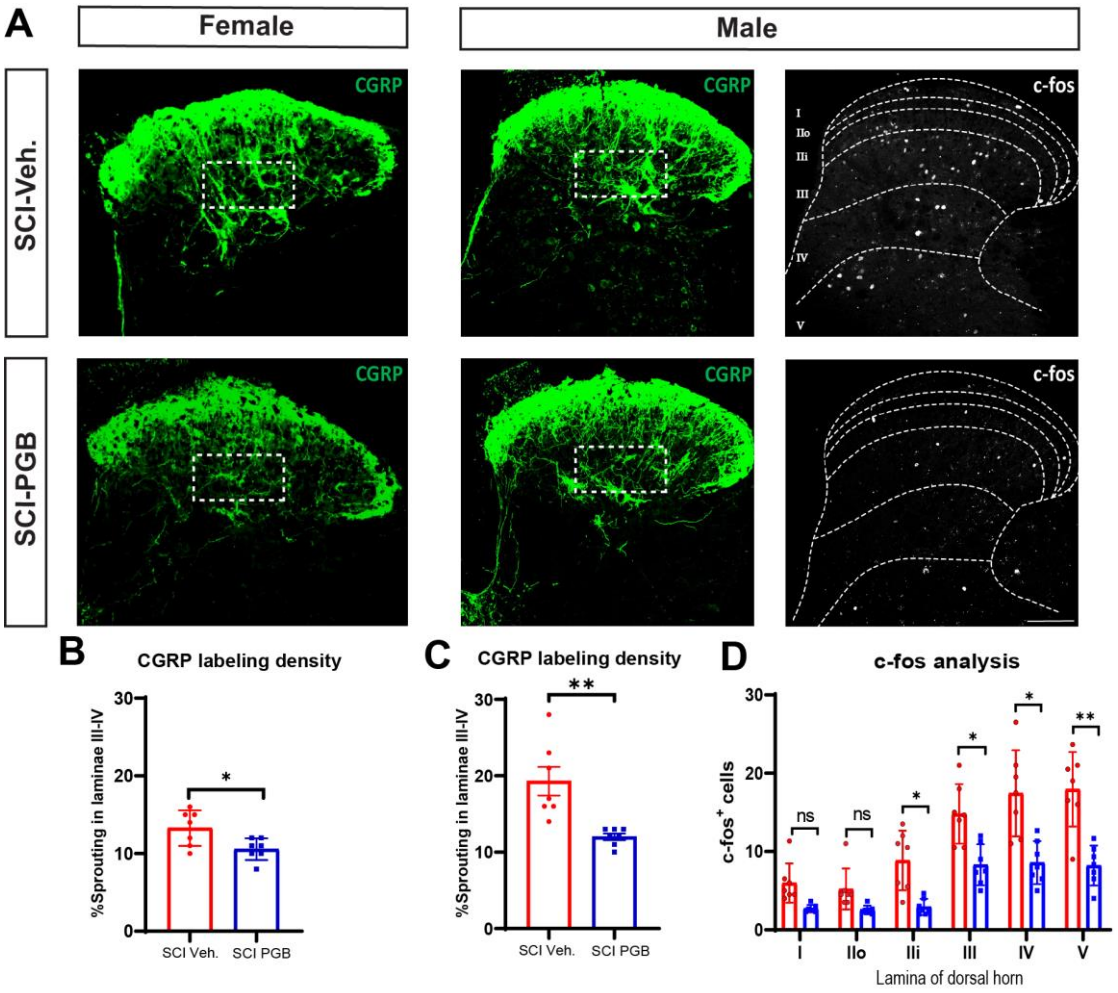

Figure 8 Prophylactic PGB treatment reduces SCI-induced CGRP⁺ fiber plasticity and neuronal activation below injury level in the lumbar spinal cord. A) CGRP and c-fos immunostaining of L4-L6 spinal cord of SCI-PGB and SCI-Veh. (T11 contusion) mice. **B, C)** Prophylactic PGB treatment stopped the aberrant plasticity of CGRP⁺ fibers in laminae III-IV, P=0.0149 in females, P=0.0026 in males, respectively (Unpaired t-test mean ± SD). **D)** In males, the number of activated c-fos⁺ neurons in the dorsal horn shows a significant effect of treatment (Repeated-measures 2-way ANOVA, P=0.0003; Sidak's pairwise comparisons SCI-PGB with SCI-Veh. lamina IIi P=0.032, lamina III P=0.02, lamina IV P=0.026, lamina V P=0.005). * P<0.05, ** P<0.01, ns= not significant, n = 7/group. Scale bar: 100 µm.

PGB has been shown to provide neuroprotective effects previously[93–95], therefore to rule out neuroprotection at the lesion site, I analyzed white matter sparing of the lesion epicenter (using eriochrome cyanine staining) as well as the lesion length. Notably, there were no discernible differences in white matter sparing or lesion length between the SCI-PGB and SCI-Veh. mice (Figure 9 A-E).

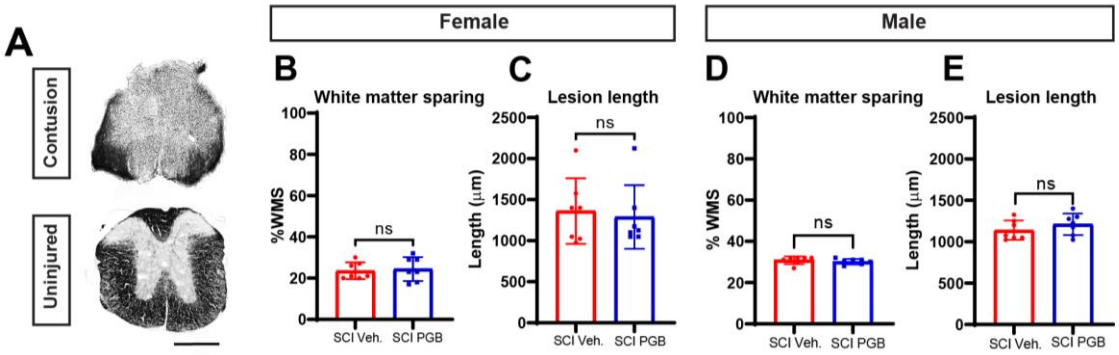

Figure 9 Prophylactic PGB treatment has no effect on white matter sparing or lesion length after SCI. A) Eriochrome cyanine stained coronal sectioned of SCI and uninjured mice (scale bar: 500 µm). **B-E)** Prophylactic PGB has no effect on white matter sparing or lesion length in females or males. Unpaired t-test mean ± SD, ns= not significant, n = 7/group.

Other studies have shown that gabapentinoids reduce inflammatory mediators[96–98]. Interestingly, I observed a reduction in the intensity of microglia labeled ionized calcium-binding adapter molecule 1 (Iba1) in the dorsal horn of both female (*** P<0.001) and male (* P<0.05) mice with prophylactic PGB treatment at one-week post-injury time point (Figure 10 A-C).

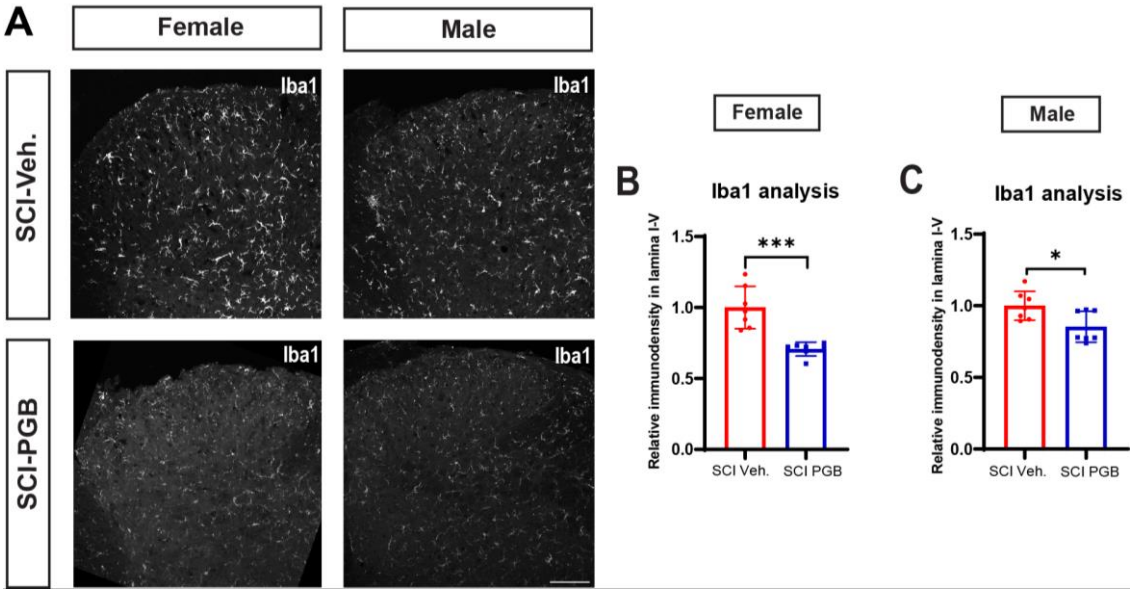

Figure 10 Prophylactic PGB treatment reduces microglia reactivity below injury level in the lumbar spinal cord, one-week post-SCI. A) Iba1 immunostaining of lumbar spinal cord of SCI-PGB and SCI-Veh. female and male mice. **B, C)** Prophylactic PGB significantly reduced Iba1 intensity in dorsal horn in both females (P=0.0003) and males (P=0.022; unpaired t-test mean ± SD). * P<0.05, *** P<0.001, ns= not significant, n = 7/group. Scale bar: 100 µm.

Studies have suggested that another mediator of mechanical allodynia is protein kinase C gamma (PKCγ). This crucial intracellular signaling kinase is primarily found in a subgroup of excitatory interneurons within the inner region of lamina II (IIi). It has been suggested that PKCγ intensity and the number of PKCγ^{+} cells in regions outside of lamina IIi increase after SCI-induced mechanical allodynia[99,100]. However, my results indicate that PKCɣ intensity in lamina IIi (Figure 11 A-C) and the number of PKCɣ$^{+}$ cells below lamina IIi (Figure 11 D and E) were not significantly altered after treatment, suggesting a different route of pain alleviation for PGB.

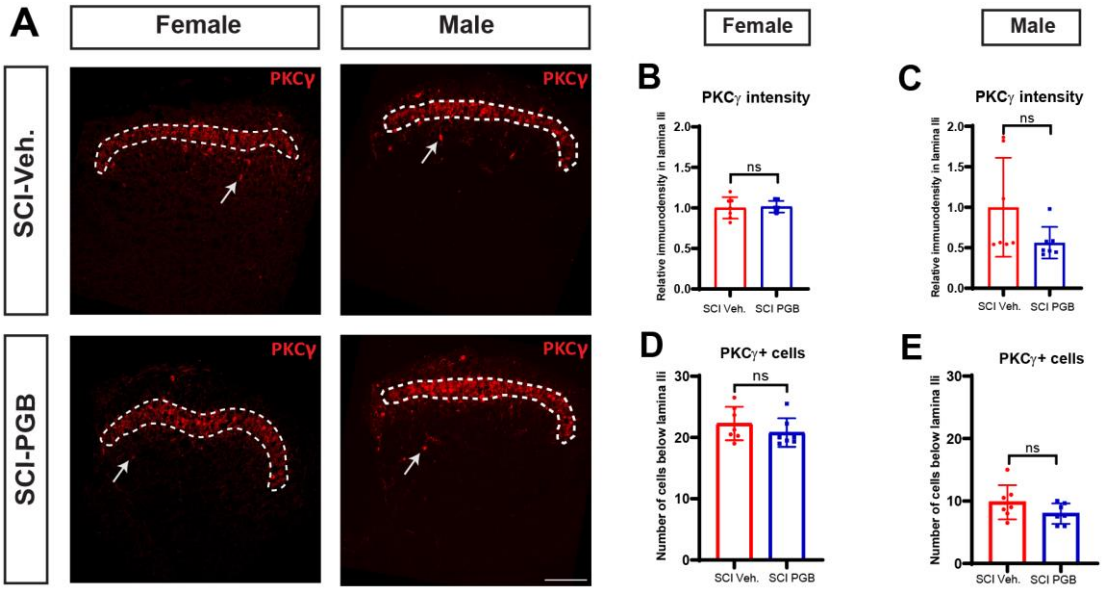

Figure 11 Prophylactic PGB treatment has no effect on PKCγ in the dorsal horn of the lumbar spinal cord after SCI. A) PKCγ immunostaining of below injury level dorsal horn of L4-L6 spinal cord of SCI-PGB and SCI-Veh. (T11 contusion) mice (scale bar: 100 µm). **B, C)** Prophylactic PGB treatment did not affect PKCγ intensity in lamina IIi. **D, E)** The number of PKCγ^{+} cells below lamina IIi were unaffected by PGB treatment. Unpaired t-test mean ± SD, ns= not significant, n = 7/group.

Studies show that after injury, potassium (K^+)/chloride (Cl^-) cotransporter 2 (KCC2) levels decrease in laminae I-II, contributing to allodynia by reducing spinal inhibition[101]. Training after injury can upregulate KCC2, leading to beneficial effects on allodynia[102]. However, PGB treatment did not cause any changes in KCC2 levels in laminae I-II (Figure 12 A and B).

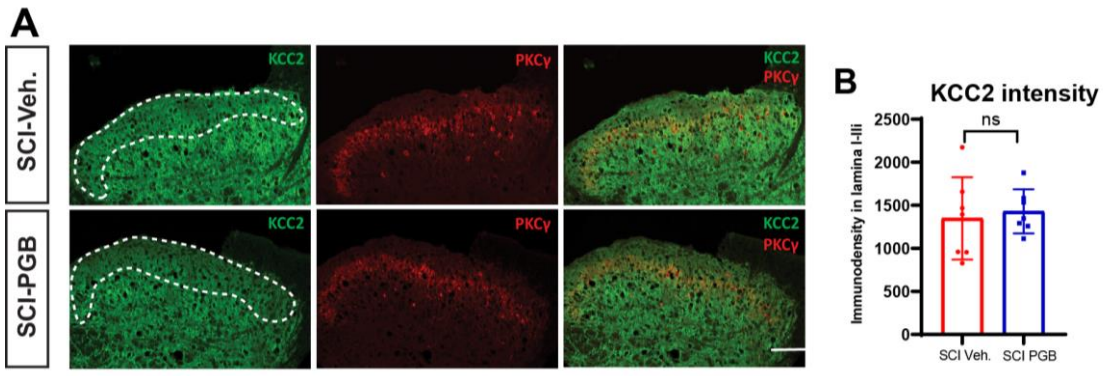

Figure 12 Prophylactic PGB treatment has no effect on KCC2 intensity in the dorsal horn of the lumbar spinal cord after SCI. A) KCC2 immunostaining of dorsal horn of L4-L6 spinal cords of SCI-PGB and SCI-Veh. treated female mice (scale bar: 100 µm). **B)** Prophylactic PGB did not affect KCC2 intensity in laminae I-IIi. Unpaired t-test mean ± SD, ns= not significant, n = 7/group.

Descending brainstem serotonergic 5-hydroxytryptamine (5HT) fibers control hypersensitivity in the dorsal horn[103]. Despite being suggested as having neuroprotective effects[93–95], I observed that PGB treatment did not yield any significant effect on the total length of descending serotonergic 5HT fibers in the lumbar dorsal horn (Figure 13 A and B).

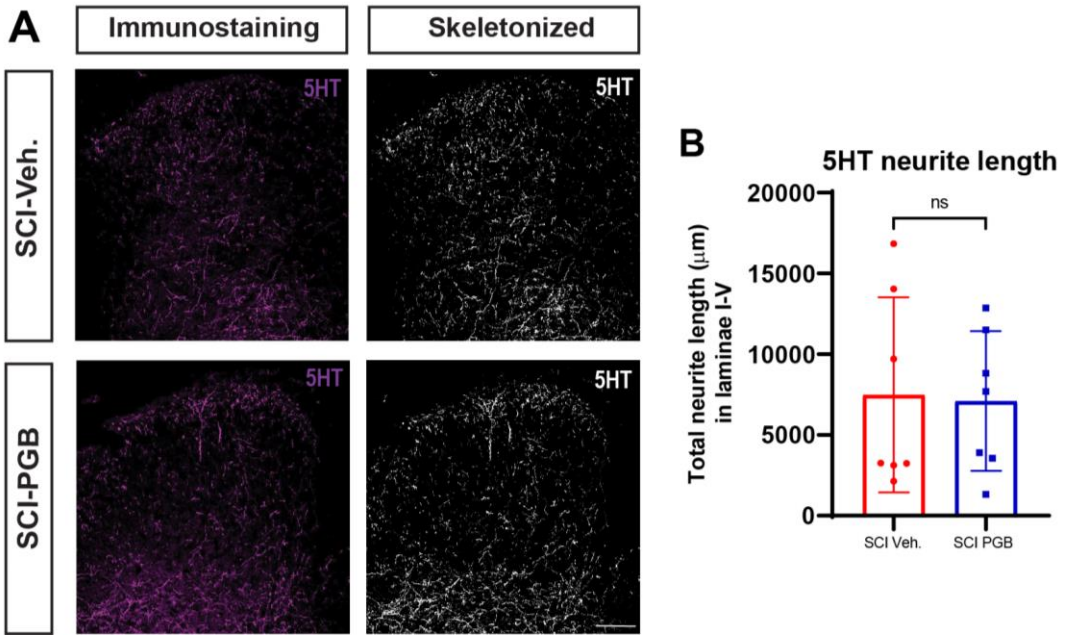

Figure 13 Prophylactic PGB treatment has no effect on 5HT fiber neuroprotection in lumbar spinal cord after SCI. A) 5HT immunostaining of the dorsal horn of L4-L6 spinal cords of SCI-PGB and SCI-Veh. treated female mice (scale bar: 100 µm). **B)** Prophylactic PGB has no effect on total length of 5HT fibers in dorsal horn. Unpaired t-test mean ± SD, ns= not significant, n = 7/group.

3.3 The prevention of mechanical hypersensitivity by pregabalin is partially conserved beyond two weeks post-discontinuation

Considering prophylactic PGB treatment prevented SCI-induced nociceptor fiber plasticity which is associated with preventing SCI-neuropathic pain, I asked if these beneficial effects are permanent, and therefore, remain following discontinuation. Female C57BL/6J mice with moderate T11 contusion (n = 13, one mouse lost a couple of hours following SCI) received either PGB (46 mg/kg, i.p., 2x/day, starting on the SCI evening, n = 6) or vehicle (n = 7) treatment for 7 dpi. Behavioral tests (mechanical and thermal sensitivity and motor function) were carried out weekly for three weeks post-SCI. Additionally, in the last week, PEAP was performed (Figure 14 A).

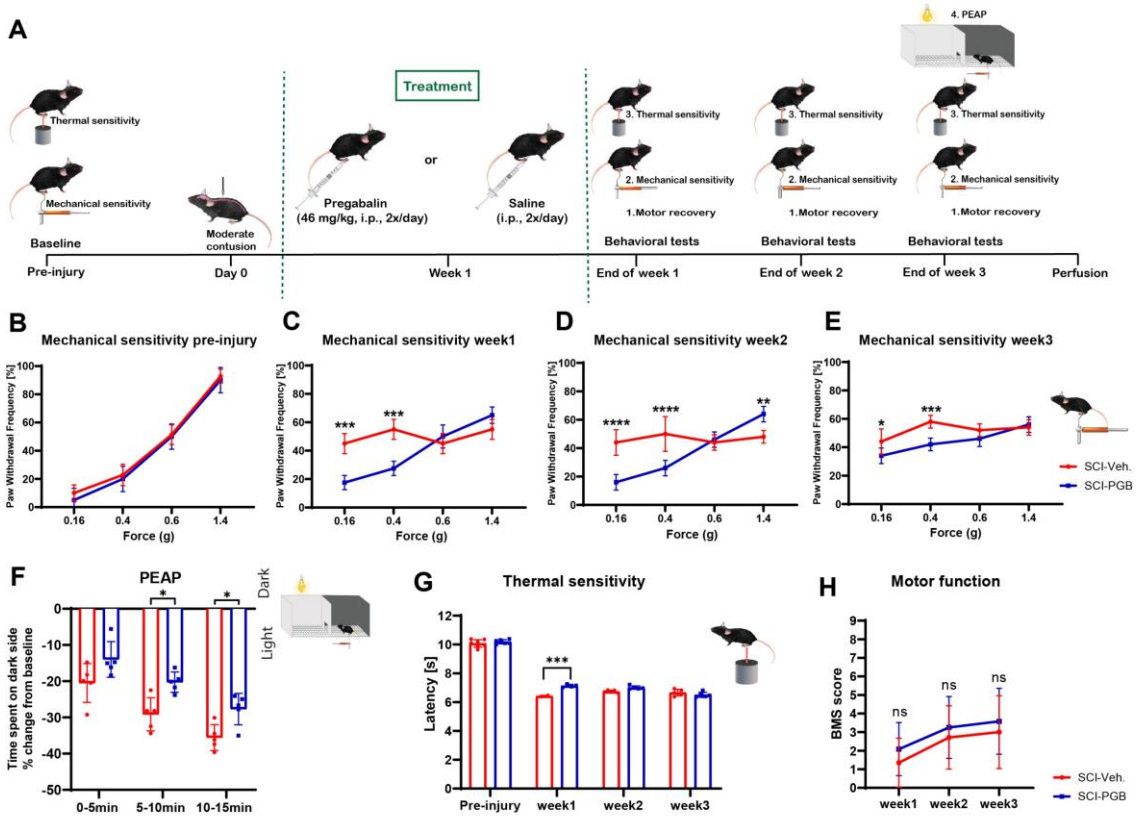

Figure 14 Seven-day PGB treatment has lasting effects on mechanical sensitivity for nearly 2 weeks post-PGB removal. A) Timeline of experiment: Starting on the SCI evening, the mice were injected with PGB (46 mg/kg i.p., 2x/day, n=6) or saline (n=7) for 7 dpi. Weekly behavioral tests were conducted for three weeks after SCI. The female mice were tested for motor function (BMS) as well as mechanical (von Frey hair filaments) and thermal (Hargreaves) sensitivity. In the last week mice were additionally tested for PEAP. **B)** Mechanical sensitivity pre-injury (SCI-PGB n=6, SCI-Veh. n=7) **C)** Mechanical sensitivity at 9 dpi (PGB treatment up to 7 dpi) shows a significant reduction of mechanical allodynia, (2-way ANOVA group differences, P=0.0357, Sidak's pairwise comparisons, *** P<0.001; SCI-PGB n=4, SCI-Veh. n=2, not all mice could undergo testing at this time point due to inadequate weight support). **D)** Mechanical sensitivity at 14 dpi (7 days after removal of PGB) shows the reduction of mechanical allodynia (0.16 g and 0.4 g) still remains (SCI-PGB n=5, SCI-Veh. n=5; 2-Way ANOVA group differences, P=0.0389: Sidak's pairwise comparisons; SCI-PGB with SCI-Veh. **** P<0.0001, ** P<0.01). **E)** Mechanical sensitivity at 21 dpi (14 days after removal of PGB) shows the effect on mechanical allodynia decreases, however remains significant (SCI-PGB n=5, SCI-Veh. n=5; 2-Way ANOVA group differences, P= 0.0163: Sidak's pairwise comparisons, *** P<0.001, *P<0.05). **F)** Supraspinal processing of nociception using the PEAP on 21 dpi (0.16 g filament) shows that although both SCI-PGB and SCI-Veh. change their chamber preference in the presence of the stimulus compared to their baselines, this is less pronounced for those that received PGB treatment (2-way ANOVA, group differences P=0.0059, Sidak's pairwise comparisons to SCI-Veh., * P<0.05; SCI-PGB n=5, SCI-Veh. n=5). **G)** Thermal hyperalgesia shows a significant reduction in SCI-PGB only at 9 dpi (2-way ANOVA group differences, P=0.0004, Sidak's pairwise comparisons, *** P<0.001). However, the effect does not persist 1 or 2 weeks after PGB removal. **H)** Motor function is not altered by PGB (SCI-PGB n=6, SCI-Veh. n=7). Mixed-effects 2-way ANOVA followed by post hoc Sidak's test for mechanical and thermal sensitivity and PEAP, unpaired t-test for motor function, mean ± SD.

The analgesic effects of PGB remain robust even one week after withdrawal of the treatment (P<0.0001 for 0.16 and 0.4 g, Figure 14 B-D) yet during the second week after discontinuation, the effect size decreased but remained significant (*P<0.05 and *** P<0.001 for 0.16 and 0.4 g, Figure 14 E). Similarly, two weeks post-removal, PGB had a reduced but significant impact on the PEAP (P<0.05, Figure 14 F). In contrast, the effect of PGB treatment on thermal sensitivity did not have a lasting effect and ended shortly after discontinuation of treatment (Figure 14 G). Similar to previous results, no difference between the treated and untreated groups in motor function (BMS) was

observed (Figure 14 H). Confirming the lingering mechanical analgesic effect 2 weeks after PGB discontinuation, I observed reduced CGRP$^+$ fibers in laminae III-IV of the dorsal horn ($P<0.05$, Figure 15 A and B), which suggests the importance of nociceptor maladaptive plasticity in conveying mechanical allodynia.

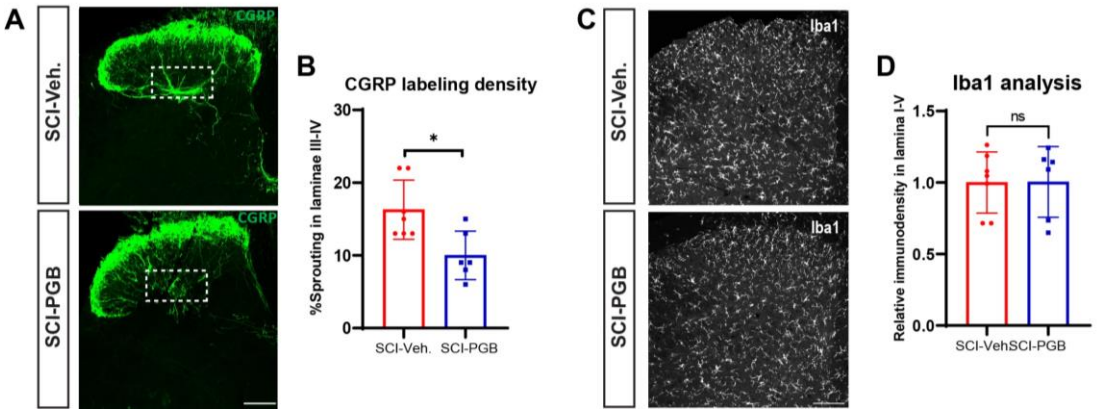

Figure 15 Seven-day PGB treatment has lasting effects on the reduction of CGRP$^+$ fiber plasticity but not Iba1 intensity two weeks following removal. A) CGRP immunostaining of L4-L6 spinal cord of SCI-PGB (one week of treatment + two weeks post-removal) and SCI-Veh. mice. **B)** Prophylactic PGB treatment has lasting effect on the aberrant plasticity of CGRP-expressing fibers in laminae III-IV after removal, P=0.0120. **C)** Iba1 immunostaining of dorsal horn of lumbar spinal cord of SCI-PGB and SCI-Veh. treated mice 2 weeks after treatment discontinuation. **D)** No significant difference was observed in Iba1 intensity in dorsal horn. Unpaired t-test mean ± SD, * P<0.05, ns= not significant, SCI-PGB n=6, SCI-Veh. n=7. Scale bar: 100 µm.

Even though in the one-week study there was a reduction of inflammatory agents after prophylactic PGB treatment, three weeks post-SCI no notable distinctions were identified in the intensity of Iba1 within the dorsal horn of the lumbar spinal cord among the groups (Figure 15 C and D). No significant differences were observed in white matter sparing at lesion epicenter or lesion length, indicating that the observed effects are not due to neuroprotection (Figure 16 B and C). Similarly, further analysis showed that PKCɣ intensity in lamina IIi (Figure 17 B) and the number of PKCɣ+ cells below lamina IIi (Figure 17 C) were not significantly altered after PGB treatment discontinuation.

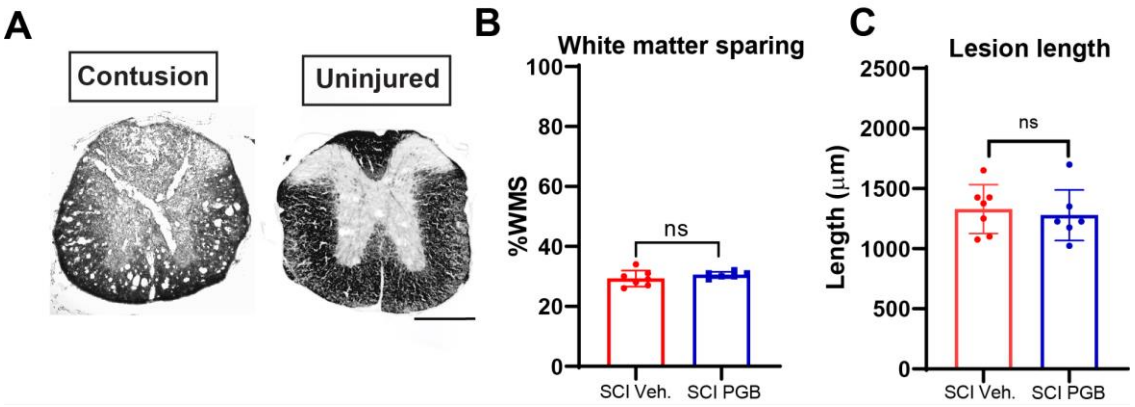

Figure 16 Discontinuation of prophylactic PGB treatment following SCI has no effect on white matter sparing or lesion extent. A) Eriochrome cyanine stained coronal sectioned of SCI and uninjured mice (Scale bar: 500 µm). **B, C)** Prophylactic PGB discontinuation has no effect on white matter sparing or lesion length. Unpaired t-test mean ± SD, ns= not significant, SCI-PGB n=6, SCI-Veh. n = 7.

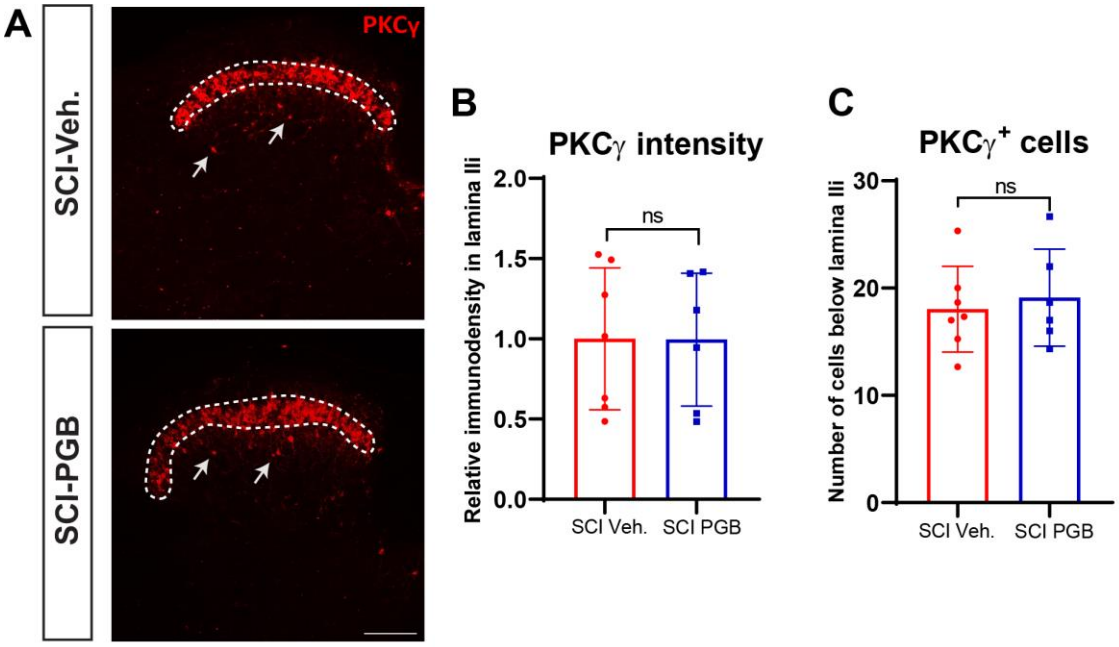

Figure 17 Discontinuation of prophylactic PGB treatment following SCI has no effect on PKCγ in the lumbar spinal cord. A) PKCγ immunostaining of the dorsal horn of L4-L6 spinal cords of SCI-PGB and SCI-Veh. female mice (Scale bar: 100 µm). **B)** Removal of prophylactic PGB treatment did not affect PKCγ intensity in lamina IIi. **C)** The number of PKCγ⁺ cells below lamina IIi were unaffected by removal of PGB treatment. Unpaired t-test mean ± SD, ns= not significant, SCI-PGB n=6, SCI-Veh. n = 7.

3.4 Nociceptors contribute to SCI-induce neuropathic pain through voltage-gated calcium channels

The α2δ-2 subunit of the voltage-gated calcium channels (VGCCs) is a target of high affinity of PGB. Given nociceptor plasticity correlates with mechanical allodynia, I sought to probe this classical pharmacological mechanism of PGB through genetic means by conditionally knocking out α2δ-2 subunit (CACNA2D2) in nociceptors (utilizing nociceptor specific SNS^{Cre} mice). Male heterozygous (8-12 weeks old) $SNS^{CACNA2D2}$ (n = 9) and control $CACNA2D2^{fl/WT}$ mice (n = 9) underwent moderate T11 spinal cord contusion injury (Figure 18 A). The partial knockout (SCI-Part. KO, $SNS^{CACNA2D2}$) mice showed significantly less response to mechanical stimuli with greater force even before SCI (**** P<0.0001 for 0.6 and 1.4 g, Figure 18 B). After SCI, the partial KO mice did not develop mechanical allodynia (**** P<0.0001 for 0.16 and 0.4 g, Figure 18 C-E) or thermal hyperalgesia (**** P<0.0001, Figure 18 F) for three weeks post-SCI. PEAP confirmed that mechanical allodynia did not develop in partial KO mice (**** P<0.0001, Figure 18 G). Again, motor scores remained similar between the two groups during the entire experiment (Figure 18 H). Interestingly through this mouse breeding only 10.5% of the female offspring were double positive for both SNS^{Cre} and $CACNA2D2^{fl/WT}$ (partial knockout in nociceptors), while 35% of the male offspring were double positive (details in Table 17). Although the breeding efforts produced fewer $SNS^{CACNA2D2}$ females than males, with limited female partial knockout mice (n = 3), a strikingly similar difference as the male mice was observed (Figure 19). These results show the importance of the nociceptor population in conveying mechanical and thermal sensitivity and highlight the role of VGCC α2δ-2 subunit in SCI-induced below-level neuropathic pain.

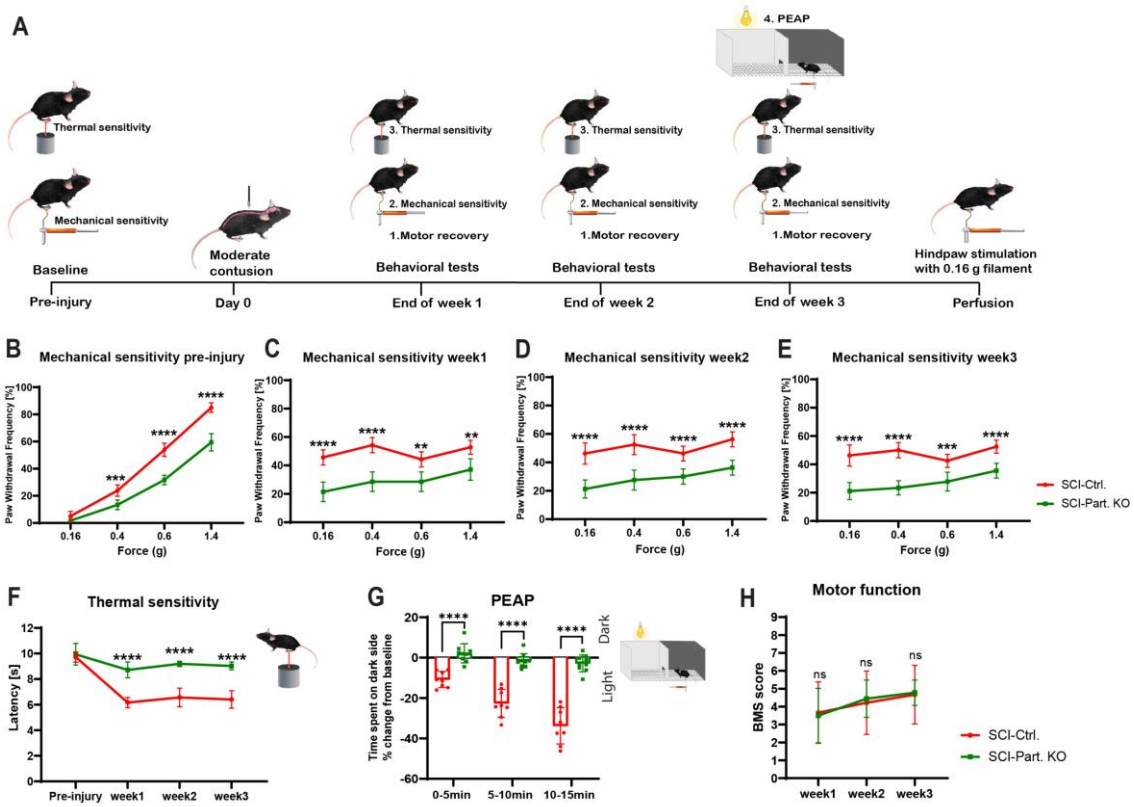

Figure 18 Partial knockout of CACNA2D2 in nociceptors of male mice stops the development of mechanical allodynia and thermal hyperalgesia following SCI. A) Timeline of CACNA2D2 nociceptor partial knockout ($SNS^{CACNA2D2}$) study: Baseline testing followed by a moderate T11 contusion and weekly behavioral tests (BMS, von Frey hair filaments, Hargreaves) for three weeks post-SCI (partial knockout $SNS^{CACNA2D2}$, n=9; control $CACNA2D2^{fl/WT}$, n=9). In the last week mice were additionally tested for PEAP. Prior to perfusion, the hindpaws were stimulated with a non-noxious mechanical stimulus. **B)** Mechanical sensitivity is significantly reduced in partial knockout mice even before SCI occurs (2-way ANOVA with Sidak's pairwise comparisons, *** P<0.001, **** P<0.0001; n=9/group). **C-E)** SCI-induced mechanical allodynia (non-noxious filaments: 0.16 g and 0.4g) exhibited a substantial reduction in partial knockout mice following SCI, and this effect persisted for three weeks post-SCI. (2-Way ANOVA with Sidak's pairwise comparisons; SCI-Ctrl with SCI-Part. KO ** P<0.01, *** P<0.001, **** P<0.0001; week1 n=7/group; week2 n=8/group; week3 partial knockout n=9, control n=8). **F)** Thermal hyperalgesia does not develop in the partial knockout mice for the three weeks post-SCI (2-way ANOVA with Sidak's pairwise comparisons, **** P<0.0001). **G)** PEAP (using 0.16 g filament) confirms that SCI-Part. KO lacks mechanical allodynia development (2-way ANOVA with Sidak's pairwise comparisons, **** P<0.0001, partial knockout n=9, control n=8). **H)** Motor function is not altered in SCI-Part. KO compared to control mice (ns= not significant, n=9/group). Mixed-effects 2-way ANOVA followed by Sidak's post hoc test for mechanical and thermal sensitivity and PEAP, unpaired t-test for motor recovery, mean ± SD.

Table 17. SNS^{CACNA2D2} breeding and offspring details

Sex	Number of pups that reached adulthood	Number of SNS^{CACNA2D2} mice	% SNS^{CACNA2D2}
Female	38	4	10.5%
Male	40	14	35%

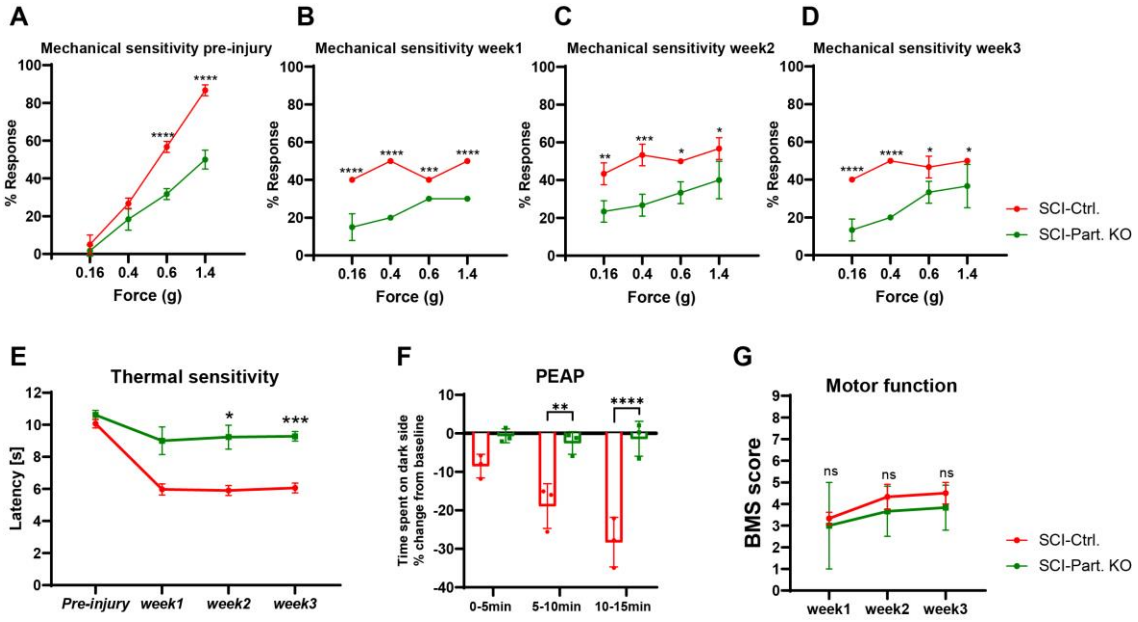

Figure 19 Partial CACNA2D2 nociceptor-specific knockout in female mice has a similar beneficial effect as males after SCI. A) Some mechanical sensitivity is significantly reduced in partial knockout female mice even before SCI occurs (2-way ANOVA with Sidak's pairwise comparisons, **** P<0.0001). **B-D)** SCI-induced mechanical allodynia (non-noxious filaments: 0.16 g and 0.4g) exhibited a substantial reduction in partial knockout mice following SCI, and this effect persisted for three weeks post-SCI. (2-Way ANOVA with Sidak's pairwise comparisons; SCI-Ctrl with SCI-Part. KO **** P<0.0001, *** P<0.001, ** P<0.01, * P<0.05; week1 partial knockout n=2, control n=3; week2 n=3/group; week3 n=3/group). **E)** Thermal hyperalgesia shows a reduction in partial knockout mice following SCI (2-way ANOVA with Sidak's pairwise comparisons, *** P<0.001, * P<0.05) **F)** PEAP (using 0.16 g filament) confirms that SCI-Part. KO lacks mechanical allodynia development (2-way ANOVA with Sidak's pairwise comparisons, **** P<0.0001, ** P<0.01; n=3/group). **G)** Motor function is not altered in SCI-Part. KO compared to control mice (ns= not significant, n=3/group). Mixed-effects 2-way ANOVA followed by Sidak's post hoc test for mechanical and thermal sensitivity and PEAP, unpaired t-test for motor recovery.

To confirm the specificity of this novel knockout, I have shown that there is significantly less CACNA2D2 intensity in TrkA^{+} (marker for nociceptors) fibers (* P<0.05) in partial nociceptor knockout lumbar DRG (L4-L6). Furthermore, no significant difference of CACNA2D2 intensity was observed in non-nociceptive large diameter (≥ 40 µm) TrkA^{-} DRG (Figure 20 A-C)[104,105]. Moreover, the intensity of pCAMKII in TrkA^{+} nociceptors decreased significantly (**** P<0.0001) in the DRG of partial nociceptor knockout mice (Figure 21 A and B). Additionally, in the TrkA^{+} fibers of these mice, there was a significant reduction (** P<0.01) in the nuclear pCREB/CREB (Figure 22 A and B).

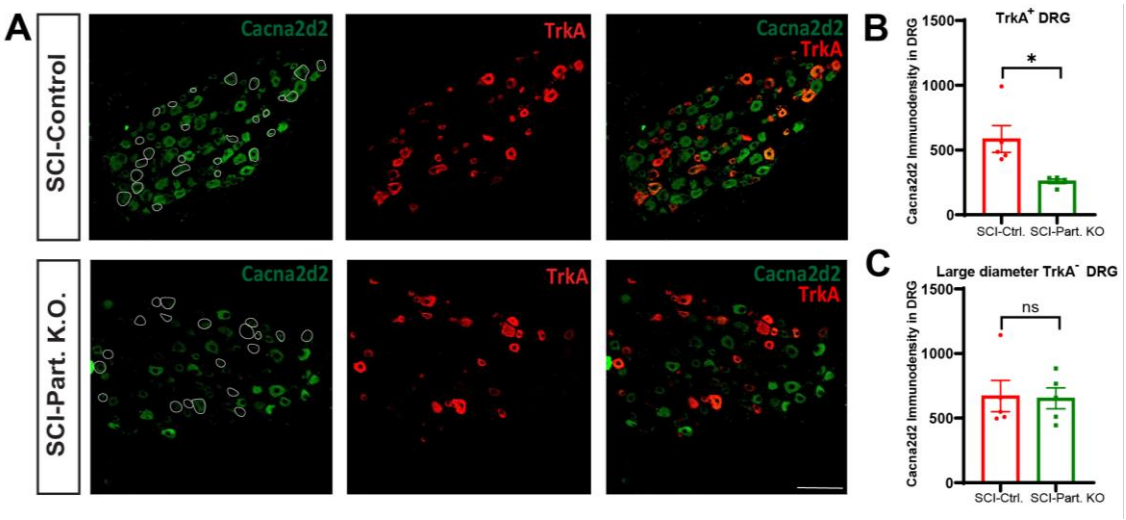

Figure 20 Significant reduction in CACNA2D2 intensity in the nociceptors after partial α2δ-2 subunit of VGCCs nociceptor-specific knockout. A) Immunostaining of L4-L6 DRG for CACNA2D2 and TrkA (Scale bar: 100 µm)**. B)** Partial nociceptor knockout mice have significantly less CACNA2D2 intensity in the nociceptors stained with TrkA. **C)** No difference was observed in CACNA2D2 intensity in large diameter (≥ 40 µm) TrkA^{-} DRG (n = 5/group). Unpaired t-test mean ± SD, * P<0.05, ns= not significant.

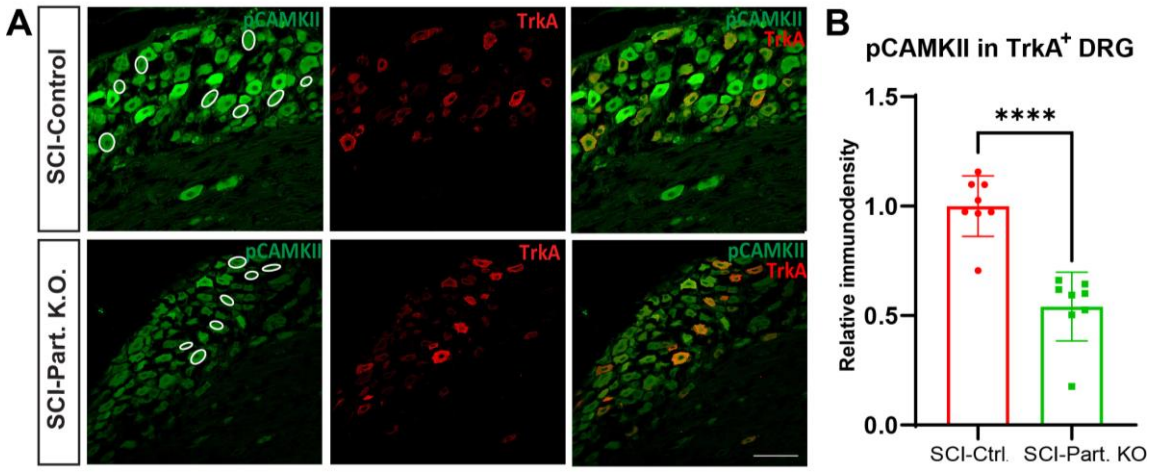

Figure 21 Significant reduction in pCAMKII intensity in the nociceptors after partial α2δ-2 subunit of VGCCs nociceptor-specific knockout. A) Immunostaining of L4-L6 DRG for pCAMKII and TrkA (Scale bar: 100 µm)**. B)** Partial nociceptor knockout mice have significantly less pCAMKII intensity in the nociceptors stained with TrkA (n = 8/group). Unpaired t-test mean ± SD, **** P<0.0001, ns= not significant.

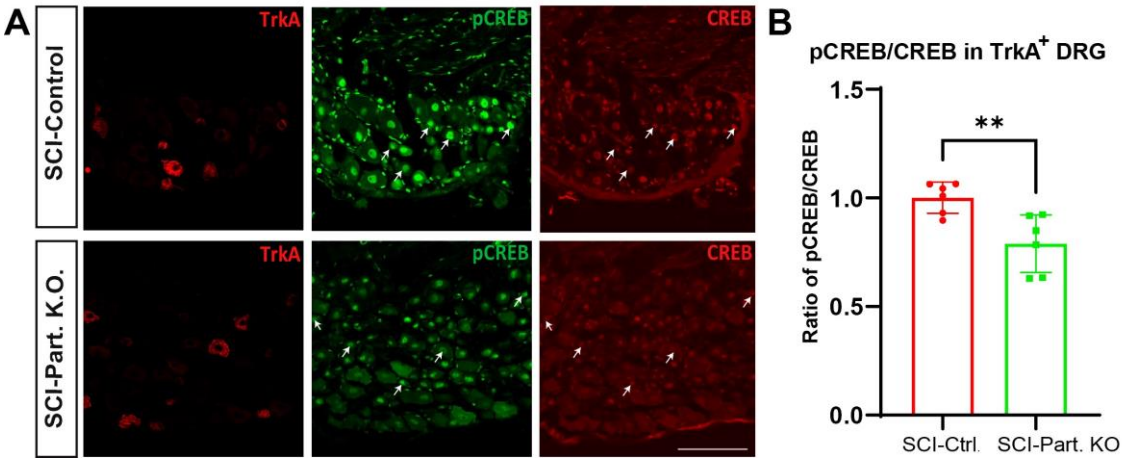

Figure 22 Significant reduction in nuclear pCREB/CREB intensity in the nociceptors after partial α2δ-2 subunit of VGCCs nociceptor-specific knockout. A) Immunostaining of L4-L6 DRG for TrkA, pCREB and CREB (Scale bar: 100 µm)**. B)** Partial nociceptor knockout mice have significantly less pCREB/CREB intensity in the nociceptors stained with TrkA (n = 6/group). Unpaired t-test mean ± SD, ** P<0.01, ns= not significant.

Analysis of the L4-L6 spinal cord indicated that partial knockout SCI male mice exhibited a significant reduction in CGRP^{+} fiber labeling in laminae III-IV (**

P<0.01, Figure 23 A, B). c-fos staining revealed dorsal horn neuronal activation significantly reduced in the SCI-Part. KO mice (P<0.0001) in laminae III-V compared to SCI-control (Figure 23 A and C). This lowered activation resembles what I observed after PGB treatment. No notable distinctions were identified in the intensity of Iba1 within the dorsal horn of the lumbar spinal cord at three weeks post-SCI (Figure 23 D and E). Suggesting that microglia activation is not responsible for the maintenance of SCI-induced mechanical allodynia.

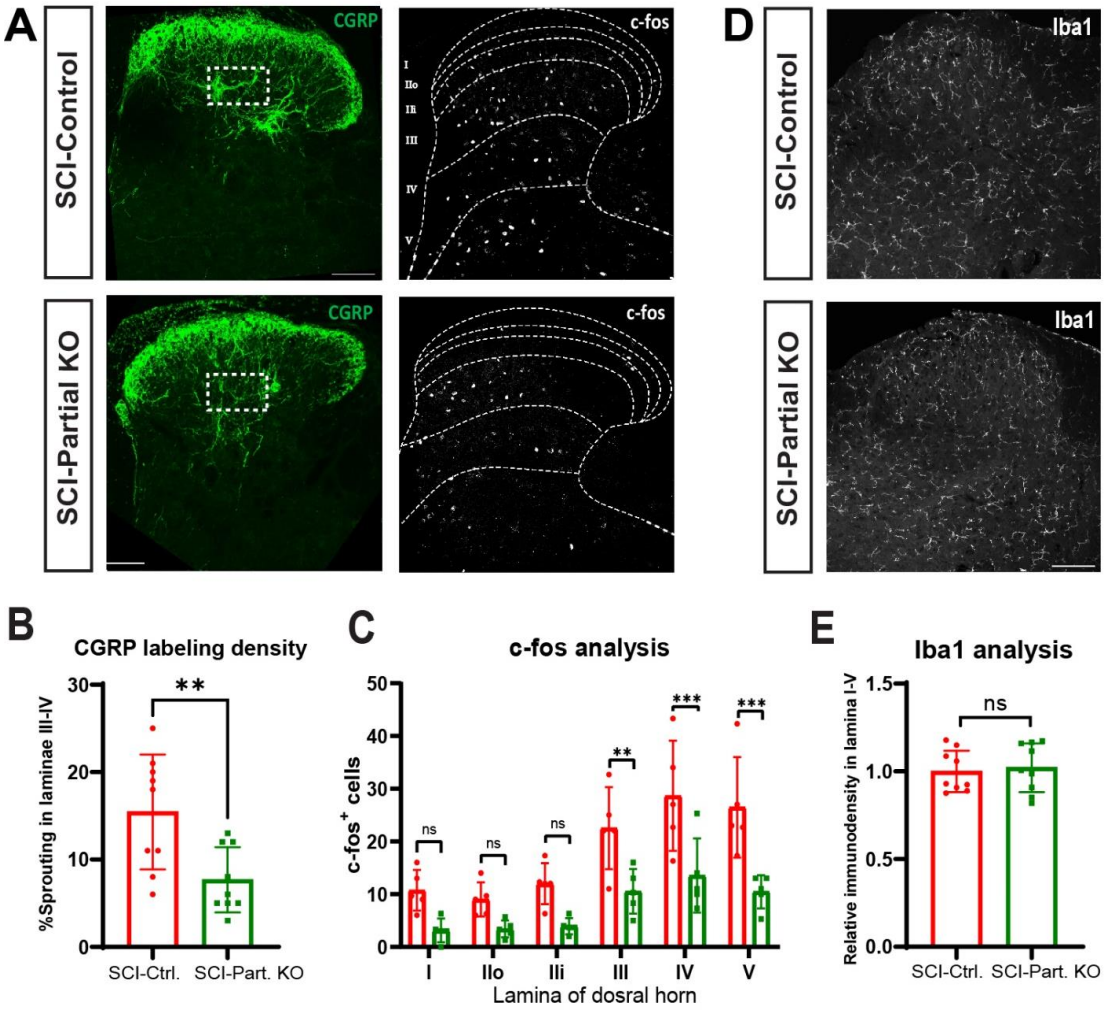

Figure 23 Partial knockout of CACNA2D2 in nociceptors reduces SCI-induced CGRP-expressing fiber plasticity and neuronal activation in laminae III-V but has no effect on Iba1 levels below injury level in the dorsal horn of lumbar spinal cord. A) CGRP and c-fos immunostaining of the dorsal horn of L4-L6 spinal cord of SCI-Part. KO and SCI-Ctrl. male mice (T11 contusion). **B)** Partial knockout of nociceptor CACNA2D2 stopped the aberrant plasticity of CGRP-expressing fibers in laminae III-IV, P=0.0071 (unpaired t-test mean ± SD). **C)** Reduced c-fos$^+$ neuronal activation in partial nociceptor knockout mice (Repeated measures 2-way ANOVA with Sidak's pairwise comparisons; lamina III P=0.0097, lamina IV P=0.0007, lamina V P=0.0003) **D, E)** No significant difference was observed in Iba1 intensity in dorsal horn. Unpaired t-test mean ± SD ** P<0.01, *** P<0.001, ns= not significant, n = 9/group. Scale bar: 100 µm.

Furthermore, I wanted to know if partially inhibiting the nociceptors through CACNA2D2 knockout would also influence other mechanisms of SCI such as the PKCɣ layer. However, similar to PGB study, neither PKCɣ intensity in lamina IIi nor the number of PKCɣ$^+$ cells below lamina IIi were altered (Figure 24 A-C). Furthermore, no significant differences were observed in white matter sparing at lesion epicenter or lesion length, indicating that the observed effects are not due to differences in lesion extent (Figure 25 A-C).

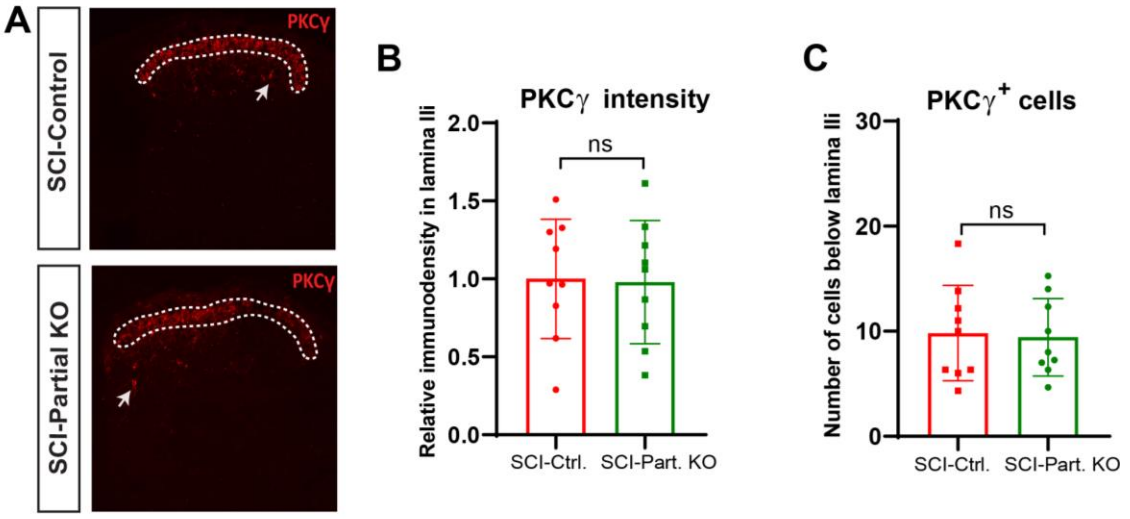

Figure 24 Partial CACNA2D2 nociceptor-specific knockout does not alter PKCγ levels in the lumbar spinal cord after SCI. A) PKCγ immunostaining of the dorsal horn of L4-L6 spinal cords of SCI-Part. KO and SCI-Ctrl. male mice (Scale bar: 100 µm). **B)** Partial nociceptor knockout of the α2δ-2 subunit did not affect PKCγ intensity in lamina IIi. **F)** The number of PKCγ$^+$ cells below lamina IIi were unaffected by partial nociceptor knockout of the α2δ-2 subunit (n = 9/group). Unpaired t-test mean ± SD, ns= not significant.

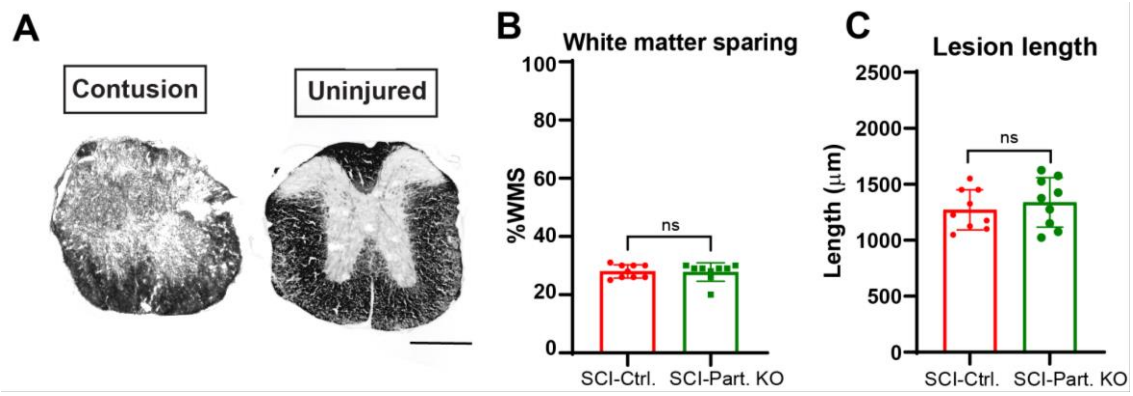

Figure 25 White matter sparing and lesion length remains similar in partial knockout and control mice after SCI. A) Eriochrome cyanine stained coronal sections of SCI and uninjured mice (Scale bar = 500 µm). **B, C)** White matter sparing and lesion length remained similar in control and partial knockout mice (n = 9/group). Unpaired t-test mean ± SD, ns= not significant.

Discussion

4. Discussion

The present work demonstrates the important role that uninjured peripheral nociceptors play in the development of below level neuropathic pain following SCI. Medical intervention through prophylactic PGB treatment can alleviate neuropathic pain and limit the plasticity of nociceptors below the SCI level. Furthermore, limiting the activation of nociceptors by knocking down PGB target α2δ-2 subunit of VGCCs specifically in nociceptors, disrupts the arousal of SCI-induced neuropathic pain as well as the aberrant plasticity of nociceptors.

4.1 Nociceptors plasticity contributes to neuropathic pain

The findings of my study provide insights into the structural plasticity of nociceptors following SCI and its correlation with neuropathic pain. This study shows that following a spinal cord contusion there is a significant increase in the volume of nociceptors in laminae III, IV, and V of the dorsal horn, indicating ventral sprouting, which is associated with the development of mechanical allodynia and thermal hyperalgesia.

Studies have reported that approximately 80% (82 ± 3.0%) of all DRG neurons express $SNS^{tdTomato}$, categorized into peptidergic and non-peptidergic fibers with nociceptive functions[104]. Specifically, about 50% (45.1 ± 3.9%) of $SNS^{tdTomato+}$ fibers have been identified as $CGRP^{+}$ (peptidergic)[104]. Given the potential argument that CGRP levels might rise following SCI, I have used $SNS^{tdTomato}$ animals to discount the possibility of increased CGRP release being responsible for the observed structural changes, which show an increase in nociceptive fiber volume. In line with my findings, prior research has established a compelling association between mechanical allodynia, thermal hypersensitivity, and aberrant plasticity of the nociceptive fibers in the dorsal horn. This correlation underscores the intricate interplay between sensory modalities and the maladaptive changes occurring in deeper regions of the spinal cord[80,91,92,106]. Furthermore, nociceptors display hypersensitivity after SCI in both rodents and patients with neuropathic pain[81], which indicates the important role they might

play in SCI-neuropathic pain. Confirming the central role of nociceptors, I noticed that reducing the activity of these fibers through a knockout approach led to a decrease in both neuropathic pain and the maladaptive structural changes associated with it.

Moreover, it is documented that following chronic constriction injury, the injection of semaphorin, a repulsive axonal guidance factor, into the spinal cord resulted in the attenuation of mechanical allodynia and heat hyperalgesia, along with a decrease in nociceptive fiber density within the deep dorsal horn[107]. Furthermore, antisense oligodeoxynucleotide knockdown of $Na_v1.8$ (nociceptor specific) after SCI, suppressed the spontaneous activity of the DRG and reduced ongoing SCI mechanical and thermal pain[108].

Interestingly I observed a significant increase in the volume of nociceptors in laminae III-V after SCI. Based on my observations there was a 1.06-fold increase in laminae I-IIi, a 2.65-fold increase in lamina III, a 1.79-fold increase in lamina IV, and a 1.57-fold increase in lamina V after SCI. Confirming these observations, Brennan et al.[89] have shown that SCI leads to a 1.2-fold increase in the proportional area of $CGRP^+$ fibers in laminae I–II and a 1.5-fold increase in laminae III–V compared to sham levels. Additionally, through c-fos staining I found that laminae III-V show the highest level of activation following SCI. These laminae house a large population of WDR neurons involved in transmitting pain signals. The WDR neurons play a significant role in the development and maintenance of neuropathic pain following SCI. Research suggests that SCI can trigger hyperexcitability in WDR neurons, contributing to the induction and maintenance of central neuropathic pain[109,110]. The abnormal plasticity of $CGRP^+$ nociceptors could potentially contribute to increased input to WDR neurons, thereby enhancing pain signal transmission via the spinothalamic tract[14].

4.2 Effect of Gabapentinoids on nociceptor plasticity and neuropathic pain

I have shown that following SCI, prophylactic PGB treatment can stop the arousal of mechanical allodynia and reduce the sprouting of peptidergic ($CGRP^+$) nociceptors into the deeper laminae of the dorsal horn. Furthermore, in the PGB treated mice, there was a significant reduction in c-fos staining specially in laminae IIi-V. Interestingly, it has been demonstrated that gabapentinoids have preferential impact on specific subsets of DRG neurons, specifically small $IB4^-$ (peptidergic), and medium-sized neurons displayed greater sensitivity to the effects of gabapentinoids compared to large and small $IB4^+$ neurons (non-peptidergic)[111]. Similar to my observations, Brennan et al.[89] did not observe $CGRP^+$ fiber plasticity in SCI mice treated with GBP.

Even though some studies suggest that PGB can help with motor recovery after SCI[112], I did not observe any effect on motor function of the PGB treated mice. However, it should be noted that the BMS is a very general score and not detailed enough to distinguish between fine motor functions. Therefore, I cannot conclude that PGB did not have any effect on fine motor function. Moreover, in all my studies involving PGB, treatment was administered for only one week. It's possible that a longer treatment duration, as observed in the other study, may be necessary to actualize effects on motor recovery.

α2δ proteins have been shown to be key regulators of synapse formation and plasticity[113]. Apart from their functions as auxiliary subunits of VGCCs in synaptic transmission, these proteins also play multiple postsynaptic roles in promoting synapse formation, facilitating trans-synaptic communication, and modulating the function of glutamate receptors[28,29,114–118]. Therefore, the sustained effects of PGB treatment on reducing mechanical allodynia and nociceptor fiber plasticity even after the cessation of treatment may be attributed to modulation of maladaptive synaptic formation post-SCI.

Since α2δ-1 expression extends beyond neurons, it should be considered that the possibility that the advantageous effects of PGB may also arise from other α2δ-1-dependent mechanisms that are not directly linked to synapses.

Importantly, it is worth noting that α2δ-1 exhibits expression in non-CNS tissues, including cardiac tissue, smooth muscle, and endocrine organs[35]. In contrast, α2δ-2 is primarily found in the CNS[35]. GBP and PGB, both interact with VGCCs; however, they exhibit selectivity for different α2δ calcium channel subunits. Specifically, GBP demonstrates a stronger affinity for the α2δ-1 subunit, whereas PGB displays greater specificity for α2δ-2[53]. Therefore, my attention was directed towards α2δ-2 subunit of nociceptors and I used transgenic knockout mice to study them further.

4.3 Effect of α2δ-2 subunit of VGCCs on nociceptor plasticity and neuropathic pain

α2δ subunit plays a pivotal role in modulating the excitability of DRG neurons and the manifestation of neuropathic pain[33]. For instance, when mice are genetically modified to overexpress the α2δ-1 subunit, they exhibit a neuropathic phenotype characterized by hyperalgesia and tactile allodynia even in the absence of nerve injury. Interestingly, Cacna2d2, which encodes α2δ-2 subunit, demonstrates predominant expression in the peptidergic population of nociceptors, while Cacna2d1 (which encodes α2δ-1) is expressed in both peptidergic and non-peptidergic nociceptors[104]. A recent study with Cacna2d2 KO mice indicates isoform-specific functions that α2δ-1 cannot compensate for. This suggests that various α2δ isoforms might have different functional roles[119].

Importantly, I showed even a partial knockout of α2δ-2 in nociceptors results in a strikingly similar pattern of alleviation of mechanical allodynia and aberrant plasticity as prophylactic PGB treatment. Moreover, α2δ-2 partial knockout mice exhibited a more pronounced effect on the reduction of thermal sensitivity compared to PGB treatment. Comparable to prophylactic PGB treatment, the partial knockout mice exhibited a significant reduction in the plasticity of $CGRP^{+}$ nociceptors in the deeper laminae of the dorsal horn. Furthermore, a similar pattern of c-fos activation was observed in the partial knockout and the PGB treated mice, confirming the important role of nociceptors

in response to mechanical allodynia. Furthermore, this validates that the deeper laminae of the dorsal horn are involved in transmission of mechanical allodynia. PGB could influence various neuronal populations, potentially affecting growth patterns, however, the selective impact on nociceptors in partial KO mice suggests that the observed effects stem from nociceptor activity reduction, thereby internally diminishing growth.

I have also shown that in the partial knockout mice, there is a significant reduction in the intensity of pCAMKII as well as nuclear pCREB/CREB in the $TrkA^+$ nociceptors, suggesting that Ca^{2+} signaling could be reduced in nociceptors of these mice. Reinforcing my observations, the data obtained from *in vitro* expression studies strongly implies that the disruption of α2δ-2 expression in ducky mice (complete knockout of Cacna2d2) leads to a decrease in the Ca^{2+} channel current in cells expressing Cacna2d2. Electrophysiological recordings show that in mutant ducky mice, Purkinje cells, which highly express $Ca_v2.1$[27,31,113], have ∼30% reduced somatic calcium currents[27]. Moreover, measurements conducted on inner hair cells of the spontaneous Cacna2d2 mutant ducky mice demonstrate a reduction in exocytosis[114]. In addition to the reduction in somatic calcium current, du^{2j}/du^{2j} mice displayed a significant decline in spontaneous Purkinje cell firing and a decrease in firing regularity, indicating a broader impact on neuronal activity. Moreover, these mice displayed changes in the expression levels of various genes linked to Purkinje cell function, such as a decrease in tenascin-C gene expression. Interestingly, $du^{2J}/+$ mice show a significant reduction in firing rate in Purkinje cells, correlating with the observed reduction in α2δ-2[120].

4.4 Role of microglia in neuropathic pain

Spinal microglia are recognized for their rapid response to nerve injury, primarily due to the membrane expression of a diverse array of receptor proteins involved in detecting damage-associated molecular patterns[121]. Studies indicate a significant rise in Iba1 expression levels at 7 days post SCI[122], alongside increased Iba1 mRNA expression in the spinal cord at different time points after

contusion[123]. My findings are in accordance with other studies which show that gabapentinoids reduce inflammatory mediators[95–98]. According to studies, there might be a sex-dependent aspect to inflammatory responses following SCI[124]. However, I did not observe any significant differences. The α2δ-1 and α2δ-2 subunits are not expressed in microglia or astrocytes[78,125], therefore, the effect of gabapentinoids on microglia is believed to be indirect[75] through reduced neuronal activation by inhibiting the calcium channel currents[126].

My finding indicates that PGB exerts an influence on microglial activation, a key component of neuroinflammation, in both sexes. By observing decreased Iba1 intensity, it could be inferred that PGB contributes to the modulation of microglial reactivity, potentially leading to an alleviation of pain in both male and females. However, my findings in the PGB discontinuation study with females imply that upon discontinuation of PGB, the previously observed reduction in Iba1 intensity regresses, thereby indicating that the sustained effects on mitigating mechanical allodynia and inhibiting $CGRP^+$ fiber plasticity cannot be solely attributed to alterations in Iba1 levels. Moreover, three weeks post-SCI, no notable difference in Iba-1 levels was detected in partial KO mice. This suggests that PGB's mechanism for reducing inflammation may extend beyond its impact solely on nociceptors, potentially involving broader pathways.

4.5 Further mechanisms of neuropathic pain

SCI leads to reduced inhibitory control in the spinal cord. It has been shown that SCI leads to downregulation of Cl^- extruder KCC2 in the spinal cord segments below the injury level. A downregulation in dorsal horn is correlated with allodynia and a downregulation in ventral horn is corelated with spasticity[101,127]. Training after injury can upregulate KCC2, leading to beneficial effects on spasticity and allodynia[102]. However, I observe no significant effect on KCC2 intensity following prophylactic PGB treatment.

PGB has also been suggested to have neuroprotective effects[93–95]. I have investigated possible neuroprotective effects of prophylactic PGB in the lesion

area as well as the descending 5-HT fibers of the lumbar spinal cord. I did not observe any effect on lesion length or the white matter sparing, suggesting negligible neuroprotection at the site of injury in both the one-week PGB study and the 3-week PGB discontinuation study. Furthermore, I investigated possible PGB neuroprotective effects on 5HT axons, which originate from the brainstem and are often impaired after SCI. Damaged 5HT neurons could be involved in the autonomic hyperreflexia, spasms and chronic pain after SCI[103,128]. However, in my studies PGB did not show any impact on the overall extent of 5HT distribution in the lumbar gray matter. However, extended treatment and observation periods may be necessary to comprehensively evaluate PGB's neuroprotective effects. In the study by Assis et al.[93], PGB treatment was administered for nearly one month. Moreover, outcomes could be influenced by factors such as the type and severity of injury.

Studies have suggested that another mediator of mechanical allodynia is PKCγ expressing excitatory interneurons of lamina IIi, and that PKCγ expression and the number of PKCγ$^+$ cells in regions outside of lamina IIi increase after SCI[99,100]. However, I did not observe any significant effect of PGB treatment or partial KO of α2δ-2 subunit on PKCγ intensity or the number of PKCγ$^+$ cells. All these observations suggest that although neuropathic pain is a complex and multifactorial pathophysiology, and many different factors may be involved, nociceptor activation and aberrant plasticity could be one of the main mechanisms involved. Therefore, future studies blocking the activation of peripheral nociceptors could lead to potential novel treatments for below level neuropathic pain after SCI.

4.6 Sex differences in neuropathic pain development

Affirming the observations of McFarlane et al.[129], my studies revealed no indications of sex differences in the development of neuropathic pain nor the mechanisms of pain alleviation. Both males and females exhibited similar responses in the arousal of SCI-induced neuropathic pain and its prevention through prophylactic PGB treatment. For the impact of prophylactic

treatment on thermal sensitivity, I noted a trend among females, but no significant difference was observed compared to control mice in the one-week PGB study. However, a significant difference emerged in males. I believe this discrepancy may be attributed to variations and the lower number of female mice at the one-week post-injury time point. The validation of prophylactic PGB's significant effect on female thermal sensitivity at the one-week post-injury timepoint is supported by a PGB discontinuation study conducted on females, where a notable reduction in thermal sensitivity was observed one-week post-injury after PGB prophylactic treatment. Therefore, I believe that the small differences observed can not be attributed to sex differences. It should be noted that I observed a lower number of PKCγ^{+} cells below lamina IIi in male mice compared to females. This was unexpected, as I anticipated more cells in males due to the staining and imaging method used (free-floating with thicker sections and Z-stack imaging in males). However, because the staining and imaging techniques differed between males and females, direct comparison into this potential difference was not possible and further investigation is warranted.

Conclusions

and

Future Perspective

5. Conclusions and Future Perspective

My study reveals the direct role of nociceptor plasticity post-SCI in causing the onset of mechanical allodynia and thermal hyperalgesia. The subsequent exploration of PGB treatment effectively prevented the development of mechanical allodynia in both female and male mice, with surprisingly sustained effects even 2 weeks after discontinuation. Prophylactic PGB had a lasting effect on stopping the $CGRP^+$ nociceptor fiber aberrant plasticity even after discontinuation. Furthermore, the impact of PGB on the acute modulation of microglial activation provides crucial insights into the multifaceted nature of neuropathic pain.

This study further explored aberrant nociceptive plasticity by selectively knocking out the α2δ-2 subunit of VGCCs in nociceptors. The partial knockout mice exhibited resistance to mechanical and thermal hyperalgesia, but also showed reduction in $CGRP^+$ nociceptor fiber plasticity. These results validate the role of the α2δ-2 subunit in conveying SCI-induced mechanical and thermal sensitivity.

The altered state of nociceptors emerges as a key player in the amplification and perpetuation of neuropathic pain signals. These findings support the significance of nociceptors in the development of neuropathic pain after SCI. Prophylactic treatment with PGB not only alleviates pain but also limits the plasticity of nociceptors, emphasizing the therapeutic potential of targeting nociceptor activation.

Looking ahead, further investigation is needed to identify the specific neuronal populations that exhibit c-fos activation following mechanical allodynia. Furthermore, electrophysiological studies of the partial KO mice may reveal alterations in action potential firing, synaptic transmission, and pain-related neuronal activity, providing valuable insights into the specific contributions of α2δ-2 subunits to nociceptor function and pain processing. Moreover, RNAseq of the DRG of these mice could reveal significant insights into the alterations in gene expression profiles that may underlie the observed changes in nociceptor function and pain sensitivity post-SCI. Additionally, investigating the long-term

implications of PGB treatment and the specific signaling pathways involved in the prevention of neuropathic pain could enhance our understanding and guide the development of more targeted therapies. Furthermore, studies in the future could focus on potential beneficial effects of specific $Na_v1.8$ inhibitors to block nociceptor hyperexcitability, dorsal horn plasticity and neuropathic pain.

Bibliography

6. Bibliography

1. Palandi, J., Bobinski, F., de Oliveira, G. M. & Ilha, J. Neuropathic pain after spinal cord injury and physical exercise in animal models: A systematic review and meta-analysis. *Neurosci Biobehav Rev* **108**, 781–795 (2020).

2. Burke, D., Fullen, B. M., Stokes, D. & Lennon, O. Neuropathic pain prevalence following spinal cord injury: A systematic review and meta-analysis. *European Journal of Pain* **21**, 29–44 (2017).

3. Hagen, E. M. & Rekand, T. Management of Neuropathic Pain Associated with Spinal Cord Injury. *Pain Ther* **4**, 51–65 (2015).

4. van Velzen, M., Dahan, A. & Niesters, M. Neuropathic Pain: Challenges and Opportunities. *Frontiers in Pain Research* **1**, 566258 (2020).

5. Emery, E. C. & Ernfors, P. Dorsal root ganglion neuron types and their functional specialization. *The Oxford Handbook of the Neurobiology of Pain, J.N. Wood, ed. (Oxford University Press)* (2018).

6. Li, C., Wang, S., Chen, Y. & Zhang, X. Somatosensory Neuron Typing with High-Coverage Single-Cell RNA Sequencing and Functional Analysis. *Neurosci Bull* **34**, 200–207 (2018).

7. Ma, Q. A functional subdivision within the somatosensory system and its implications for pain research. *Neuron110* **110**, 749–769 (2022).

8. Kupari, J. *et al.* Single cell transcriptomics of primate sensory neurons identifies cell types associated with chronic pain. *Nature Communications 2021 12:1* **12**, 1–15 (2021).

9. Li, C. L. *et al.* Somatosensory neuron types identified by high-coverage single-cell RNA-sequencing and functional heterogeneity. *Cell Research 2016 26:1* **26**, 83–102 (2015).

10. Usoskin, D. *et al.* Unbiased classification of sensory neuron types by large-scale single-cell RNA sequencing. *Nature Neuroscience 2014 18:1* **18**, 145–153 (2014).

11. Sharma, N. *et al.* The emergence of transcriptional identity in somatosensory neurons. *Nature 2020 577:7790* **577**, 392–398 (2020).

12. Sengul, G. & Watson, C. Ascending and Descending Pathways in the Spinal Cord. *The Rat Nervous System: Fourth Edition* 115–130 (2015) doi:10.1016/B978-0-12-374245-2.00008-5.

13. Watson, C., George, P. & Gulgun, K. The Spinal Cord: A Christopher and Dana Reeve Foundation Text and Atlas. *Academic press* https://books.google.de/books?hl=en&lr=&id=uxw3Li9067wC&oi=fnd&pg=PP1&dq=the+spinal+cord+a+christopher+and+dana+reeve+foundation+text+and+atlas&ots=NuMhu8wi9M&sig=5GvQeSqGIVnkt445ogqodfhN8_s&redir_esc=y#v=onepage&q=the%20spinal%20cord%20a%20christopher%20and%20dana%20reeve%20foundation%20text%20and%20atlas&f=false (2009).

14. Liu, F. Y. *et al.* Electrophysiological properties of spinal wide dynamic range neurons in neuropathic pain rats following spinal nerve ligation. *Neurosci Bull* **27**, 1 (2011).

15. Price, D. D. Spinothalamic Tract Neurons, in Deep Dorsal Horn. *Encyclopedia of Pain* 2278–2282 (2007) doi:10.1007/978-3-540-29805-2_4173.

16. Price, D. D. & Dubner, R. Neurons that subserve the sensory-discriminative aspects of pain. *Pain* **3**, 307–338 (1977).

17. Price, D. D., Dubner, R. & Hu, J. W. Trigeminothalamic neurons in nucleus caudalis responsive to tactile, thermal, and nociceptive stimulation of monkey's face. *https://doi.org/10.1152/jn.1976.39.5.936* **39**, 936–953 (1976).

18. Price, D. D., Hayes, R. L., Ruda, M. & Dubner, R. Spatial and temporal transformations of input to spinothalamic tract neurons and their relation to somatic sensations. *https://doi.org/10.1152/jn.1978.41.4.933* **41**, 933–947 (1978).

19. Coghill, R. C., Mayer, D. J. & Price, D. D. The roles of spatial recruitment and discharge frequency in spinal cord coding of pain: a combined electrophysiological and imaging investigation. *Pain* **53**, 295–309 (1993).

20. Khasabov, S. G. *et al.* Spinal Neurons that Possess the Substance P Receptor Are Required for the Development of Central Sensitization. *Journal of Neuroscience* **22**, 9086–9098 (2002).

21. Suzuki, R., Morcuende, S., Webber, M., Hunt, S. P. & Dickenson, A. H. Superficial NK1-expressing neurons control spinal excitability through activation of descending pathways. *Nature Neuroscience 2002 5:12* **5**, 1319–1326 (2002).

22. Dolphin, A. C. Voltage-gated calcium channel α2δ subunits: an assessment of proposed novel roles. *F1000Res* **7**, (2018).

23. Arikkath, J. & Campbell, K. P. Auxiliary subunits: essential components of the voltage-gated calcium channel complex. *Curr Opin Neurobiol* **13**, 298–307 (2003).

24. Patel, R. & Dickenson, A. H. Mechanisms of the gabapentinoids and α2δ-1 calcium channel subunit in neuropathic pain. *Pharmacol Res Perspect* **4**, e00205 (2016).

25. Kadurin, I. *et al.* Proteolytic maturation of α2δ represents a checkpoint for activation and neuronal trafficking of latent calcium channels. *Elife* **5**, (2016).

26. Brodbeck, J. *et al.* The ducky mutation in Cacna2d2 results in altered Purkinje cell morphology and is associated with the expression of a truncated α2δ-2 protein with abnormal function. *Journal of Biological Chemistry* **277**, 7684–7693 (2002).

27. Barclay, J. *et al.* Ducky Mouse Phenotype of Epilepsy and Ataxia Is Associated with Mutations in the Cacna2d2 Gene and Decreased Calcium Channel Current in Cerebellar Purkinje Cells. *Journal of Neuroscience* **21**, 6095–6104 (2001).

28. Eroglu, Ç. *et al.* Gabapentin Receptor α2δ-1 Is a Neuronal Thrombospondin Receptor Responsible for Excitatory CNS Synaptogenesis. *Cell* **139**, 380–392 (2009).

29. Kurshan, P. T., Oztan, A. & Schwarz, T. L. Presynaptic α2δ-3 is required for synaptic morphogenesis independent of its Ca2+-channel functions. *Nat Neurosci* **12**, 1415–1423 (2009).

30. Hoppa, M. B., Lana, B., Margas, W., Dolphin, A. C. & Ryan, T. A. α2δ expression sets presynaptic calcium channel abundance and release probability. *Nature* **486**, 122–125 (2012).

31. Cole, R. L. *et al.* Differential distribution of voltage-gated calcium channel alpha-2 delta (α2δ) subunit mRNA-containing cells in the rat central nervous system and the dorsal root ganglia. *Journal of Comparative Neurology* **491**, 246–269 (2005).

32. Taylor, C. P. & Garrido, R. Immunostaining of rat brain, spinal cord, sensory neurons and skeletal muscle for calcium channel alpha2-delta (α2-δ) type 1 protein. *Neuroscience* **155**, 510–521 (2008).

33. Li, C. Y. *et al.* Calcium channel α2δ1 subunit mediates spinal hyperexcitability in pain modulation. *Pain* **125**, 20–34 (2006).

34. Bauer, C. S. *et al.* The Increased Trafficking of the Calcium Channel Subunit α2δ-1 to Presynaptic Terminals in Neuropathic Pain Is Inhibited by the α2δ Ligand Pregabalin. *Journal of Neuroscience* **29**, 4076–4088 (2009).

35. Dolphin, A. C. The α2δ subunits of voltage-gated calcium channels. *Biochimica et Biophysica Acta (BBA) - Biomembranes* **1828**, 1541–1549 (2013).

36. Perkins, J. R. *et al.* A comparison of RNA-seq and exon arrays for whole genome transcription profiling of the L5 spinal nerve transection model of neuropathic pain in the rat. *Mol Pain* **10**, (2014).

37. Newton, R. A., Bingham, S., Case, P. C., Sanger, G. J. & Lawson, S. N. Dorsal root ganglion neurons show increased expression of the calcium channel α2δ-1 subunit following partial sciatic nerve injury. *Molecular Brain Research* **95**, 1–8 (2001).

38. Luo, Z. D. *et al.* Upregulation of Dorsal Root Ganglion α2δ Calcium Channel Subunit and Its Correlation with Allodynia in Spinal Nerve-Injured Rats. *Journal of Neuroscience* **21**, 1868–1875 (2001).

39. Patel, R. *et al.* α2δ-1 Gene Deletion Affects Somatosensory Neuron Function and Delays Mechanical Hypersensitivity in Response to Peripheral Nerve Damage. *Journal of Neuroscience* **33**, 16412–16426 (2013).

40. Lawson, S. N. Phenotype and function of somatic primary afferent nociceptive neurones with C-, Aδ- or Aα/β-fibres. *Exp Physiol* **87**, 239–244 (2002).

41. Li, C. Y., Song, Y. H., Higuera, E. S. & Luo, Z. D. Spinal Dorsal Horn Calcium Channel α2δ-1 Subunit Upregulation Contributes to Peripheral Nerve Injury-Induced Tactile Allodynia. *Journal of Neuroscience* **24**, 8494–8499 (2004).

42. Wang, H. *et al.* Chronic neuropathic pain is accompanied by global changes in gene expression and shares pathobiology with neurodegenerative diseases. *Neuroscience* **114**, 529–546 (2002).

43. Boroujerdi, A. *et al.* Injury discharges regulate calcium channel alpha-2-delta-1 subunit upregulation in the dorsal horn that contributes to initiation of neuropathic pain. *Pain* **139**, 358–366 (2008).

44. Li, Z. *et al.* Pregabalin is a potent and selective ligand for α2δ-1 and α2δ-2 calcium channel subunits. *Eur J Pharmacol* **667**, 80–90 (2011).

45. Bockbrader, H. N. *et al.* A comparison of the pharmacokinetics and pharmacodynamics of pregabalin and gabapentin. *Clin Pharmacokinet* **49**, 661–669 (2010).

46. Taylor, C. P., Angelotti, T. & Fauman, E. Pharmacology and mechanism of action of pregabalin: The calcium channel α2–δ (alpha2–delta) subunit as a target for antiepileptic drug discovery. *Epilepsy Res* **73**, 137–150 (2007).

47. Lanneau, C. *et al.* Gabapentin is not a GABAB receptor agonist. *Neuropharmacology* **41**, 965–975 (2001).

48. Jensen, A. A. *et al.* The Anticonvulsant Gabapentin (Neurontin) Does Not Act through γ-Aminobutyric Acid-B Receptors. *Mol Pharmacol* **61**, 1377–1384 (2002).

49. Tong, C. *et al.* Pregabalin and Gabapentin in Patients with Spinal Cord Injury-Related Neuropathic Pain: A Network Meta-Analysis. *Pain Ther* **10**, 1497 (2021).

50. Davari, M. *et al.* Pregabalin and gabapentin in neuropathic pain management after spinal cord injury: a systematic review and meta-analysis. *Korean J Pain* **33**, 3 (2020).

51. Marais, E., Klugbauer, N. & Hofmann, F. Calcium Channel α2δ Subunits—Structure and Gabapentin Binding. *Mol Pharmacol* **59**, 1243–1248 (2001).

52. Cheng, J. K. & Chiou, L. C. Mechanisms of the Antinociceptive Action of Gabapentin. *J Pharmacol Sci* **100**, 471–486 (2006).

53. Gong, H. C., Hang, J., Kohler, W., Li, L. & Su, T. Z. Tissue-specific expression and gabapentin-binding properties of calcium channel α2δ subunit subtypes. *Journal of Membrane Biology* **184**, 35–43 (2001).

54. Dooley, D. J., Donovan, C. M. & Pugsley, T. A. Stimulus-dependent modulation of norepinephrine release from rat neocortical slices by gabapentin and pregabalin. *Journal of Pharmacology and Experimental Therapeutics* **295**, 1086–1093 (2000).

55. Dooley, D. J., Mieske, C. A. & Borosky, S. A. Inhibition of K+-evoked glutamate release from rat neocortical and hippocampal slices by gabapentin. *Neurosci Lett* **280**, 107–110 (2000).

56. Fink, K. *et al.* Inhibition of neuronal Ca2+ influx by gabapentin and pregabalin in the human neocortex. *Neuropharmacology* **42**, 229–236 (2002).

57. Tran-Van-Minh, A. & Dolphin, A. C. The α2δ Ligand Gabapentin Inhibits the Rab11-Dependent Recycling of the Calcium Channel Subunit α2δ-2. *Journal of Neuroscience* **30**, 12856–12867 (2010).

58. Hendrich, J. *et al.* Pharmacological disruption of calcium channel trafficking by the α2δ ligand gabapentin. *Proc Natl Acad Sci U S A* **105**, 3628–3633 (2008).

59. Heblich, F., Van Minh, A. T., Hendrich, J., Watschinger, K. & Dolphin, A. C. Time course and specificity of the pharmacological disruption of the trafficking of voltage-gated calcium channels by gabapentin. *Channels* **2**, 4–9 (2008).

60. Cassidy, J. S., Ferron, L., Kadurin, I., Pratt, W. S. & Dolphin, A. C. Functional exofacially tagged N-type calcium channels elucidate the interaction with auxiliary α2δ-1 subunits. *Proc Natl Acad Sci U S A* **111**, 8979–8984 (2014).

61. Miranpuri, G. S. *et al.* Role of Microglia and Astrocytes in Spinal Cord Injury Induced Neuropathic Pain. *Ann Neurosci* **28**, 219–228 (2021).

62. Tateda, S. *et al.* Rapamycin suppresses microglial activation and reduces the development of neuropathic pain after spinal cord injury. *Journal of Orthopaedic Research* **35**, 93–103 (2017).

63. Schomberg, D. & Olson, J. K. Immune responses of microglia in the spinal cord: Contribution to pain states. *Exp Neurol* **234**, 262–270 (2012).

64. Gwak, Y. S. & Hulsebosch, C. E. Remote astrocytic and microglial activation modulates neuronal hyperexcitability and below-level neuropathic pain after spinal injury in rat. *Neuroscience* **161**, 895–903 (2009).

65. Detloff, M. R. *et al.* Remote activation of microglia and pro-inflammatory cytokines predict the onset and severity of below-level neuropathic pain after spinal cord injury in rats. *Exp Neurol* **212**, 337–347 (2008).

66. Hains, B. C. & Waxman, S. G. Development/Plasticity/Repair Activated Microglia Contribute to the Maintenance of Chronic Pain after Spinal Cord Injury. (2006) doi:10.1523/JNEUROSCI.0003-06.2006.

67. Jin, S. X., Zhuang, Z. Y., Woolf, C. J. & Ji, R. R. p38 Mitogen-Activated Protein Kinase Is Activated after a Spinal Nerve Ligation in Spinal Cord Microglia and Dorsal Root Ganglion Neurons and Contributes to the Generation of Neuropathic Pain. *Journal of Neuroscience* **23**, 4017–4022 (2003).

68. Okubo, M. *et al.* Macrophage-Colony Stimulating Factor Derived from Injured Primary Afferent Induces Proliferation of Spinal Microglia and Neuropathic Pain in Rats. *PLoS One* **11**, e0153375 (2016).

69. Guan, Z. *et al.* Injured sensory neuron–derived CSF1 induces microglial proliferation and DAP12-dependent pain. *Nature Neuroscience 2016 19:1* **19**, 94–101 (2015).

70. Scholz, J. & Woolf, C. J. The neuropathic pain triad: neurons, immune cells and glia. *Nature Neuroscience 2007 10:11* **10**, 1361–1368 (2007).

71. Trang, T., Beggs, S., Wan, X. & Salter, M. W. P2X4-Receptor-Mediated Synthesis and Release of Brain-Derived Neurotrophic Factor in Microglia Is Dependent on Calcium and p38-Mitogen-Activated Protein Kinase Activation. *Journal of Neuroscience* **29**, 3518–3528 (2009).

72. Coull, J. A. M. *et al.* BDNF from microglia causes the shift in neuronal anion gradient underlying neuropathic pain. *Nature 2005 438:7070* **438**, 1017–1021 (2005).

73. Hildebrand, M. E. *et al.* Potentiation of Synaptic GluN2B NMDAR Currents by Fyn Kinase Is Gated through BDNF-Mediated Disinhibition in Spinal Pain Processing. *CellReports* **17**, 2753–2765 (2016).

74. Inoue, K. & Tsuda, M. Microglia in neuropathic pain: cellular and molecular mechanisms and therapeutic potential. *Nature Reviews Neuroscience 2018 19:3* **19**, 138–152 (2018).

75. Zajączkowska, R. *et al.* Mirogabalin Decreases Pain-like Behaviors by Inhibiting the Microglial/Macrophage Activation, p38MAPK Signaling, and Pronociceptive CCL2 and CCL5 Release in a Mouse Model of Neuropathic Pain. *Pharmaceuticals 2023, Vol. 16, Page 1023* **16**, 1023 (2023).

76. Rosa, A. S., Freitas, M. F., Rocha, I. R. C. & Chacur, M. Gabapentin decreases microglial cells and reverses bilateral hyperalgesia and allodynia in rats with chronic myositis. *Eur J Pharmacol* **799**, 111–117 (2017).

77. Wodarski, R., Clark, A. K., Grist, J., Marchand, F. & Malcangio, M. Gabapentin reverses microglial activation in the spinal cord of streptozotocin-induced diabetic rats. *European Journal of Pain* **13**, 807–811 (2009).

78. Ahmad, K. A. *et al.* Microglial IL-10 and β-endorphin expression mediates gabapentinoids antineuropathic pain. *Brain Behav Immun* **95**, 344–361 (2021).

79. Nees, T. A. *et al.* Early-onset treadmill training reduces mechanical allodynia and modulates calcitonin gene-related peptide fiber density in lamina III/IV in a mouse model of spinal cord contusion injury. *Pain* **157**, 687–697 (2016).

80. Sliwinski, C., Nees, T. A., Puttagunta, R., Weidner, N. & Blesch, A. Sensorimotor activity partially ameliorates pain and reduces nociceptive fiber density in the chronically injured spinal cord. *J Neurotrauma* **35**, 2222–2238 (2018).

81. Sliwinski, C. *et al.* Contribution of mechanoreceptors to spinal cord injury–induced mechanical allodynia. *Pain* (2023).

82. Basso, D. M. *et al.* Basso Mouse Scale for Locomotion Detects Differences in Recovery after Spinal Cord Injury in Five Common Mouse Strains. *J Neurotrauma* **23**, 635–659 (2006).

83. Gan, Z., Li, H., Naser, P. V., Oswald, M. J. & Kuner, R. Suppression of neuropathic pain and comorbidities by recurrent cycles of repetitive transcranial direct current motor cortex stimulation in mice. *Sci Rep* **11**, 1–17 (2021).

84. Gan, Z. *et al.* Repetitive non-invasive prefrontal stimulation reverses neuropathic pain via neural remodelling in mice. *Prog Neurobiol* **201**, 102009 (2021).

85. Hargreaves, K., Dubner, R., Brown, F., Flores, C. & Joris, J. A new and sensitive method for measuring thermal nociception in cutaneous hyperalgesia. *Pain* **32**, 77–88 (1988).

86. Madisen, L. *et al.* A robust and high-throughput Cre reporting and characterization system for the whole mouse brain. *Nat Neurosci* **13**, 133–140 (2009).

87. Agarwal, N., Offermanns, S. & Kuner, R. Conditional gene deletion in primary nociceptive neurons of trigeminal ganglia and dorsal root ganglia. *genesis* **38**, 122–129 (2004).

88. Watson, C. & Harrison, M. The location of the major ascending and descending spinal cord tracts in all spinal cord segments in the mouse: actual and extrapolated. *Anatomical record* **295**, 1692–1697 (2012).

89. Brennan, F. H. *et al.* Acute post-injury blockade of α2δ-1 calcium channel subunits prevents pathological autonomic plasticity after spinal cord injury. *Cell Rep* **34**, (2021).

90. Liu, S. *et al.* Pre-Synaptic GABAA in NaV1.8+ Primary Afferents Is Required for the Development of Punctate but Not Dynamic Mechanical Allodynia following CFA Inflammation. *Cells* **11**, 2390 (2022).

91. Kalous, A., Osborne, P. B. & Keast, J. R. Acute and chronic changes in dorsal horn innervation by primary afferents and descending supraspinal pathways after spinal cord injury. *Journal of Comparative Neurology* **504**, 238–253 (2007).

92. Ondarza, A. B., Ye, Z. & Hulsebosch, C. E. Direct evidence of primary afferent sprouting in distant segments following spinal cord injury in the rat: colocalization of GAP-43 and CGRP. *Exp Neurol* **184**, 373–380 (2003).

93. Assis, A. D., Chiarotto, G. B., Simões, G. F. & Oliveira, A. L. R. Pregabalin-induced neuroprotection and gait improvement in dystrophic MDX mice. *Molecular and Cellular Neuroscience* **114**, 103632 (2021).

94. Hundehege, P. *et al.* Targeting Voltage-Dependent Calcium Channels with Pregabalin Exerts a Direct Neuroprotective Effect in an Animal Model of Multiple Sclerosis. *Neurosignals* **26**, 77–93 (2019).

95. Ha, K. Y., Carragee, E., Cheng, I., Kwon, S. E. & Kim, Y. H. Pregabalin as a Neuroprotector after Spinal Cord Injury in Rats: Biochemical Analysis and Effect on Glial Cells. *J Korean Med Sci* **26**, 404–411 (2011).

96. Anfuso, C. D. *et al.* Gabapentin attenuates ocular inflammation: In vitro and in vivo studies. *Front Pharmacol* **8**, 173 (2017).

97. Daneshdoust, D. *et al.* Pregabalin enhances myelin repair and attenuates glial activation in lysolecithin-induced demyelination model of rat optic chiasm. *Neuroscience* **344**, 148–156 (2017).

98. Dias, J. M. *et al.* Gabapentin, a Synthetic Analogue of Gamma Aminobutyric Acid, Reverses Systemic Acute Inflammation and Oxidative Stress in Mice. *Inflammation* **37**, 1826–1836 (2014).

99. Peirs, C., Williams, S.-P. G., Ross, S. E., Goulding, M. & Seal Correspondence, R. P. PKCg neurons are important for mechanical allodynia in neuropathic injuries d CCK and tVGLUT3 neurons in deeper laminae convey both types of injuries d The Maf + subset of CCK neurons encompasses tVGLUT3 and conveys dynamic allodynia. *Neuron* **109**, 73-90.e7 (2021).

100. Kerr, B. J. & David, S. Pain behaviors after spinal cord contusion injury in two commonly used mouse strains. *Exp Neurol* **206**, 240–247 (2007).

101. Talifu, Z. *et al.* The role of KCC2 and NKCC1 in spinal cord injury: From physiology to pathology. *Front Physiol* **13**, 1045520 (2022).

102. Tashiro, S. *et al.* BDNF Induced by Treadmill Training Contributes to the Suppression of Spasticity and Allodynia After Spinal Cord Injury via Upregulation of KCC2. *Neurorehabil Neural Repair* **29**, 677–689 (2015).

103. Bee, L. A. & Dickenson, A. H. Descending facilitation from the brainstem determines behavioural and neuronal hypersensitivity following nerve injury and efficacy of pregabalin. *Pain* **140**, 209–223 (2008).

104. Chiu, I. M. *et al.* Transcriptional profiling at whole population and single cell levels reveals somatosensory neuron molecular diversity. *Elife* **3**, (2014).

105. Fang, X. *et al.* trkA Is Expressed in Nociceptive Neurons and Influences Electrophysiological Properties via Nav1.8 Expression in Rapidly Conducting Nociceptors. *Journal of Neuroscience* **25**, 4868–4878 (2005).

106. Detloff, M. R. *et al.* Delayed Exercise Is Ineffective at Reversing Aberrant Nociceptive Afferent Plasticity or Neuropathic Pain after Spinal Cord Injury in Rats. *Neurorehabil Neural Repair* **30**, 685–700 (2016).

107. Hayashi, M. *et al.* Intrathecally administered Sema3A protein attenuates neuropathic pain behavior in rats with chronic constriction injury of the sciatic nerve. *Neurosci Res* **69**, 17–24 (2011).

108. Yang, Q. *et al.* Persistent Pain after Spinal Cord Injury Is Maintained by Primary Afferent Activity. *Journal of Neuroscience* **34**, 10765–10769 (2014).

109. Gwak, Y. S. *et al.* Activation of Spinal GABA Receptors Attenuates Chronic Central Neuropathic Pain after Spinal Cord Injury. *https://home.liebertpub.com/neu* **23**, 1111–1124 (2006).

110. Zhang, H., Xie, W. & Xie, Y. Spinal cord injury triggers sensitization of wide dynamic range dorsal horn neurons in segments rostral to the injury. *Brain Res* **1055**, 103–110 (2005).

111. Biggs, J. E. *et al.* Analysis of the long-term actions of gabapentin and pregabalin in dorsal root ganglia and substantia gelatinosa. *J Neurophysiol* **112**, 2398–2412 (2014).

112. Freda Warner, A. M. *et al.* Early Administration of Gabapentinoids Improves Motor Recovery after Human Spinal Cord Injury. *CellReports* **18**, 1614–1618 (2017).

113. Dolphin, A. C. Calcium channel auxiliary α2δ and β subunits: trafficking and one step beyond. *Nat Rev Neurosci* **13**, 542–555 (2012).

114. Fell, B. *et al.* α2δ2 Controls the Function and Trans-Synaptic Coupling of Cav1.3 Channels in Mouse Inner Hair Cells and Is Essential for Normal Hearing. *Journal of Neuroscience* **36**, 11024–11036 (2016).

115. Wang, T., Jones, R. T., Whippen, J. M. & Davis Correspondence, G. W. α2δ-3 is required for rapid transsynaptic homeostatic signaling. *CellReports* **16**, 2875–2888 (2016).

116. Brockhaus, J. *et al.* α-Neurexins Together with α2δ-1 Auxiliary Subunits Regulate Ca2+ Influx through Cav2.1 Channels. *Journal of Neuroscience* **38**, 8277–8294 (2018).

117. Chen, J. *et al.* The α2δ-1-NMDA Receptor Complex Is Critically Involved in Neuropathic Pain Development and Gabapentin Therapeutic Actions. *Cell Rep* **22**, 2307–2321 (2018).

118. Geisler, S. *et al.* Presynaptic α2δ-2 Calcium Channel Subunits Regulate Postsynaptic GABAA Receptor Abundance and Axonal Wiring. *Journal of Neuroscience* **39**, 2581–2605 (2019).

119. Beeson, K. A., Beeson, R., Westbrook, G. L. & Schnell, E. α2δ-2 Protein Controls Structure and Function at the Cerebellar Climbing Fiber Synapse. *Journal of Neuroscience* **40**, 2403–2415 (2020).

120. Donato, R. *et al.* The ducky2J Mutation in Cacna2d2 Results in Reduced Spontaneous Purkinje Cell Activity and Altered Gene Expression. *Journal of Neuroscience* **26**, 12576–12586 (2006).

121. Calvo, M. & Bennett, D. L. H. The mechanisms of microgliosis and pain following peripheral nerve injury. *Exp Neurol* **234**, 271–282 (2012).

122. Fu, H. *et al.* Depletion of microglia exacerbates injury and impairs function recovery after spinal cord injury in mice. *Cell Death & Disease 2020 11:7* **11**, 1–12 (2020).

123. Akhmetzyanova, E. R. *et al.* Increasing Severity of Spinal Cord Injury Results in Microglia/Macrophages With Annular-Shaped Morphology and No Change in Expression of CD40 and Tumor Growth Factor-β During the Chronic Post-injury Stage. *Front Mol Neurosci* **14**, 802558 (2022).

124. Stewart, A. N. *et al.* Acute inflammatory profiles differ with sex and age after spinal cord injury. *J Neuroinflammation* **18**, 1–16 (2021).

125. Yang, J. Le *et al.* Gabapentin reduces CX3CL1 signaling and blocks spinal microglial activation in monoarthritic rats. *Mol Brain* **5**, 1–12 (2012).

126. Kitano, Y. *et al.* Effects of mirogabalin, a novel ligand for the α2δ subunit of voltage-gated calcium channels, on N-type calcium channel currents of rat dorsal root ganglion culture neurons. *Pharmazie* **74**, 147–149 (2019).

127. Boulenguez, P. *et al.* Down-regulation of the potassium-chloride cotransporter KCC2 contributes to spasticity after spinal cord injury. *Nature Medicine 2010 16:3* **16**, 302–307 (2010).

128. Fauss, G. N. K., Hudson, K. E. & Grau, J. W. Role of Descending Serotonergic Fibers in the Development of Pathophysiology after Spinal Cord Injury (SCI): Contribution to Chronic Pain, Spasticity, and Autonomic Dysreflexia. *Biology (Basel)* **11**, (2022).

129. McFarlane, K. *et al.* Effect of Sex on Motor Function, Lesion Size, and Neuropathic Pain after Contusion Spinal Cord Injury in Mice. *J Neurotrauma* **37**, 1983–1990 (2020).

130. Willis, W. D., Zhang, X., Honda, C. N. & Giesler, G. J. A critical review of the role of the proposed VMpo nucleus in pain. *J Pain* **3**, 79–94 (2002).

131. Dolphin, A. C. & Lee, A. Presynaptic calcium channels: specialized control of synaptic neurotransmitter release. *Nature Reviews Neuroscience 2020 21:4* **21**, 213–229 (2020).